PHYSICAL REVIEW D **88,** 094004 (2013)

Isospin asymmetries in $B \to (K^*, \rho)\gamma/l^+l^-$ and $B \to Kl^+l^-$ in and beyond the standard model

James Lyon* and Roman Zwicky†

School of Physics and Astronomy, University of Edinburgh, Edinburgh EH9 3JZ, United Kingdom

(Received 5 June 2013; published 11 November 2013)

We compute the isospin asymmetries in $B \to (K^*, \rho)\gamma$ and $B \to (K, K^*, \rho)l^+l^-$ for low lepton pair invariant mass q^2, within the Standard Model (SM) and beyond the SM in a generic dimension six operator basis. Within the SM the CP-averaged isospin asymmetries for $B \to (K, K^*, \rho)ll$, between $1\ \mathrm{GeV}^2 \leq q^2 \leq 4m_c^2$, are predicted to be small (below 1.5%) though with significant cancellation. In the SM the non-CP-averaged asymmetries for $B \to \rho ll$ deviate by $\approx \pm 5\%$ from the CP-averaged ones. We provide physical arguments, based on resonances, of why isospin asymmetries have to decrease for large q^2 (towards the endpoint). Two types of isospin violating effects are computed: ultraviolet isospin violation due to differences between operators coupling to up and down quarks, and infrared isospin violation where a photon is emitted from the spectator quark and is hence proportional to the difference between the up- and down-quark charges. These isospin violating processes may be subdivided into weak annihilation (WA), quark loop spectator scattering, and a chromomagnetic contribution. Furthermore we discuss generic selection rules based on parity and angular momentum for the $B \to Kll$ transition as well as specific selection rules valid for WA at leading order in the strong coupling constant. We clarify that the relation between the K and the longitudinal part of the K^* only holds for leading twist and for left-handed currents. In general the $B \to \rho ll$ and $B \to K^*ll$ isospin asymmetries are structurally different yet the closeness of α_{CKM} to 90° allows us to construct a (quasi)null test for the SM out of the respective isospin symmetries. We provide and discuss an update on $\mathcal{B}(B^0 \to K^{*0}\gamma)/\mathcal{B}(B_s \to \phi\gamma)$ which is sensitive to WA.

DOI: 10.1103/PhysRevD.88.094004 PACS numbers: 12.38.−t, 12.38.Lg, 13.20.He

I. INTRODUCTION

The isospin asymmetry in $B \to K^*ll$ gave, in recent years, some indication of being of opposite sign to the Standard Model (SM) prediction [1]. This trend has not been confirmed by the new LHCb data in the year of 2012 [2], yet in $B \to Kll$ a negative deviation from zero has been measured at the level of 4σ taking into account the entire q^2 spectrum. The isospin asymmetry in $B \to Kll$ is expected to be small in the SM and therefore it is important to assess this observable. Isospin asymmetries of the $B \to K^*\gamma$ and $B \to \rho\gamma$ [3] are found to agree and deviate by 2 standard deviations from the SM giving rise to constraints and curiosity for future measurements, respectively.

Independent of any signs of deviation, the isospin asymmetry contributes to the microscopic investigation of flavor changing neutral currents. It is sensitive to a large number of four Fermi operators of the $\Delta F = 1$-type and complements the constraints from nonleptonic decays.

In this paper we consider two types of isospin violating effects: *ultraviolet (UV) isospin violation* due to unequal coupling of up and down quarks to Fermi operators as well as *infrared (IR) isospin violation from spectator emission* of the intermediate photon which is therefore proportional to the charge difference of up and down quarks. The latter mainly results from processes for which the large energy release of the b-quark is transferred to the spectator quark which then emits an energetic photon as the external kinematics require. The processes are depicted in Fig. 1 and are from left to right: weak annihilation (WA), quark loop spectator scattering (QLSS), and the contribution from the chromomagnetic operator which we shall simply denote by $\mathcal{O}_8$ hereafter. Isospin effects in quantum chromodynamical (QCD) quantities such as masses and decay constants are known to be just below the subpercent level, to be discussed later on, and therefore small in comparison to the precision accessible to near future experiments.

In this paper we have computed WA in light-cone sum rules (LCSR), extending earlier results for $q^2 = 0$ [4,5], QLSS within QCD factorization (QCDF), and $\mathcal{O}_8$ we take from our recent computation [6]. Furthermore we include a complete set of dimension six operators relevant at leading order of the strong coupling constant $\alpha_s = g_s^2/4\pi$. By mapping a specific model into an operator basis, such as the family model considered in [7], one can get the effects with our estimates.

Various aspects of the isospin asymmetry in $B \to K$, $K^*l^+l^-$ decay have been calculated previously. The closely related decay $B \to V\gamma$ has been computed using QCD factorization (QCDF) in [8] and using a mixture of QCDF and LCSR in [9]. A program computing the isospin asymmetry $B \to K^*\gamma$ in the minimal supersymmetric SM has been reported in [10]. $B \to K$, $K^*l^+l^-$ was computed using QCDF in [11], and a mixed approach was recently employed for $B \to Kll$ in [12]. In this paper we improve on

*J.D.Lyon@sms.ed.ac.uk
†Roman.Zwicky@ed.ac.uk

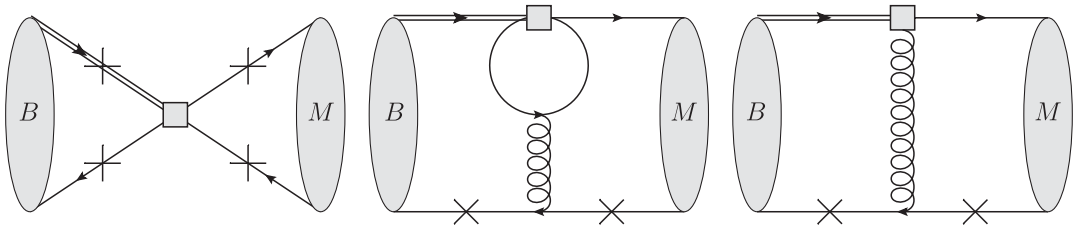

FIG. 1. Isospin violating processes included in our calculation. Crosses indicate possible photon emission points. Throughout this paper double lines stand for the b-quark flavor. Left: weak annihilation; middle: quark loops with spectator scattering; right: chromomagnetic operator $\mathcal{O}_8$. Note that in WA we have indicated photon emission from quarks with Q_b charge as well as WA is sensitive to UV isospin violation where the four Fermi operators with spectator quarks u and d appear in unequal proportion.

these works by including a complete basis of dimension six operators for WA and QLSS, our recent $\mathcal{O}_8$ computation [6], and the complete set of twist-3 terms for WA.

Essential results of the paper are that the isospin asymmetries of $B \to K, K^*, \rho ll$ are small in the SM; especially and systematically for high q^2. The isospin asymmetries of the K^* and ρ mesons turn out to be very similar at small q^2 up to form factor ratios due to the, presumably, accidental closeness of the Cabibbo-Kobayashi-Maskawa (CKM) angle α_{CKM} to 90°. This prompts us to define a quantity δ_{a_I} which serves as a (quasi)null test of the SM. The results of the generic dimension six operators are given in the form of tables and complement constraints from nonleptonic decays and $B \to (K^*, \rho)\gamma$ decays, which we discuss.

This work is written in the language of $B \to K/K^*$ transition. Adaptation to other light vector mesons is generally straightforward, with the exception of WA for $B^0 \to \rho^0$ and $B_s \to \phi$ transitions which we discuss in the corresponding section in some detail. The paper is organized as follows: In Sec. II we present formulas for pseudoscalar and vector meson decay rates in terms of helicity amplitudes, the relation of the latter to form factors and quark loop functions, and finally formulas for the isospin asymmetries in a linear approximation. In Sec. III the complete operator basis of dimension six operators contributing at $\mathcal{O}(\alpha_s^0)$ to the WA subprocess is given; with results in Sec. III D and detailed formulas in Appendix F 3. In Sec. IV we present the complete dimension six operator basis contributing to QLSS at order $\mathcal{O}(\alpha_s)$ along with results computed in QCDF. In Sec. V we present the $B \to K^* ll$ and $B \to K^*\gamma$ isospin asymmetries. In Sec. V A we discuss selection rules: those applicable to any scalar → scalar ll decay in V A 1, those particular to WA in the factorization approximation V A 2, and we also discuss to what extent the K distribution amplitude (DA) does or does not correspond to the $K_\parallel^*$ in V A 3. In Sec. V B we discuss q^2 dependence of the isospin asymmetries, and in Sec. V C we discuss the kaon isospin asymmetries in the SM, respectively. In Sec. VI we present the isospin asymmetry of $B \to \rho\gamma/ll$ as well as an extension of the operator basis for the ρ^0 channel. In Sec. VII we cover aspects of isospin beyond the SM (BSM): in VII A we (briefly) discuss constraints and in VII B we propose the ratio of the $K^*\gamma$ and $\rho\gamma$ asymmetries as a (quasi)null test of the SM. We end the paper with a summary and conclusions in Sec. VIII.

We give an updated prediction for $\mathcal{B}(B^0 \to K^{*0}\gamma)/\mathcal{B}(B_s \to \phi\gamma)$ in Appendix A, which was recently measured by LHCb. Various explicit results can be found in Appendix F, such as numbers for the generic dimension six operator basis for all isospin asymmetries discussed in this paper in Appendix F 1. Aspects of gauge invariance of the WA and QLSS computations, which turn out to be rather intricate, can be found in Appendix D.

II. DECAY RATE AND FORM FACTORS

The effective Hamiltonian in the SM, to be extended in upcoming sections, is parametrized by

$$\mathcal{H}_{\mathrm{eff}} = \frac{G_F}{\sqrt{2}}\Big(\sum_{i=1}^{2}(\lambda_u C_i \mathcal{O}_i^u + \lambda_c C_i \mathcal{O}_i^c) - \lambda_t \sum_{i=3}^{10} C_i \mathcal{O}_i\Big),$$
$$\lambda_i \equiv V_{is}^* V_{ib}, \tag{1}$$

where the $b \to s$ unitarity relation reads $\lambda_u + \lambda_c + \lambda_t = 0$. The basis is given by [13]

$$\begin{aligned}
\mathcal{O}_1^q &= (\bar{s}_i q_j)_{V-A}(\bar{q}_j b_i)_{V-A},\\
\mathcal{O}_2^q &= (\bar{s}_i q_i)_{V-A}(\bar{q}_j b_j)_{V-A},\\
\mathcal{O}_3 &= (\bar{s}_i b_i)_{V-A}\sum_q (\bar{q}_j q_j)_{V-A},\\
\mathcal{O}_4 &= (\bar{s}_i b_j)_{V-A}\sum_q (\bar{q}_j q_i)_{V-A},\\
\mathcal{O}_5 &= (\bar{s}_i b_i)_{V-A}\sum_q (\bar{q}_j q_j)_{V+A},\\
\mathcal{O}_6 &= (\bar{s}_i b_j)_{V-A}\sum_q (\bar{q}_j q_i)_{V+A},\\
\mathcal{O}_7 &= -\frac{e m_b}{8\pi^2}\bar{s}\sigma\cdot F(1+\gamma_5)b,\\
\mathcal{O}_8 &= -\frac{g_s m_b}{8\pi^2}\bar{s}\sigma\cdot G(1+\gamma_5)b,\\
\mathcal{O}_9 &= \frac{\alpha}{2\pi}(\bar{l}\gamma^\mu l)(\bar{s}\gamma_\mu(1-\gamma_5)b),\\
\mathcal{O}_{10} &= \frac{\alpha}{2\pi}(\bar{l}\gamma^\mu\gamma_5 l)(\bar{s}\gamma_\mu(1-\gamma_5)b),
\end{aligned} \tag{2}$$

where i, j are color indices, $(\bar{s}b)_{V\pm A} = \bar{s}\gamma^\mu(1 \pm \gamma_5)b$ and $\mathcal{O}'_{7-10}$ will denote the operators with opposite chirality as usual, and we have taken the opposite sign of $\mathcal{O}_{7,8}$.[1] These are the same conventions as in [14]. Details of the calculation of the Wilson coefficients C_{1-10} are given in Appendix E 3. Furthermore, $e = \sqrt{4\pi\alpha} > 0$ where α is the fine structure constant and G_F is the Fermi constant.

We parametrize the amplitude as follows:

$$
\begin{aligned}
&{}_{\text{out}}\langle M(p) l^+(l_1) l^-(l_2) \mid B(p+q)\rangle_{\text{in}} \\
&\quad = \frac{G_F}{\sqrt{2}} \lambda_t \frac{\alpha m_b}{q^2 \pi} \Big(\bar{u}(l_1)\gamma_\mu v(l_2) \sum_i \mathcal{T}_i^V P_i^\mu \\
&\qquad + \bar{u}(l_1)\gamma_\mu\gamma_5 v(l_2) \sum_i \mathcal{T}_i^A P_i^\mu \Big) \delta^{(4)}(q - l_1 - l_2), \qquad (3)
\end{aligned}
$$

where M stands, throughout this work, for a light vector (K^*, ρ) or pseudoscalar (K) meson. The symbols u, v correspond to lepton polarization spinors of mass dimension $1/2$ and $q = l_1 + l_2$ is the total momentum of the lepton pair. For lepton coupling we only allow V and A couplings as present in the SM. The isospin violating contributions all proceed through a photon and thus have a vectorial coupling. The axial coupling is included as it originates through Z penguins and box diagrams which are significant in the SM. In this work we do not include non-SM lepton couplings. The basis tensors P_i^μ [6] are the standard choice for penguin form factors

$$
\begin{aligned}
K^*\colon\ & P_1^\mu = 2\epsilon^{\mu\nu\rho\sigma}\eta_\nu^* p_\sigma q_\rho, \\
& P_2^\mu = i[(m_B^2 - m_{K^*}^2)\eta^{*\mu} - (\eta^*\cdot q)(2p+q)^\mu], \\
& P_3^\mu = i(\eta^*\cdot q)\Big[q_\mu - \frac{q^2}{m_B^2 - m_{K^*}^2}(2p+q)^\mu \Big], \qquad (4) \\
K\colon\ & P_T^\mu = \frac{1}{m_B + m_K}[(m_B^2 - m_K^2)q^\mu - q^2(2p+q)^\mu],
\end{aligned}
$$

in the sense that $\mathcal{T}_i^V = C_7 T_i(q^2) + \text{corrections}$.[2] The basis for pseudoscalar and vector meson decays are P_T^μ and $P_{1,2,3}^\mu$, respectively. Note we have implicitly assumed $m_l = 0$ as otherwise there is additional direction proportional to q^μ which vanishes for the V but is proportional to m_l for A. The four vector η denotes the vector meson polarization. We use the Bjorken and Drell convention for the Levi-Civita tensor $\epsilon_{0123} = +1$. In discussing physical quantities and problems it will prove advantageous to go over to the so-called *helicity basis*:

$$
\begin{pmatrix} h_0 \\ h_+ \\ h_- \end{pmatrix} = \underbrace{\begin{pmatrix} 0 & a & b \\ 1/\sqrt{2} & -c/\sqrt{2} & 0 \\ 1/\sqrt{2} & +c/\sqrt{2} & 0 \end{pmatrix}}_{\equiv B} \begin{pmatrix} \mathcal{T}_1 \\ \mathcal{T}_2 \\ \mathcal{T}_3 \end{pmatrix}, \qquad (5)
$$

which corresponds to 0, $\pm$[3] polarization of the vector meson. Basis tensors corresponding to $h_{0,\pm}$ are given in Appendix C. The variables a, b, c in the basis transformation matrix are given by

$$
\begin{aligned}
(a,b) &\equiv \sqrt{\frac{\hat{q}^2}{8}} \frac{1}{\hat{m}_V} \Big(\frac{1 + 3\hat{m}_V^2 - \hat{q}^2}{\sqrt{\lambda_V}}, \frac{-\sqrt{\lambda_V}}{1 - \hat{m}_V^2} \Big), \\
c &\equiv \frac{1 - \hat{m}_V^2}{\sqrt{\lambda_V}} = 1 + \mathcal{O}(\hat{q}^2),
\end{aligned}
$$

where here and below hatted quantities are normalized with respect to the B-meson mass, $\hat{q}^2 \equiv q^2/m_B^2$, $\hat{m}_V^2 \equiv m_V^2/m_B^2$ and λ_V is the Källén-function with normalized entries:

$$
\begin{aligned}
\lambda_V &\equiv \lambda_V(1, \hat{m}_V^2, \hat{q}^2) \\
&= ((1+\hat{m}_V)^2 - \hat{q}^2)((1-\hat{m}_V)^2 - \hat{q}^2). \qquad (6)
\end{aligned}
$$

For the K meson there is no polarization and no freedom in choosing a basis.

The decay rates are given by[4]

$$
\begin{aligned}
&\frac{d\Gamma}{dq^2}[B \to K^* l^+ l^-] \\
&\quad = \Big[\frac{\lambda_V^{3/2}}{q^2} \Big] \Big(\frac{\alpha}{4\pi} \Big)^2 c_F c_L \sum_{i=V,A} [|h_+^i|^2 + |h_-^i|^2 + |h_0^i|^2], \qquad (7)
\end{aligned}
$$

$$
\frac{d\Gamma}{dq^2}[B \to K l^+ l^-] = \Big[\frac{\lambda_P^{3/2}}{2(m_B + m_K)^2} \Big] \Big(\frac{\alpha}{4\pi} \Big)^2 c_F c_L \sum_{i=V,A} |h_T^i|^2, \qquad (8)
$$

$$
\Gamma[B \to K^* \gamma] = \Big[\frac{3}{4}\lambda_V^{3/2} \Big] \Big(\frac{\alpha}{4\pi} \Big) c_F [|h_+^V|^2 + |h_-^V|^2]|_{q^2=0}, \qquad (9)
$$

where $c_F \equiv (G_F^2 |\lambda_t|^2 m_b^2 m_B^3/12\pi^3)$, $h_T^i \equiv \mathcal{T}_T^i$, and $c_L = (1 + 2m_l^2/q^2)\sqrt{1 - 4m_l^2/q^2}$ accounts for nonzero lepton mass. An important observation is that for $m_V \to 0$ the rate remains bounded[5] provided that

[1] This corresponds to a covariant derivative $D_\mu = \partial_\mu - iQeA_\mu - ig_s A_\mu$ and interaction vertex $+i(Qe + g_s \frac{\lambda^a}{2})\gamma^\mu$ in agreement with [14] but differing from [4,5,13,15].

[2] The $\mathcal{T}_i^V$ differ from the ones in [14] in that we include the contributions of C_9 as well.

[3] The direction 0 and $\pm$ are also known as the longitudinal and transversal polarization directions.

[4] The IR sensitive $1/q^2$ factor in the $B \to V l l$ rate for $m_l \to 0$ is compensated by a virtual lepton loop in the limit $q^2 \to 0$ as the collinear lepton pair is indistinguishable from a photon. This corresponds to the famous Bloch-Nordsieck cancellation mechanism. Furthermore we note that $|h_0|^2 \sim q^2$ by virtue of (6) and (5) and corresponds to the well-known decoupling of the zero helicity mode towards $q^2 \to 0$. In the differential rate into the pseudoscalar (8) the q^2 has been factored out from $|h_T|^2$ to cancel the explicit pole.

[5] Note we do not want to invoke the $m_V \to 0$ limit *per se* as it is well known that massless and massive representations differ in a discontinuous fashion.

$$h_0^i = \mathcal{O}(m_V^0) \Rightarrow \mathcal{T}_2^i = \frac{\lambda_V}{(1-\hat{m}_V^2)(1+3\hat{m}_V^2-\hat{q}^2)}\mathcal{T}_3^i + \mathcal{O}(m_V). \quad (10)$$

This expression reduces to the form we have given in our previous work [6] in the appendix in the $m_V \to 0$ limit. In essence the relation between $\mathcal{T}_2$ and $\mathcal{T}_3$ cancels the explicit $1/m_V$ in h_0 which appears through (5) and (6). Note in the SM $h_+ \ll h_-$ by virtue of the V-A interactions. In [14], which operates in the heavy quark limit, $h_+ \to 0$. In our work h_+ is vital as we allow for right-handed structures that violate isospin.

The axial lepton amplitudes $\mathcal{T}_i^A$ arise only from the $\mathcal{O}_{10}$ operator and are given in terms of standard form factors by

$$\mathcal{T}_1^A = \frac{C_{10}q^2V(q^2)}{2m_b(m_B+m_{K^*})}, \qquad \mathcal{T}_3^A = -C_{10}\frac{m_{K^*}}{m_b}A_3(q^2),$$
$$\mathcal{T}_2^A = \frac{C_{10}q^2A_1(q^2)}{2m_b(m_B-m_{K^*})}, \qquad \mathcal{T}_T^A = C_{10}\frac{m_B+m_K}{2m_b}f_+(q^2). \quad (11)$$

We will split the vector lepton amplitudes into isospin sensitive and insensitive parts denoted by $\mathcal{T}^q$ and $\mathcal{T}^0$, respectively, with q being the light flavor of the B meson:

$$\mathcal{T}_i^V = \mathcal{T}_i^{V,0} + \mathcal{T}_i^{V,q},$$
$$\mathcal{T}_i^{V,q} = C_8^{\text{eff}}G_i^q(q^2) + W_i^q(q^2) + S_i^q(q^2). \quad (12)$$

Note, we have absorbed the Wilson coefficient (WC) for WA and QLSS into the functions $W_i^q(q^2)$ and $S_i^q(q^2)$, respectively, as there are quite a few of them. The WC $C_{7,8,9}^{\text{eff}}$ correspond to scheme and basis independent WCs which include quark loop contributions and will be defined further below. The symmetric part is approximated throughout this work by the $C_{7,9}^{\text{eff}}$ contributions, which in terms of standard form factors is given by

$$\mathcal{T}_1^{V,0}(q^2) = \frac{C_9^{\text{eff}}(q^2)q^2V(q^2)}{2m_b(m_B+m_{K^*})} + C_7^{\text{eff}}T_1(q^2),$$
$$\mathcal{T}_3^{V,0}(q^2) = -C_9^{\text{eff}}(q^2)\frac{m_{K^*}}{m_b}A_3(q^2) + C_7^{\text{eff}}T_3(q^2),$$
$$\mathcal{T}_2^{V,0}(q^2) = \frac{C_9^{\text{eff}}(q^2)q^2A_1(q^2)}{2m_b(m_B-m_{K^*})} + C_7^{\text{eff}}T_2(q^2),$$
$$\mathcal{T}_T^{V,0}(q^2) = C_9^{\text{eff}}(q^2)\frac{m_B+m_K}{2m_b}f_+(q^2) + C_7^{\text{eff}}f_T(q^2). \quad (13)$$

The isospin sensitive diagrams are shown in Fig. 1. The weak annihilation amplitude, denoted $W_i^q(q^2)$, (Fig. 1, left) originates from $\mathcal{O}_{1-6}$ and is computed using LCSR in Sec. III. Spectator scattering with a quark loop, denoted $S_i^q(q^2)$, (Fig. 1, middle) arises from $\mathcal{O}_{1-6}$ as well and is computed using QCD factorization in Sec. IV. The spectator contributions due to $\mathcal{O}_8$ (Fig. 1, right) are denoted by $G_i^q(q^2)$ and are taken from our recent work [6]. For the short distance form factors in (11) and (13) we use the fits in [16,17], recomputed with updated hadronic inputs as in [6]. Quark loop contributions, other than the ones with a gluon connecting to the spectator, are absorbed into the effective WCs. The structures proportional to the m_b mass are independent of q^2 and described by

$$C_7^{\text{eff}} = C_7 - \frac{4}{9}C_3 - \frac{4}{3}C_4 + \frac{1}{9}C_5 + \frac{1}{3}C_6,$$
$$C_8^{\text{eff}} = C_8 + \frac{4}{3}C_3 - \frac{1}{3}C_5. \quad (14)$$

The other contributions are taken care of by $C_9^{\text{eff}}(q^2)$ [18],

$$C_9^{\text{eff}}(q^2) = C_9 + Y(q^2), \quad (15)$$

where

$$Y(q^2) = h(q^2,m_c)\left(-\frac{\lambda_c}{\lambda_t}(3C_1+C_2) + 3C_3 + C_4 + 3C_5 + C_6\right) - \frac{h(q^2,m_b)}{2}(4C_3+4C_4+3C_5+C_6) - h(q^2,0)\left(\frac{\lambda_u}{\lambda_t}(3C_1+C_2) + \frac{1}{2}(C_3+3C_4)\right) + \frac{4}{27}(C_3+3C_4+8C_5), \quad (16)$$

with $h(s,m_q)$ being the photon vacuum polarization which we quote in Sec. IV B, and we restored the λ_u and λ_c factors explicitly especially in view of the fact that for the $b \to d$ transition the hierarchies differ from the $b \to s$ transitions.

A. Definition of isospin asymmetries

The experimentally accessible isospin asymmetry $a_I(q^2)$ and its CP-average $\bar{a}_I$,[6] which are functions of the lepton pair invariant mass q^2, are defined as follows:

$$a_I^{\bar{0}-}(q^2) \equiv \frac{dA_I^{\bar{0}-}}{dq^2} \equiv \frac{c_M^2 d\Gamma[\bar{B}^0 \to \bar{M}^0 l^+ l^-]/dq^2 - d\Gamma[B^- \to M^- l^+ l^-]/dq^2}{c_M^2 d\Gamma[\bar{B}^0 \to \bar{M}^0 l^+ l^-]/dq^2 + d\Gamma[B^- \to M^- l^+ l^-]/dq^2},$$
$$\bar{a}_I(q^2) \equiv \frac{1}{2}(a_I^{\bar{0}-}(q^2) + a_I^{0+}(q^2)), \quad (17)$$

where a_I^{0+} corresponds to the CP-conjugated process of $a_I^{\bar{0}-}$. The constant c_M is given by $c_K = c_{K^*} = 1$ and $c_\rho = \sqrt{2}$.[7] A similar definition without differential applies

[6] For the K^* this merely doubles the statistics and reduces experimental uncertainties in the production. For the pseudoscalar K this is essential as the K_S^0 is detected in experiment which is a linear superposition of $|s\bar{d}\rangle$ and $|d\bar{s}\rangle$ eigenstates which implies averaging.

[7] This accounts for $\rho^0 \sim (\bar{u}u - \bar{d}d)/\sqrt{2}$ since the leading decay amplitude only couples to the $\bar{d}d$ component of the ρ^0.

for the $B \to K^*/\rho\gamma$ transition. The definition above makes clear the meaning of isospin in this context: it is understood throughout this paper to mean a rotation between u and d quarks, with no corresponding rotation between b and t quarks, as is understood in the case of the electroweak precision parameter ρ for instance.

Assuming that the decay rate is dominated by $C_{7,9,10}$, only taking linear terms into account as in [8,11], we arrive at

$$\begin{aligned}
\frac{dA_I^{\bar{0}-}}{dq^2}[B \to K^* l^+ l^-] &= \frac{\sum_{i=\{0,\pm\}} \mathrm{Re}[h_i^{V,0}(q^2)\Delta_i^{V,d-u}(q^2)]}{\sum_{i=\{0,\pm\}} [|h_i^{V,0}(q^2)|^2 + |h_i^{A}(q^2)|^2]} \\
&\quad + \mathcal{O}([\Delta_i^{V,d-u}(q^2)]^2), \\
\frac{dA_I^{\bar{0}-}}{dq^2}[B \to K l^+ l^-] &= \frac{\mathrm{Re}[h_T^{V,0}(q^2)\Delta_T^{V,d-u}(q^2)]}{|h_T^{V,0}(q^2)|^2 + |h_T^{A}(q^2)|^2} \\
&\quad + \mathcal{O}([\Delta_T^{V,d-u}(q^2)]^2), \\
a_I^{\bar{0}-}[B \to K^* \gamma] &= \frac{\sum_{i=\pm} \mathrm{Re}[h_i^{V,0}(0)\Delta_i^{V,d-u}(0)]}{\sum_{i=\pm} [|h_i^{V,0}(0)|^2 + |h_i^{A}(0)|^2]} \\
&\quad + \mathcal{O}([\Delta_i^{V,d-u}(0)]^2),
\end{aligned} \tag{18}$$

where $\Delta_i^{V,d-u}(q^2) \equiv (h_i^{V,d}(q^2) - h_i^{V,u}(q^2))$. It is worth mentioning that in the above formulas we have explicitly and implicitly neglected effects from phase space differences, isospin corrections to QCD quantities such as decay constants, and the light quark masses m_q. The latter are negligibly small and QCD corrections to isospin are known to be small: for example the pseudoscalar decay constant differs by roughly 0.5% between the neutral and charged case; see e.g. [19] for a computation in chiral perturbation theory. For the B mesons isospin effects are even smaller as $m_{B^0} - m_{B^\pm} = 0.32(6)$ MeV[8] [20], which is minuscule in comparison with the heavy quark scale $\bar{\Lambda} = m_B - m_b \simeq 600$ MeV. Thus in summary it is expected that isospin violation arising from the form factors will not reach the 1% level and we shall therefore not discuss them any further.

III. WEAK ANNIHILATION CONTRIBUTION

The weak annihilation (WA) process $B^- \to W^- \to K^{(*)-}$ is described by the "tree-level" operators $\mathcal{O}_{1,2}$ in a process as shown in Fig. 1 (left). By extension, the same name is also given to diagrams with the same arrangement of quark lines involving $\mathcal{O}_{3-6}$, though they arise from renormalization running and short distance penguins.

[8]The mass difference between the two neutral kaons is about 1% and relatively large and rather exceptional as a result of the Gell-Mann–Oakes–Renner relation $m_K^2 = -2(m_q + m_s) \times \langle\bar{q}q\rangle/f_K^2 + \cdots$.

The WA contribution to $B \to K^*\gamma/l^+l^-$ has previously been computed at $\mathcal{O}(\alpha_s)$ using LCSR at $q^2 = 0$ in [4,5] and in QCD factorization at $q^2 = 0$ [21] and for $q^2 > 0$ [11,14]. We extend the LCSR computation to higher q^2 including twist-3 corrections from the $h_\parallel$ DA relevant to the longitudinal K^* component which were neglected in [11,14].

A. Complete WA basis of dimension six operators at $\mathcal{O}(\alpha_s^0)$

We include all four quark operators $\bar{q}\Gamma_1 b\bar{s}\Gamma_2 q$ which potentially contribute at $\mathcal{O}(\alpha_s^0)$[9]:

$$\begin{aligned}
&O_1^{\mathrm{WA}} \equiv \bar{q}b\bar{s}q, \qquad O_2^{\mathrm{WA}} \equiv \bar{q}\gamma_5 b\bar{s}q, \\
&O_3^{\mathrm{WA}} \equiv \bar{q}b\bar{s}\gamma_5 q, \qquad O_4^{\mathrm{WA}} \equiv \bar{q}\gamma_5 b\bar{s}\gamma_5 q, \\
&O_5^{\mathrm{WA}} \equiv \bar{q}\gamma_\mu b\bar{s}\gamma^\mu q, \qquad O_6^{\mathrm{WA}} \equiv \bar{q}\gamma_\mu\gamma_5 b\bar{s}\gamma^\mu q, \\
&O_7^{\mathrm{WA}} \equiv \bar{q}\gamma_\mu b\bar{s}\gamma^\mu\gamma_5 q, \qquad O_8^{\mathrm{WA}} \equiv \bar{q}\gamma_\mu\gamma_5 b\bar{s}\gamma^\mu\gamma_5 q, \\
&O_9^{\mathrm{WA}} \equiv \bar{q}\sigma_{\mu\nu} b\bar{s}\sigma^{\mu\nu} q, \qquad O_{10}^{\mathrm{WA}} \equiv \bar{q}\sigma_{\mu\nu}\gamma_5 b\bar{s}\sigma^{\mu\nu} q,
\end{aligned} \tag{19}$$

parametrized by the effective Hamiltonian,

$$\mathcal{H}^{\mathrm{WA,q}} = -\frac{G_F}{\sqrt{2}}\lambda_t \sum_{i=1}^{10} a_i^q O_i^{\mathrm{WA}}, \tag{20}$$

where we suppress the q superscript on the operators O_i^{WA} throughout this work. Note that at $\mathcal{O}(\alpha_s)$, as well as for the ρ^0 for $\mathcal{O}(\alpha_s^0)$ to be discussed in Sec. VI A, the size of the basis doubles as octet combinations of the type $O_1^{\mathrm{WA,8}} \equiv (1/4)\bar{q}\lambda^a b\bar{s}\lambda^a q$ contribute as well.

1. Projection on SM basis (WA in SM)

In the SM the operators (19) obey minimal flavor symmetry (MFV) [22–26] and may be expressed in the form $\bar{q}\Gamma P_L b\bar{s}P_R\Gamma q$ (2). Since WA fixes the quark flavors and couples to only a single color structure, two independent combinations of SM WCs ($\Gamma \in \{\mathbf{1}, \gamma_\mu\}$) appear in each $B \to Mll$ process. For a $bq \to sq$ process, with $q = u, d$, the couplings are given by

$$\begin{aligned}
\text{SM: scalars: } a_1^q &= -a_2^q = a_3^q = -a_4^q = -2\left(\frac{C_5}{N_c} + C_6\right), \\
\text{vectors: } a_5^q &= -a_6^q = -a_7^q = a_8^q = \left(\frac{C_3}{N_c} + C_4\right) \\
&\quad - \delta_{qu}\frac{\lambda_u}{\lambda_t}\left(\frac{C_1}{N_c} + C_2\right), \\
\text{tensors: } a_9^q &= a_{10}^q = 0,
\end{aligned} \tag{21}$$

where a_{5-8} are the only ones which are nondegenerate in q and $N_c = 3$ denotes the number of colors. The role of $\mathcal{O}_{1,2}^u$

[9]As we shall see shortly there are further selection rules e.g. parity at $\mathcal{O}(\alpha_s)$ and Lorentz covariance to all orders for the K.

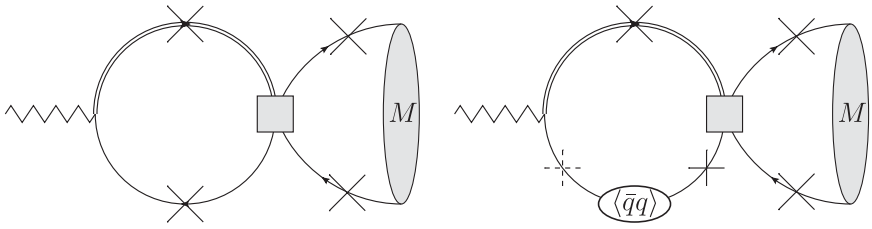

(a) Perturbative photon contributions. (b) OPE quark condensate contribution.

FIG. 2. Weak annihilation Feynman diagrams for $B \to M l^+ l^-$. The zigzag line is the B meson current insertion. Crosses mark possible photon insertions, although the contribution from the insertion at the dashed cross is zero.

in the SM is exceptional as there is no $\mathcal{O}^d_{1,2}$ counterpart. It corresponds to what we called UV isospin violation. In particular, radiation from all quarks in Fig. 1 (left) contributes to the isospin asymmetry. Therefore the isospin asymmetry in the SM is sensitive to three independent combinations of the four quark WCs C_{1-6}. Note, in the SM the effect is CKM suppressed in $b \to s$ contrary to $b \to d$. In the latter case the closeness of α_{CKM} to 90° leads to a suppression of the effect, to be discussed and exploited in further sections.

B. WA at leading order $\mathcal{O}(\alpha_s^0)$

The WA matrix element with uncontracted photon polarization tensor $\epsilon(q)_\rho$ reads

$$\begin{aligned}\mathcal{A}^{*\rho}|_{\mathrm{WA}} &= \langle X\gamma^*(\rho)|\bar{q}\Gamma_1 b\bar{s}\Gamma_2 q|B\rangle|_{\mathrm{WA}} \\ &= \underbrace{\langle X|\bar{s}\Gamma_2 q|0\rangle\langle\gamma^*(\rho)|\bar{q}\Gamma_1 b|B\rangle}_{\text{initial state radiation}} \\ &\quad + \underbrace{\langle X\gamma^*(\rho)|\bar{s}\Gamma_2 q|0\rangle\langle 0|\bar{q}\Gamma_1 b|B\rangle}_{\text{final state radiation}} + \mathcal{O}(\alpha_s).\end{aligned} \tag{22}$$

We shall call the first and second term initial (ISR) and final state radiation (FSR), respectively. The computation of these two contributions is performed, as previously stated, using LCSR and further details are deferred to Sec. III C. The computation is valid as long as q^2 is away from partonic and hadronic thresholds. This means that the ρ, ω resonance region has to be treated with care and that the computation is valid say 1–2 GeV^2 below the J/Ψ-resonance region. For $B \to V\gamma$ (partial) effects of the ρ, ω mesons are included into the photon DA [4,5,27]. For $q^2 > 1$ GeV^2 the corresponding leading twist effects are included in the quark condensate contributions and appear as $\langle\bar{q}q\rangle/q^2$ in the results. We refrain from using our computations between 0 and 1 GeV^2. A salient feature due to the resonance region is the appearance of an imaginary part. In the partonic computation this results from the photon emitted from the light valence quark of the B meson corresponding to the cross in the lower left of Fig. 2(a). In the hadronic picture this corresponds to the emission of $\rho, \omega, \ldots$ mesons and conversion into the photon; the analogous $\mathcal{O}_8$ case can be found in Ref. [6], Fig. 4 (left). In Fig. 3 we plot the $W(q^2)_T$ (12) matrix element for a_8 contribution (with $a_8 = a_8^u = a_8^d$), which illustrates the point made above.

We restrict ourselves to leading twist-2 and twist-3 DAs; cf. Appendix B 1. We neglect 3-particle DAs and quark mass corrections and thus the twist-3 2-particle DAs for the K^* may be written in terms of the twist-2 DAs via the so-called Wandzura-Wilczek relations [28]. We include the first two moments in the Gegenbauer expansion and thus have a total of four input parameters to the K^* in addition to the decay constants. The K DAs ϕ_P and ϕ_σ are also related [17], but here we use the asymptotic forms for reasons discussed in Appendix B.

In Table I the selection rules for the operators are depicted. It is apparent that selection rules are at work. We refer the reader to Sec. V A 2 where the WA selection rules in the factorization, cf. Eq. (22), approximation are discussed in some detail.

At this point, we wish to briefly discuss the issue of gauge invariance (GI) in the factorization approximation (22). At the level of the amplitude (22) electromagnetic GI, that is invariance under $\epsilon^*(q)_\mu \to \epsilon^*(q)_\mu + q_\mu$, implies:

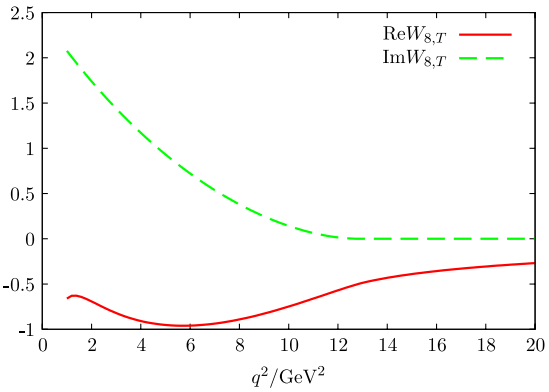

FIG. 3 (color online). WA contribution to $B \to K l l$ from the O_8^{WA} operator (19) as defined implicitly in (12). The imaginary part originates from the emission of $\rho, \omega, \ldots$ meson and conversion into the photon, which is analogous to the $\mathcal{O}_8$ contribution; cf. Fig. 4 (right) [6].

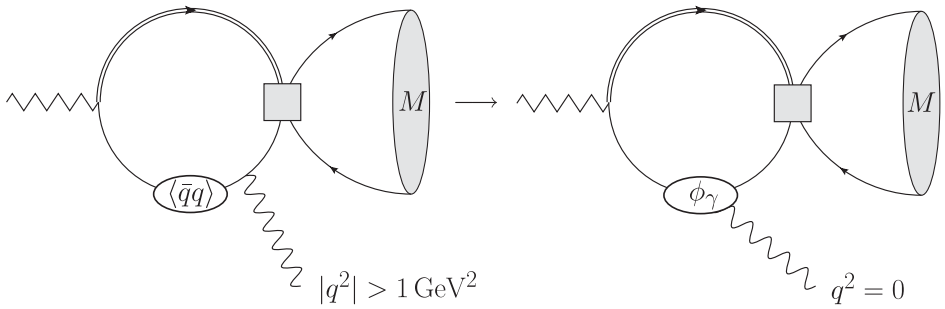

FIG. 4. Quark condensate contribution to be replaced by the photon DA contribution for $q^2 = 0$ case i.e. $B \to V\gamma$. The important point to realize is that both diagrams are gauge variant and produce, together with the other diagram in Fig. 2(b) (right), a fully gauge invariant result.

$$q_\rho \mathcal{A}^{*\rho}|_{\mathrm{WA}} = 0. \tag{23}$$

When the mesons are neutral this equation is satisfied for ISR and FSR separately. When the mesons are charged the two terms cancel each other when they are treated at the same level of approximation. From Table I we infer that for the K and K^* this is the case for $\mathcal{O}_{4,8}$ and $\mathcal{O}_{5,6}$, respectively. For the current-current operators $\mathcal{O}_{5\text{–}8}$ the final state radiation is, by virtue of the (axial) vector Ward identity (WI), equal to a contact term. This was implicitly used in [4,5] and analyzed in more clarity and detail in [29]. In the case $\mathcal{O}_4$ for the K there is ISR and FSR and no WI at hand which complicates the issue. More precisely this necessitates the same approximation scheme be used for both ISR and FSR as discussed and illustrated at length in Appendix D 1.

C. Light cone sum rules

We calculate initial state terms using the technique known as *light cone sum rules* [30,31] which originates from QCD sum rules [32,33] and the light-cone operator product expansion (LC-OPE). We extract the matrix elements required in (22) from the correlation function

$$\Pi(q^2, p_B^2) = i \int d^4x e^{-ip_B\cdot x} \langle \gamma^*(q) M(p)|T\{J_B(x)\mathcal{O}(0)\}|0\rangle, \tag{24}$$

where

$$J_B = im_b \bar{b}\gamma_5 q, \qquad \langle \bar{B}|J_B(0)|0\rangle = m_B^2 f_B \tag{25}$$

is the interpolating current for the B meson. By application of Cauchy's theorem we can express this matrix element as

TABLE I. Operators contributing to WA. The acronyms t. and cov. stand for twist and for covariance, respectively, and χ odd/even for odd/even chirality. Furthermore note the following: (i) (I,F) radiation from inital (I) and or final (F) state; (F_c) corresponds solely to a (local) contact term contribution from final state radiation. The latter are then necessarily to all orders in the twist expansion. (ii) (✓) contribution expected in initial and final state; (iii) (✗) no contribution due to parity invariance of strong interactions in the factorization approximation $\mathcal{O}(\alpha_s^0)$; (iv) (✗) no contribution, in any order of α_s and twist, as chirality necessitates a Levi-Civita tensor structure for which there are not enough independent vectors for contraction (relevant for pseudscalar final state). We should also note that $g_\perp^{(v,a)}$ and $h_\parallel^{(s,t)}$ are related to $\phi_\perp$ an $\phi_\parallel$ by Wandzura-Wilczek type relations [28]. At our level of approximation, $m_q = 0$ and no 3-particle DA, this corresponds to Eqs. (4.15/16) and (3.21/22) [28], respectively. See also Appendix B 1 for further comments. This means that when $g_\perp^{(v,a)}$ and $h_\parallel^{(s,t)}$ are computed $\phi_\parallel$ and $\phi_\perp$ are needed to render the computation gauge invariant at the relevant $\mathcal{O}(m_V)$ level. Thus for (I, F_c), contrary to (F) itself, it is not possible to properly distinguish between twist 2 and 3 which is reflected in the table.

			Operator O_n^{WA}									
		Twist	1	2	3	4	5	6	7	8	9	10
$B \to K$	cov. (α_s^0)		✗	✗	✗		✗	✗	✗		✗	✗
	χ even (ϕ_K)	2								I, F_c		
	χ odd ($\phi_{P,\sigma}$)	3				I,F						
	cov. (α_s^n, $n > 0$)		✓	✗	✗	✓	✓	✗	✗	✓	✓	✗
$B \to K^*$	cov. (α_s^0)		✗		✗				✗	✗		
	χ even ($\phi_\parallel$)	2					I	I, F_c				
	χ even ($g_\perp^{(v)}$, $g_\perp^{(a)}$)	3					I	I, F_c				
	χ odd ($\phi_\perp$)	2		F		F					I	I
	χ odd ($h_\parallel^{(t)}$, $h_\parallel^{(s)}$)	3		F								I
	cov. (α_s^n, $n > 0$)		✓	✓	✓	✓	✓	✓	✓	✓	✓	✓

$$\Pi(q^2, p_B^2) = \frac{m_B^2 f_B}{m_B^2 - p_B^2}\langle\gamma^*(q)M(p)|\mathcal{O}(0)|B(p_B)\rangle + \frac{1}{2\pi i}\oint_{\Gamma_{\rm NP}} \frac{ds}{s - p_B^2}\Pi(q^2, s), \quad (26)$$

where the integration contour $\Gamma_{\rm NP}$ separates the pole at $p_B^2 = m_B^2$ of the desired matrix element $\langle\gamma^*(q)M(p)|\mathcal{O}(0)|B(p_B)\rangle$ from all other poles and branch cuts. The matrix element in (24) may also be calculated within the LC-OPE, and after applying Cauchy's theorem to the LC-OPE result we get that, at large spacelike p_B^2,

$$\Pi(q^2, p_B^2) = \frac{1}{2\pi i}\oint_{\Gamma} \frac{ds}{s - p_B^2}\Pi^{\text{LC-OPE}}(q^2, s), \quad (27)$$

where the contour Γ encloses all poles and branch cuts of this function. The sum rule is obtained by equating the two representations (26) and (27) and making the approximation, known as semiglobal quark-hadron duality, $\Pi(q^2, s) = \Pi^{\text{LC-OPE}}(q^2, s)$ under the integral in (26). A Borel transformation is also applied to reduce the sensitivity to the duality threshold, which in this case only requires the relation

$$B_{p_B^2 \to M^2}\left[\frac{1}{x - p_B^2}\right] = \frac{e^{-x/M^2}}{M^2}, \quad (28)$$

yielding the final form of the sum rule

$$\begin{aligned}\langle\gamma^*(q)M(p)|\mathcal{O}(0)|B(p_B)\rangle &= \frac{1}{f_B m_B^2}\frac{1}{2\pi i}\int_{\Gamma\setminus\Gamma_{\rm NP}} ds \exp\left(\frac{m_B^2 - s}{M^2}\right)\Pi_P(q^2, s) \\ &\equiv \frac{1}{f_B m_B^2}\int_{\text{cut}}^{s_0} ds \exp\left(\frac{m_B^2 - s}{M^2}\right)\rho(q^2, s), \end{aligned} \quad (29)$$

where $\Gamma\setminus\Gamma_{\rm NP}$ is the difference between the integration contours in (26) and (27). The resulting contour will lie along either side of the real line and thus the final sum rule may be expressed in terms of an integral over the density function ρ on the real line from the lowest perturbative state mass (m_b^2 here) to the duality threshold s_0. In the full theory the lowest lying multiparticle state coupling to the current J_B occurs at $(m_B + 2m_\pi)^2$, and s_0 is an effective parameter which is adjusted so that the continuum contribution matches that of QCD. In practice this means that one expects $\sim(m_B + 2m_\pi)^2 \simeq 30.9\ \text{GeV}^2 < s_0 < (m_B + m_\rho)^2 \simeq 36.6\ \text{GeV}^2$ with s_0 somewhat closer to the upper boundary as the other case is α_s suppressed.

D. WA results

Due to our choice of basis for the four quark operators, it is convenient to present our results for the K^* in the following linear combinations, which is basically the helicity basis,

$$\begin{aligned} W_V^q(q^2) &= W_1^q(q^2) = \frac{1}{\sqrt{2}}(W_-(q^2) + W_+(q^2)), \\ W_A^q(q^2) &= cW_2^q(q^2) = \frac{1}{\sqrt{2}}(W_-(q^2) - W_+(q^2)), \\ W_0^q(q^2) &= aW_2^q(q^2) + bW_3^q(q^2), \end{aligned} \quad (30)$$

where V and A are the PC and PV transverse decay modes, and the constants a, b, c are defined in (5) and (6). The matrix elements $W_\iota^q(q^2)$, with $\iota \in \{T, V, A, 0\}$, are decomposed as follows:

$$W_\iota^q(q^2) = \sum_{j=1}^{10} a_j^q[F_{j,\iota}^q(q^2) + I_{j,\iota}^q(q^2)]. \quad (31)$$

The functions I and F stand for ISR and FSR and are further parametrized as

$$\begin{aligned} I_{j,\iota}^q(q^2) &= \frac{1}{f_B m_B^2}\left(\langle\bar{q}q\rangle \exp\left(\frac{m_B^2 - m_b^2}{M_{\rm WA}^2}\right)V_{j,\iota}^q(q^2) + \int_{m_b^2}^{s_0} ds \exp\left(\frac{m_B^2 - s}{M_{\rm WA}^2}\right)\rho_{j,\iota}^q(q^2, s)\right), \\ F_{j,i}^q(q^2) &= f_{K^*}^\perp f_B\left(\frac{m_B}{m_b}\right)^2 \int_0^1 f_{j,i}^q(q^2, u)du, \end{aligned} \quad (32)$$

for the K^* meson with $i \in \{V, A, 0\}$ and

$$F_{j,T}^q(q^2) = \mu_K^2 f_B^{\text{wti}}\left(\frac{m_B}{m_b}\right)^2 \int_0^1 f_{j,T}^q(q^2, u)du, \quad (33)$$

for the K meson. We take the Borel parameter $M_{\rm WA}^2 = 9(2)\ \text{GeV}$ to be the same for all WA processes, although this is not strictly necessary since in principle the results should be independent of it within a reasonable range, and a calculation involving higher twist and/or α_s corrections would usually extremize the result with respect to the Borel parameter. We take the duality threshold as $s_0 = 35(1)\ \text{GeV}^2$. The quoted uncertainty in the Borel parameter and the duality threshold are the ranges over which we vary them to provide an estimate of the error of the LCSR method. The use of f_B^{wti} in $F_{j,T}^q(q^2)$ arises because this is the only case where both physical initial and final state radiation contribute, and thus we must choose f_B^{wti} as the sum rule approximation of f_B which corresponds to our approximation of the initial state radiation contribution in order to fulfil the Ward identity:

$$f_B^{\text{wti}} = \frac{m_b^2}{f_B m_B^4}\left[\frac{3}{8\pi^2}\int_{m_b^2}^{s_0} \exp\left(\frac{m_B^2 - s}{M_{\rm WA}^2}\right)\frac{(s - m_b^2)^2}{s}ds - m_b\langle\bar{q}q\rangle \exp\left(\frac{m_B^2 - m_b^2}{M_{\rm WA}^2}\right)\right]. \quad (34)$$

This procedure is discussed further in Appendix D 1. The occurrence of f_B in $I_{j,\iota}^q$ is evaluated using the leading order sum rule including the $\langle\bar{q}q\rangle$ and $\langle\bar{q}Gq\rangle$ condensates [34]

$$(m_B^2 f_B)^2 = m_b^2 \exp\left(\frac{m_B^2 - m_b^2}{M_{f_B}^2}\right)\left(\frac{3}{8\pi^2}\int_{m_b^2}^{s_0} \exp\left(\frac{m_b^2 - s}{M_{f_B}^2}\right) \times \frac{(s-m_b^2)^2}{s} ds - m_b\langle\bar{q}q\rangle_\mu - \frac{m_b}{2M_{f_B}^2}\left(1 - \frac{m_b^2}{2M_{f_B}^2}\right)\langle\bar{q}Gq\rangle_\mu\right), \quad (35)$$

where $M_{f_B}^2 = 5.0(5)$ GeV is used. Quark condensates are taken at $\mu = 1$ GeV to be $\langle\bar{q}q\rangle = (-0.24(1)\ \text{GeV})^3$ and $\langle\bar{q}Gq\rangle = (0.8(1)\ \text{GeV})^2\,\langle\bar{q}q\rangle$ which are the same values as in [6]. The occurrence of f_B in $F_{j,i}^q$ is taken from lattice data as $f_B = 191(5)$ MeV [35,36]. Formulas for DAs of the external light mesons are given in Appendix B 1. Formulas for all functions appearing on the right-hand side of (33) are given in Appendix F 3.

E. WA at $q^2 = 0$—photon DA replaces some $\langle\bar{q}q\rangle$ contributions

The local OPE for $q^2 \neq 0$, used in diagrams like Fig. 4 (left) for the light quark propagator originating from the J_B current, results in terms like $Q_q\langle\bar{q}q\rangle/q^2$; cf. (33) which cannot be a good description at $q^2 = 0$. The resolution to this apparent paradox is to replace the this term by the photon DA[10] as sketched in Fig. 4.

This type of computation has been completed in [4,5] for the vector-current operators $\mathcal{O}_{5-8}^{\text{WA}}$. Our calculation, essentially, extends this to the complete four quark operator basis (19). Aspects of GI and contact terms as well as a difference in the $(Q_b - Q_q)\langle\bar{q}q\rangle$ contribution with reference [5] are discussed in Appendix D 3 c. We note that the latter are small and have not been included in [4].

Our results are given, such that $I_{j,i}^q(q^2) \to I_{j,i}^q|_\gamma$ in (33),

$$I_{j,i}^q|_\gamma = \frac{1}{f_B m_B^2}\left(\langle\bar{q}q\rangle \exp\left(\frac{m_B^2 - m_b^2}{M_{\text{WA}}^2}\right)V_{j,i}^{q,\gamma} + \int_{m_b^2}^{s_0} ds \exp\left(\frac{m_B^2 - s}{M_{\text{WA}}^2}\right)\rho_{j,i}^{q,\gamma}(s)\right), \quad (36)$$

where we reuse our result from $q^2 \neq 0$ for the density via

$$\rho_{j,i}^{q,\gamma}(s) = \rho_{j,i}^q(0,s) + \langle\bar{q}q\rangle\tilde{\rho}_{j,i}^{q,\gamma}(s), \quad (37)$$

and $V_{j,i}^{q,\gamma}$ and $\tilde{\rho}_{j,i}^{q,\gamma}(s)$ are given in Appendix F 6 b.

IV. QUARK LOOP SPECTATOR SCATTERING

The quark loop spectator scattering (QLSS) topology parallels the $\mathcal{O}_8$ contribution as can be seen from Fig. 1. We would expect an LCSR computation of this contribution to include some long distance (LD) contributions, in analogy with the $\mathcal{O}_8$ contribution (intermediate multiparticle states with quantum numbers $(\bar{s}q)_{J^P=0^\pm}$; cf. Fig. 4 (left) in [6]. On a computational level though spectator scattering differs from the analogous $\mathcal{O}_8$ computation by the additional nested quark loop which makes the computation rather involved; especially in view of the fact that we further expect a nontrivial analytic structure including anomalous thresholds [6]. Thus the evaluation of this contribution with LCSR is beyond the scope of this paper. We therefore resort to QCDF where it would seem that these LD contributions are, at least at leading order in $\mathcal{O}(\alpha_s)$, absent. In QCDF, QLSS has been computed previously for the $B \to K^* l^+ l^-$ [11] and for the $B \to K^*\gamma$ case in [8]. We extend these computations by including a complete basis of four quark operators. Elements of GI are discussed in Appendix D 2.

A. Complete QLSS basis of dimension six operators at $\mathcal{O}(\alpha_s)$

We now turn to the discussion of the relevant operators contributing to QLSS. The vectorial coupling of the gluon in Fig. 5 imposes efficient selection rules such that only 4 out of the 10 operator types, as listed in Eq. (19), can contribute:

$$Q_{1L(R)}^{4f} \equiv \frac{1}{4}\bar{f}\lambda^a\gamma_\mu f\bar{s}_{L(R)}\lambda^a\gamma^\mu b,$$
$$Q_{2L(R)}^{4f} \equiv \frac{1}{4}\bar{f}\lambda^a\sigma_{\mu\nu} f\bar{s}_{L(R)}\lambda^a\sigma_{\mu\nu} b. \quad (38)$$

Quark flavors and color matrices are arranged, differently from Eq. (19), in a way that is convenient for the QLSS computation. Since we shall set the light quark masses to zero the light flavor u, d, s are effectively degenerate and it proves economic to introduce the $SU(3)_F$ singlet operator

$$Q_{xL(R)}^{4SU(3)_F} \equiv (Q_{xL(R)}^{4u} + Q_{xL(R)}^{4d} + Q_{xL(R)}^{4s}), \quad x = 1,2. \quad (39)$$

Finally, the relevant effective Hamiltonian for QLSS becomes

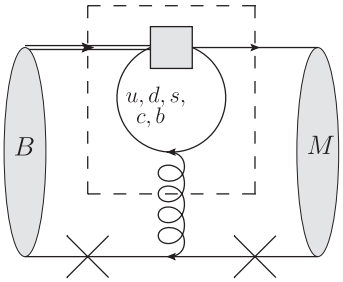

FIG. 5. Hard gluon scattering through a charm loop. Isospin symmetry violating photon insertions are indicated by crosses. The segment in the dashed box is computed first without the DAs attached to simplify the calculation.

[10]One might also pose the problem the other way around, starting from the photon DA at $q^2 = 0$ and asking how the latter is to be modified when $q^2 > 0$. The primary effect can be covered by the quark condensate contribution.

$$\mathcal{H}^{\mathrm{QLSS}} = -\frac{G_F}{\sqrt{2}}\lambda_t \sum_{x,\chi,f} s^f_{x\chi} Q^{4f}_{x\chi}, \qquad x = 1, 2, \quad \chi = L, R, \quad f = SU(3)_F, c, b, \tag{40}$$

with $s^f_{x\chi}$ being WCs. The somewhat baroque sum over the indices x, χ, f, which amounts to 12 operators at this stage, will prove economic in the end. We would like to stress that this basis in linearly independent, though not orthogonal, to the WA basis (19). This is the case as in WA the flavor f is, modulo a few exceptions, fixed by the spectator flavor and since in QLSS f is either c, b, or the sum of light flavors linear independence follows.

B. QLSS results

The computation of QLSS may be broken up into two stages: first, the intermediate process shown in the dashed box of Fig. 5 is computed, and second, the results of this computation are combined with the remainder of the diagram in Fig. 5.

To start, the intermediate process can be written, by virtue of Lorentz covariance, as

$$\begin{aligned} a^\mu &= \langle sg(r,\mu)|H_{\mathrm{eff}}|b\rangle \\ &= \sum_{i=L,R} [K^\mu_{1,i} F_{1,i}(r^2) + K^\mu_{2,i} F_{2,i}(r^2)], \end{aligned} \tag{41}$$

where r is the gluon momentum and μ is the gluon polarization index. The two tensor structures

$$\begin{aligned} K^\mu_{1,(L,R)} &= \frac{r^\mu \not{r} - r^2\gamma^\mu}{r^2} P_{L,R}, \\ K^\mu_{2,(L,R)} &= \frac{r^\mu - \not{r}\gamma^\mu}{r^2} P_{L,R}, \end{aligned} \tag{42}$$

are the only ones allowed by gauge invariance $r \cdot a = 0$.

In our parametrization (40), the functions $F_{x,\chi}$ are given by

$$F_{x,\chi} = s^{SU(3)}_{x,\chi} H_x(s,0) + s^c_{x,\chi} H_x(s,m_c) + s^b_{x,\chi} H_x(s,b), \tag{43}$$

and it is clear that $F_2 \sim m_f$, where f is the flavor of the quark running in the loop, by virtue of dimensional analysis. This means that $s^{SU(3)}_{2L(R)}$ is heavily suppressed and not present in our approximation where we set the light quark masses to zero and so only 10 of the 12 operators in (40) effectively contribute. The functions H_x result from loop integrals for the vector and tensor currents and are given by

$$\begin{aligned} H_1(s,m) &= -\frac{1}{96\pi^2}[9h(s,m) + 4], \\ H_2(s,m) &= -\frac{m}{4\pi^2} B_0(s,m^2,m^2), \end{aligned} \tag{44}$$

where the function $h(s,m_q)$ is the vacuum polarization (this form from [11]), with $z \equiv \frac{4m_q^2}{s}$,

$$\begin{aligned} h(s,m_q) = &-\frac{4}{9}\left(\log\frac{m_q^2}{\mu^2} - \frac{2}{3} - z\right) - \frac{4}{9}(2+z)\sqrt{|z-1|} \\ &\times \begin{cases} \arctan\frac{1}{\sqrt{z-1}} & z > 1 \\ \log\frac{1+\sqrt{1-z}}{\sqrt{z}} - \frac{i\pi}{2} & z \le 1 \end{cases}, \end{aligned}$$

$$B_0(s,m_q^2,m_q^2) = 2 - \log\frac{m_q^2}{\mu^2} + 2\frac{\frac{9}{4}h(s,m_q) + \log\frac{m_q^2}{\mu^2} - \frac{2}{3} - z}{2+z}, \tag{45}$$

which can be found in any standard textbook on quantum field theory.

Before quoting the full result let us detail a few points of the computation. The B meson DA used is [37,38]

$$\begin{aligned} &\langle 0|\bar{q}_\alpha(x)[x,0]b_\beta(0)|B\rangle \\ &= \frac{-if_B m_B}{4}\int_0^\infty dl_+ e^{-il_+x_-/2} \\ &\quad\times\left[\frac{1+\not{v}}{2}\{\phi_+(l_+)\not{n}_+ + \phi_-(l_+)\not{n}_-\}\gamma_5\right]_{\beta\alpha}. \end{aligned} \tag{46}$$

Definitions of the vectors and various terms involved along with a more complete version of this formula are given in Appendix B 3; however, this version of the formula contains all terms involved in our computation of the diagram in Fig. 5.

To this end let us mention that corrections of $\mathcal{O}(q^2/m_B^2)$ which come from neglecting the l_- direction of the light quark in the B-meson DA and aspects of the B-meson DA including the transverse derivative are discussed in Appendix B 3 a. Since we have restricted ourselves to $q^2 < 4m_c^2$, using the B-meson light-cone DA (46) seems reasonable. A more interesting question is to what extent the shape of the q^2 distribution is accurate or trustworthy.

We write the results directly in the helicity basis, $S_{\pm,0}$, whose transformation to the $\mathcal{T}_{1,2,3}$ basis is given in (5), for the K^* meson:

$$\begin{aligned} S^q_-(q^2) = \sqrt{2}Q_q\frac{C_F}{N_c}\frac{16\pi^3\alpha_s f_B m_B}{m_b}\int_0^1 du\Big(&F_{1,L}(\bar{u}m_B^2 + uq^2) \\ &- \frac{1}{m_B}F_{2,R}(\bar{u}m_B^2 + uq^2))\Big[\frac{f^\perp_{K^*}\phi_\perp(u)}{\bar{u}m_B^2 + uq^2} \\ &- \frac{f_{K^*}m_{K^*}}{2\lambda_+(q^2)(m_B^2 - q^2)}\left(g^{(v)}_\perp(u) - \frac{g^{(a)'}_\perp(u)}{4}\right)\Big] \\ &- \frac{F_{2,R}(\bar{u}m_B^2 + uq^2)}{m_B}\Big[\frac{f^\perp_{K^*}\phi_\perp(u)u(m_B^2 - q^2)}{2(\bar{u}m_B^2 + uq^2)^2} \\ &- \frac{f_{K^*}m_{K^*}}{2\lambda_+(q^2)(m_B^2 - q^2)}\frac{g^{(a)}_\perp(u)}{4\bar{u}}\Big], \end{aligned} \tag{47}$$

$$S^q_+(q^2) = (L \leftrightarrow R), \tag{48}$$

$$d \cdot S_0^{q,V}(q^2) = -Q_q \frac{C_F}{N_c} \frac{32\pi^3 \alpha_s f_B m_B}{m_b} \frac{f_{K^*} m_{K^*}}{\lambda_-(q^2)(m_B^2 - q^2)} \times \int_0^1 du \phi_\parallel(u) \Big[F_{1,A}(\bar{u} m_B^2 + u q^2) + \frac{m_B}{\bar{u}(m_B^2 - q^2)} F_{2,A}(\bar{u} m_B^2 + u q^2) \Big], \quad (49)$$

with $d \equiv -\frac{\sqrt{2} m_B m_V}{\sqrt{q^2} E}$. For the K meson we get

$$S_T^q(q^2) = -Q_q \frac{C_F}{N_c} \frac{(m_B + m_K) 16\pi^3 \alpha_s f_B f_K}{m_B m_b \lambda_-(q^2)} \int_0^1 du \phi_K(u) \times \Big[F_{1,V}(\bar{u} m_B^2 + u q^2) - \frac{m_B}{\bar{u}(m_B^2 - q^2)} F_{2,V}(\bar{u} m_B^2 + u q^2) \Big], \quad (50)$$

where we have used $F_{1,V(A)}(s) \equiv F_{1,R}(s) \pm F_{1,L}(s)$ for the sake of compact notation. At this point we would like to specify some details of the computation. There are two types of terms that appear:

$$X_1 = \int_0^\infty dl_+ \phi_\pm(l_+) H_1(l_+), \quad (51)$$

$$X_2 = \int_0^\infty dl_+ \phi_\pm(l_+) \frac{H_2(l_+)}{l_+ - q^2/m_B - i\epsilon}, \quad (52)$$

where the kernels $H(l_+)$ are smooth and the denominator in the second term originates from a propagator which in turn cancels for the type one term. The following recipe is applied:

$$X_1 \to \Big(\int_0^\infty dl_+ \phi_\pm(l_+) \Big) H_1(0) = \text{constant} \cdot H_1(0), \quad (53)$$

$$X_2 \to \Big(\int_0^\infty dl_+ \frac{\phi_\pm(l_+)}{l_+ - q^2/m_B - i\epsilon} \Big) H_2(\bar{l}_+) = \frac{H_2(\bar{l}_+)}{\lambda_\pm(q^2)}, \quad (54)$$

where $\bar{l}_+ \equiv q^2/m_B$, $1/\lambda_\pm(q^2)$ is further detailed in Appendix B 3. The term in (47) proportional to $\phi_\perp(u)$ is of the first type and all others are of the second type as can be seen in Eqs. (47)–(50). The equation (47) disagrees with Eq. (24) in Ref. [11] by a factor of 2 in the $g_\perp^{(v,a)}$ term but agrees with the result in [8] in the limit $q^2 \to 0$. The definitions of the B-meson moment functions $\lambda_\pm(q^2)$ and the K and K^* DA functions are given in Appendix B 1. An important remark is that the Wandzura-Wilczek type equations of motions ($m_s = 0$) (B5) for the K^* have been used.

We note that we have included the K^* DAs $\phi_\parallel$, $\phi_\perp$, and $g_\perp^{(v,a)}$. In light of Table I it might seem that we should have also included $h_\parallel^{(s,t)}$; however, here we are considering the leading $1/m_B$ term, so it is the $g_\perp^{(v,a)}$ term which requires justification. It is included because the $\phi_\perp$ coefficient does not contain a $1/\lambda_\pm$ factor as it might, and therefore occurs at the same power of $1/m_B$ as $g_\perp^{(v,a)}$. Since the $\phi_\parallel$ term comes with a $1/\lambda_\pm$ factor, an $h_\parallel^{(s,t)}$ term would be $\mathcal{O}(1/m_B)$ suppressed so we neglect it.

It should be noted that there is an endpoint (infrared) divergence proportional to $F_{2,(R,L)}(0)$ in $S_\pm(q^2 \to 0)$ arising from the $\bar{u} \to 0$ integration region which is of the same type as $\mathcal{O}_8$. There are three ways to deal with it: (i) only use it for $q^2 > 0$ in which case an IR sensitivity remains; (ii) employ the cutoff model [8,11], or (iii) perform a local subtraction to render the QCDF result finite and then use the IR finite result from LCSR [6] to compensate. We choose option (iii). To get an infrared finite result we write

$$F_{2,i}(r^2) = [F_{2,i}(0)]_{\text{LCSR}} + [F_{2,i}(r^2) - F_{2,i}(0)]_{\text{QCDF}}, \quad (55)$$

where the contribution of each term in square brackets to $B \to K^{(*)} ll$ is computed as indicated in the subscript. The LCSR term is therefore a local operator and the $\mathcal{O}_8$ result [6] applies, and the QCDF term vanishes for $r^2 \to 0$ restoring IR finiteness of (47) at $q^2 = 0$. The slightly inconsistent feature is that the LCSR computation contains LD contributions which are not present at this level of approximation in QCDF as explained at the very beginning of this section.

At last we wish to add some remarks about imaginary parts. In the partonic picture the charm quark can go on shell, whose importance has been emphasised in [39], as is visible from the formulas. Fortunately the momentum that enters the charm loop depends on the momentum fraction of the light meson as $\bar{u} m_B^2 + u q^2$ and is sufficiently smeared out that a partonic description seems tolerable. Conversely the interpretation of such effects in the real hadronic world would be a $D\bar{D}$ threshold for which is, compared to a single resonance, sufficiently tame to be described by partons within our quoted uncertainties.

C. Projection on SM basis (QLSS in the SM)

In the SM using naïve dimensional regularization we have [11]

$$\text{SM: } F_{1,L}(s) = \frac{3}{32\pi^2} \Big[h(s, m_c) \Big(-\frac{\lambda_c}{\lambda_t} C_2 + C_4 + C_6 \Big) + h(s, m_b)(C_3 + C_4 + C_6) + h(s, 0) \Big(-\frac{\lambda_u}{\lambda_t} C_2 + C_3 + 3C_4 + 3C_6 \Big) - \frac{8}{27}(C_3 - C_5 - 15C_6) \Big],$$
$$F_{1,R}(s) = 0, \quad (56)$$

$$F_{2,R}(s) = \frac{m_b}{8\pi^2}(C_8^{\text{eff}} - C_8),$$
$$F_{2,L}(s) = \frac{m_s}{8\pi^2}(C_8^{\text{eff}} - C_8) \to 0 + \mathcal{O}(m_s). \quad (57)$$

The MFV symmetry of the SM implies that $F_{1,R} = 0$. The operators $Q_{2\chi}^{4f}$ are not present in the SM in $d = 4$ but give contributions in the spirit of evanescent operators in naive dimensional regularization. They render the effective WC C_8^{eff} scheme independent [40,41]. It is worth pointing out that in the SM the charm loop dominates as it originates from $\mathcal{O}_2^c$ which is proportional to a large WC $C_2 \approx 1$ and is not CKM suppressed. All other WCs are small as can be seen in Table VIII.

V. ISOSPIN ASYMMETRIES $B \to K^{(*)}\gamma/ll$

We shall first make a few generic remarks on selection rules and related issues in Sec. V A, reflect on the q^2 behavior from various viewpoints in Sec. V B and then discuss the isospin asymmetries of $B \to K^{(*)}$ in the SM in Sec. V C. Discussion of isospin asymmetry beyond the SM is deferred to Sec. VII.

A. Generic remarks on selection rules

In total there are 32 operators potentially contributing to the isospin asymmetry at the level of $\mathcal{O}(\alpha_s)$ correction we are considering. Schematically they decompose as follows:

$$32 = 2_{\mathcal{O}_8^{(\prime)}(2)} + 20_{\text{WA}(19)} + 10_{\text{QLSS}(38)} \tag{58}$$

where the prime denotes $V + A$ chirality as previously defined. We note that $\mathcal{O}_{2L(R)}^{SU(3)}$ gives no contribution in the limit of all light quark masses set to zero since it is proportional to m_f as pointed out in Sec. IV B. The number 32 will be reduced further for the K and K^* below.

We shall discuss below general selection rules for the K in Sec. V A 1 before discussing more specific selection rules for WA in the factorization approximation in Sec. V A 2 and then comment on the (non)relation between the K and $K_\parallel^*$ amplitude in Sec. V A 3.

1. Parity and angular momentum selection rule for K

For the K there is a parity selection rule. We note that

$$B[0^-] \to K[0^-](\gamma^*[1^-] \to l^+l^-[1^-]) \Rightarrow p \text{ wave; i.e. } l = 1, \tag{59}$$

where $[J^P]$ denotes total angular momentum and parity, respectively, and l is the spatial angular momentum of the decay product. Thus the left-hand side (LHS) and right-hand side (RHS) of the decay have odd parity and the decay is therefore induced by parity conserving (PC) operators. This means that operators of the type $\bar{s}\ldots\gamma_5 q\bar{q}\ldots b$, $\bar{s}\ldots q\bar{q}\ldots\gamma_5 b$, where $\ldots$ stands for strings of γ matrices not including γ_5, do not contribute. This reduces the number of operators for the K (by a factor of 2) down to $1_{\mathcal{O}_8}$ and 5_{QLSS} using the notation of Eq. (58). It seems worthwhile to emphasize that the selection rules are generic. In the next subsection we are going to discuss WA in the factorization approximation (22) for which there are additional selection rules.

2. WA selection rules in the factorization approximation

In the factorization approximation, automatic at $\mathcal{O}(\alpha_s^0)$ we are considering for WA, there are more stringent selection rules. They come from the fact that the Dirac traces of the B meson and the K^* meson close separately, and so γ_5 matrices cannot be commuted from one end to the other. Selection rules arising due to this effect derive from the matrix element which does not emit the photon, i.e. the initial state in a FSR diagram and vice versa. We call the matrix element imposing the selection rule the local matrix element (LME) since it is the matrix element of an external state coupling to a local operator.

The $O_{9,10}^{\text{WA}}$ operators must be considered separately: in the case of the K they do not contribute in the factorization approximation since the LME will be a pseudoscalar coupling to an antisymmetric tensor operator and no such tensor can be formed from a single vector. On the other hand in the case of the K^* both operators contribute since an antisymmetric tensor $p^{[\mu}\eta^{\nu]}$ is available and by $\epsilon^{\mu\nu\rho\sigma}\sigma_{\rho\sigma} = 2i\sigma^{\mu\nu}\gamma_5$ the two different parities are trivially related. For $O_{1\ldots8}^{\text{WA}}$, the LME will impose a selection rule since the external state will only couple to a local scalar or vector operator of the correct parity. This reduces the number of applicable operators by a factor of 2. If this is further combined with the global parity constraint for the K case so for $B \to Kll$ only 2 of the 8 operators remain.

Combining these rules we expect $8/2 + 2 = 6$ and $8/2/2 + 0 = 2$ operators to contribute to WA in the factorization approximation for the K^* and the K, respectively. This is indeed the case as the reader may verify from Table I or Table II. With respect to the latter table note that we have not taken into account the degeneracy in $q = u$, d in the previous wording and this is why the numbers are 12 and 4 rather than 6 and 2.

3. On the (non)relation between $K_\parallel^*$ and K

There is some conventional wisdom, throughout the literature, that the longitudinal polarization of the K^* corresponds to that of the K. We shall argue that this is true in the SM at leading twist and falls apart thereafter.

The main points follow from the fact the longitudinal polarization can be decomposed as follows:

TABLE II. Operators contributing to isospin in $B \to K^{(*)}ll$. In square brackets we denote the number of operators that are present in the SM for the respective channel. In this counting we neglect C_8' as $C_8'/C_8 \simeq m_s/m_b$.

	$C_8^{(\prime)}$	WA	Eq. (19)	QLSS	Eq. (19)	Total
K^*	2[1]	12[3]	$a_{2,4,5,6,9,10}^q$	10[3]	all no $i = 2$, $f = SU(3)$	24[7]
K	1[1]	4[3]	$a_{4,8}^q$	5[3]	idem no $\chi = A$	10[7]

$$\eta(0)^\mu \equiv \eta_\parallel^\mu = \frac{p^\mu}{m_{K^*}} + (q^\mu \mathcal{O}(m_{K^*}) + p^\mu \mathcal{O}(m_{K^*})). \quad (60)$$

Thus at leading twist, $m_{K^*}^2 = 0$, we see that $\eta_\parallel^\mu$ and p^μ play the same role. Since the former is a pseudovector and the latter is a vector we also see that they couple to opposite parity: K only couples to PC operators, as pointed out in Sec. VA 1, and $K_\parallel^*$ only couples to PV operators. Due to the V-A interactions in the SM there is a link between the corresponding WCs and this makes it clear that the statement at the beginning of this subsection is true.

On the other hand it is then also clear that the presence of right-handed currents, i.e. $V + A$ interactions, invalidates the statement. Furthermore the $\mathcal{O}(m_{K^*})$ corrections, by virtue of (60), are going to bring in new structures as well and we can therefore not expect the correspondence to hold at twist 4. Examples include the following:

(i) *Working example at leading twist:* From the formulas in Appendix F 3 one infers that the parity related O_6^{WA} and O_8^{WA} contributions are (indeed) proportional to each other $[a_6(K_\parallel^*) \sim a_8(K)]$.

(ii) *Nonworking example at nonleading twist:* From Table I we infer that O_4^{WA} couples to ISR for the K but the corresponding PV operator O_2^{WA} does not for the K^*.

The latter point deserves some further explanation. Should there be an extension of the correspondence from $\phi_{p,\sigma}$ to K^* amplitudes then it would be through the same chirality DA and necessarily involve the chiral-odd DA $\phi_\perp$ and $h_\parallel^{(s,t)}$ in Table I. That this cannot hold can also be seen as follows: the chiral-odd K^* 2-particle DAs included in our calculation have independent coefficients to the chiral-even ones. In the case of the K this is not so: the chiral-odd DAs are fully constrained by equations of motion and arise from finite quark masses, 3-particle and higher twist DAs, and chiral symmetry breaking, the last of which is the only effect we include.

4. Implications of selection rules on twist-expansion hierarchy

In practice selection rules such as the ones depicted in Table I enforce a rethinking of the matters of the twist expansion. More precisely we mean that if a large WC does not contribute at leading twist but say only at next leading twist then it does not seem wise to truncate at leading twist. Thus in practice this implies that one should expand to the twist order such that all sizeable WC, allowed by the fundamental selection rules such as the ones quoted in Sec. VA 1, contribute to the amplitude.

The K shall serve as an explicit example. For the latter we see that at leading and next leading twist a_8^q and a_4^q contribute which correspond to $(C_3/N_c + C_4)$ and $(C_5/N_c + C_6)$ in the SM (21). From the size of the WC VIII, we infer that the latter could be of importance especially in view of the fact that the next leading twist DA $\phi_{p,\sigma}$ is known to be chirally enhanced which can be inferred from its normalization (B1). The reader is referred to Figs. 6 and 8 to convince himself or herself of this fact.

B. Generic remarks on q^2 dependence

Below we add a few generic remarks on the q^2 dependence ranging from the validity the LCSR up to pointing out the dominant contributions. The latter are particularly useful for understanding the isospin asymmetries within and beyond the SM.

(i) *Physical spectrum and approximation ranges:* the physical spectrum of the decays ranges from $4m_l^2 < q^2 < (m_B - m_K^{(*)})^2 = 22.9(19.3)\ \mathrm{GeV}^2$. In this work we compute the isospin asymmetries at low q^2 (large recoil) where the LCSR (WA and $\mathcal{O}_8$) and QCDF (QLSS) results are naturally trustworthy. We restrict ourselves to the interval of $[1, 8]\ \mathrm{GeV}^2$ whose boundary is limited by the nearby ω, ρ, ρ' resonances from below and the charmonium resonances, commencing at $q^2 = m_{J/\Psi}^2 \simeq (3.1\ \mathrm{GeV})^2 \simeq 9.6\ \mathrm{GeV}^2$, from above. While it is plausible to assess effects of the latter close to these regions we consider it too difficult to asses them locally and thus refrain from doing so.

(ii) *Isospin asymmetry in $B \to K^* ll$ decreases for high q^2:* to understand the possible size of isospin asymmetry for a given WC as a function of q^2 it is helpful to look at the WCs $C_{9,10}$ and note the following:

(a) They are large as compared to the other WC (cf. Table VIII), partially as a result of a $1/\sin\theta_W^2 \simeq 4$ enhancement, where θ_W is the Glashow-Weinberg angle.

(b) We may write the leading terms in the $B \to Mll$ decay rate as

$$\begin{aligned} h_T &\sim [C_{9,10}^{\mathrm{eff}} \mathcal{O}(1) + C_7^{\mathrm{eff}} \mathcal{O}(1)], \\ h_0 &\sim \sqrt{q^2}[C_{9,10}^{\mathrm{eff}} \mathcal{O}(1) + C_7^{\mathrm{eff}} \mathcal{O}(1)], \\ h_\pm &\sim [C_{9,10}^{\mathrm{eff}} \mathcal{O}(q^2/m_B^2) + C_7^{\mathrm{eff}} \mathcal{O}(1)]. \end{aligned} \quad (61)$$

This behavior can be inferred from Eqs. (5), (13), and (11). Another way to look at it is to realize that $C_{9,10}$ should never be sensitive to $1/q^2$ in front of the rate as they are *not* generated by an intermediate photon but through intermediate Z bosons and box diagrams.

We therefore see that at low q^2 in $B \to K^* ll$ isospin violating terms only compete against C_7^{eff}, but at high q^2 they must compete with the much larger $C_{9,10}$ and hence the asymmetry decreases for large q^2. In $B \to Kll$ no such argument applies as in h_T C_7^{eff} and $C_{9,10}$ are on equal footing.

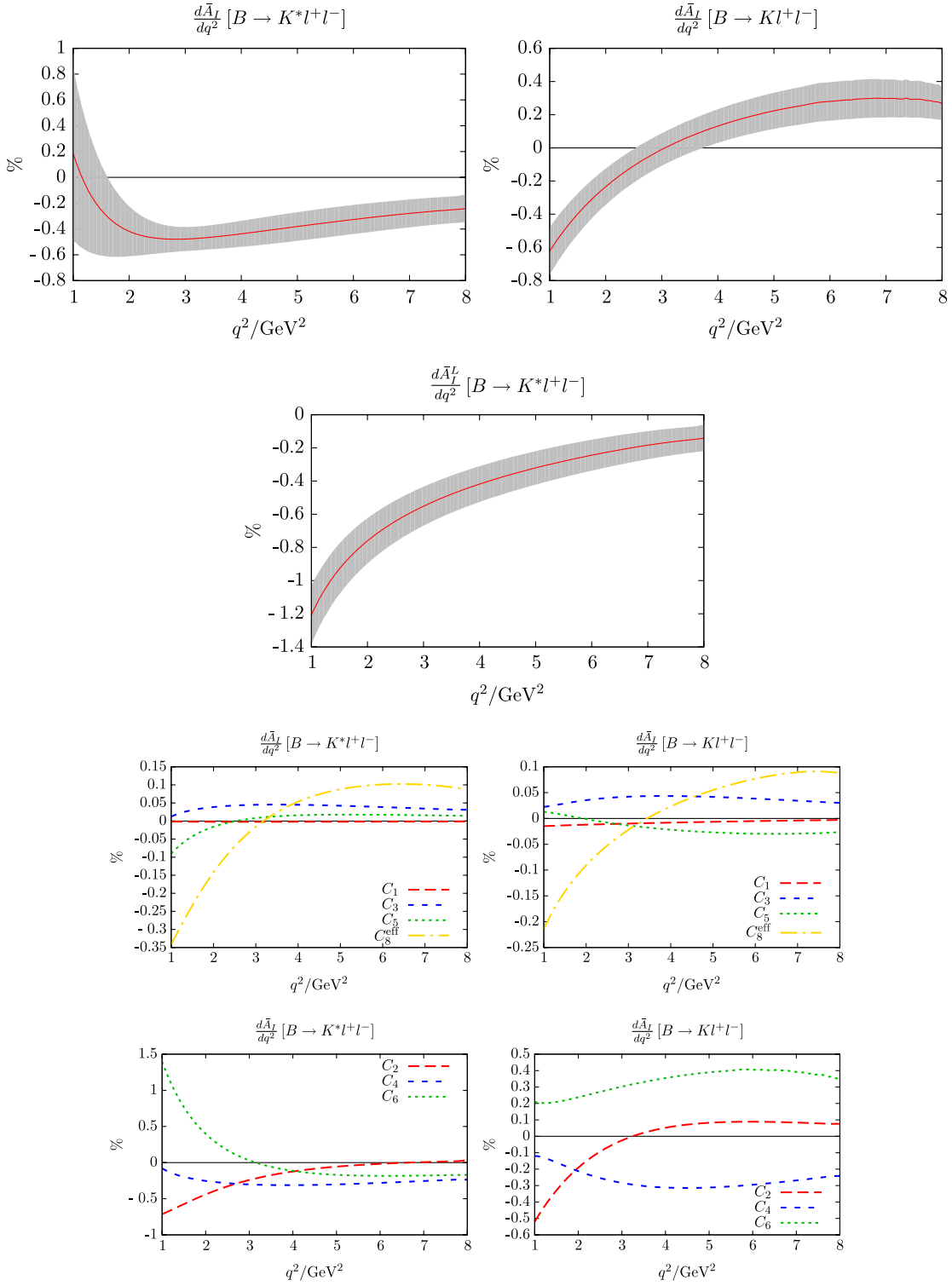

FIG. 6 (color online). Left (right), top: Isospin asymmetry for $B \to K^{(*)} ll$ with grey error bands. We have plotted the isospin asymmetry for the longitudinal part of the K^* meson denoted by subscript L. Left (right), middle, and bottom: Contribution of different SM operators to the isospin asymmetry in $B \to K^{(*)} ll$. The bottom ones are the sizeable contributions. The dominance of $[C_6 + (C_5/3)]$ has been found previously. Its decrease is due to the relevant operators O_{1-4}^{WA} entering at subleading twist in the longitudinal part which is dominant at high q^2. See Appendix E 2 for details of the calculation of the grey error band.

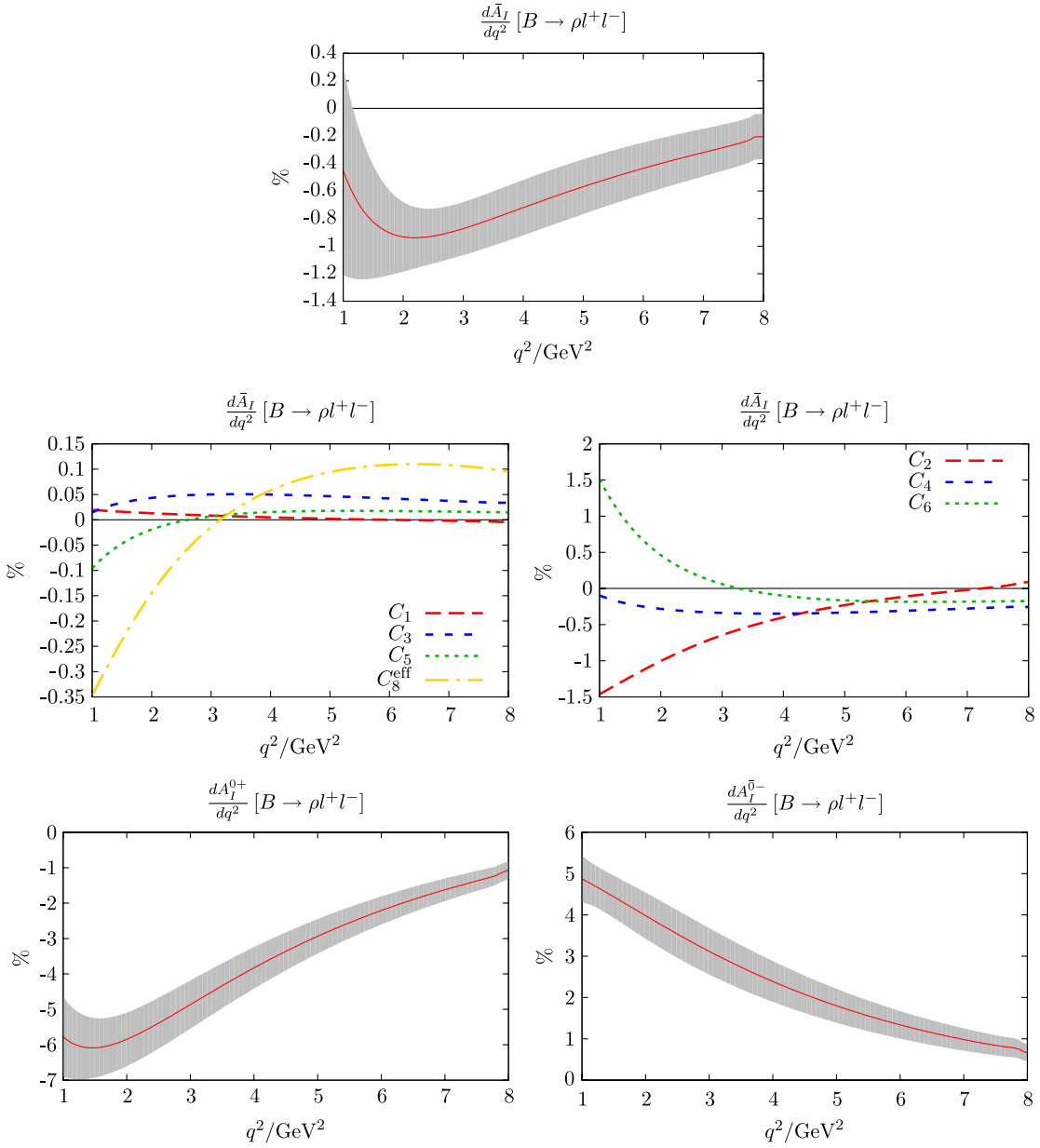

FIG. 7 (color online). Top: Isospin asymmetry for $B \to \rho ll$ with grey error bands. Left (right), middle: Contribution of different SM operators to the isospin asymmetry in $B \to \rho ll$. The graph on the right shows sizeable contributions. Note that unlike at $q^2 = 0$ the C_2 contribution is comparable to the C_6 contribution here; this is due to a small weak phase arising from C_9^{eff} alleviating the $\cos\alpha_{\mathrm{CKM}}$ suppression a little. See Appendix E 2 for details of the calculation of the grey error band. Left (right), bottom: Isospin asymmetry for $B \to \rho ll$ not CP-averaged $b \to d$ and $\bar{b} \to \bar{d}$ type. They do add up to the CP average (top) but do deviate significantly from the latter as a result of strong and weak phases as discussed in Sec. VI C. No such effect is observed for the K^* as explained in some detail in that section.

(iii) *High* $q^2 \leq (m_B - m_K^{(*)})^2$ *region:* In this paper we have not assessed the isospin asymmetry at high q^2, that is low recoil, *per se*. We shall discuss it from two viewpoints which fortunately lead to the same conclusion, namely, that the isospin violating effects get smaller for large q^2; that is to say the short-distance form factor contribution with small isospin effects are dominant.

Form factor contributions (FFCs) in the high-q^2 region. In that region the $C_{7,9,10}$ FFC are expected to be enhanced by the presence of the nearby resonance at $q^2 = m_{B_s^*}^2$, which can be foreseen from the plots and form factor parametrizations in [16] whereas no such enhancement is present in the isospin violating (IVQE) terms.[11] Let us add that IVQE terms, arising from intermediate off-shell photons, will be enhanced by light resonances

[11]This statement is only corrected by UV isospin violating effects in WA at $\mathcal{O}(\alpha_s)$.

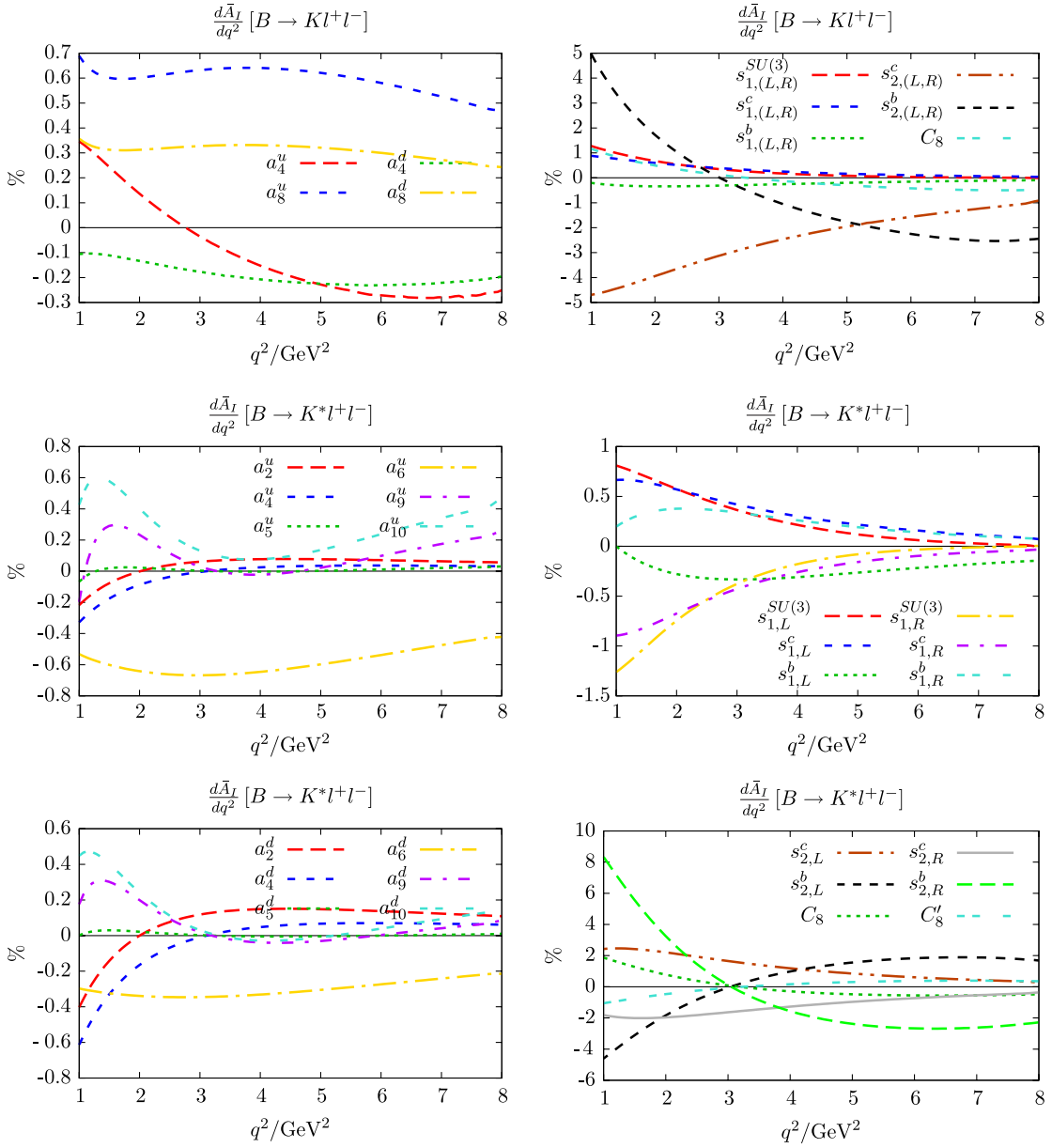

FIG. 8 (color online). Breakdown of contributions of WA (a_i), QLSS ($s^f_{x,\chi}$), and $\mathcal{O}_8^{(\prime)}$ to the isospin asymmetry $B \to K^{(*)}ll$ in the linear approximation (18). We have split the contributions as detailed in Table II into different graphs in order to make them more readable. Note that we use $a_i^q = 0.1$ and $s^f_{x,\chi} = 1$ to produce these figures, as in the tables.

at $q^2 = m_\rho^2, m_\omega^2, \ldots$, as can be seen for example in Fig. 3, and also by a heavy resonance $\Upsilon(\bar{b}b)$. Thus in summary the isospin asymmetry is expected to be suppressed both by small WCs and competing with a resonant isospin-symmetric term, and thus should be very small at high q^2.

Low recoil OPE: Some time ago an OPE in q^2 and m_b^2 was proposed [42] for the low recoil region, which was implemented into phenomenology [43] and reinvestigated from a theoretical viewpoint in [44]. In this language the FFC come as dimension three matrix elements and IVQE originate from higher dimensional operators (dimension six for WA and dimension five for QLSS and $\mathcal{O}_8$) and are therefore naturally small.

C. Isospin asymmetries $B \to K^{(*)}\gamma/ll$ in the SM

The plots of the $B \to K^{(*)}ll$ isospin asymmetries are given in Fig. 6, including a plot of the longitudinal part (zero helicity) of the K^* DA, and the values are tabulated in Table X (Appendix F 1). Important aspects on which operators or WC contribute were discussed in the previous subsection. The feature that is obvious is that the isospin asymmetry is small on the scale of -100% to 100% for $B \to K^{(*)}ll$ for $q^2 > 1\ \mathrm{GeV}^2$; specifically below the 2%

TABLE III. SM operators contributing to the isospin asymmetry $\mathcal{O}_{1-6,8}$ and operators not contributing to the asymmetry $\mathcal{O}_{7,9,10}$. This table summarizes the discussion in Sec. V C. WC denotes whether the operator is generated by a tree or penguin process. CKM denotes the CKM suppression, and $\lambda \simeq 0.22$ stands for the Wolfenstein parameter. In anticipation of $B \to \rho ll$ we have indicated the CKM hierarchy for $b \to d$ in parenthesis. M.E. denotes whether the matrix element is a tree or loop level process.

$b \to s(d)$		WA		QLSS		$\mathcal{O}_8$	
$\mathcal{O}_X$	WC	CKM	M.E.	CKM	M.E.	CKM	M.E.
$\mathcal{O}_{1,2}$	tree	$\lambda_u \sim \lambda^4(\lambda^3)$	tree	$\lambda_c \sim \lambda^2(\lambda^3)$	loop	...	...
$\mathcal{O}_{3\text{-}6}$	penguin	$\lambda_t \sim \lambda^2(\lambda^3)$	tree	$\lambda_t \sim \lambda^2(\lambda^3)$	loop	...	...
$\mathcal{O}_8$	penguin	...	...	...	...	$\lambda_t \sim \lambda^2(\lambda^3)$	loop
$\mathcal{O}_7$	penguin	not isospin sensitive and dominates low q^2					
$\mathcal{O}_{9,10}$	penguin/box	not isospin sensitive and dominates high q^2					

level. Qualitatively they agree with previous determination e.g. $B \to K^* ll$ [11] and $B \to Kll$ [12].[12] A few qualitative remarks on the size of the contributions can be found in the caption. Generically the asymmetries are dominated by WA which can also be inferred indirectly from Fig. 8 in the next subsection. Let us quote here the world average of the $B \to K^*\gamma$ isospin asymmetry from the Heavy Flavor Averaging Group (HFAG) [3]

$$\bar{a}_I(K^*\gamma)_{\text{HFAG}} = 5.2(2.6)\%, \qquad \bar{a}_I(K^*\gamma)_{\text{LZ}} = 4.9(2.6)\%, \tag{62}$$

which compared with our value turns out to be really close. Our value is also close to values previously found by [8,9,11]. The calculation of the theoretical uncertainty is detailed in Appendix E 2. To what extent this constrains the dimension six operators and therefore $B \to K^{(*)} ll$ is discussed in Sec. VII A.

Let us briefly discuss the three contributions in Fig. 1 considered in this paper.

(i) *WA:* The SM contributions $[a_i^q]^{\text{SM}}$ (21) are given in terms of the C_i in Eq. (21). For WA one has to distinguish between $\bar{q}b\bar{s}q$ operators (omitting the Lorentz indices) as generated from tree and penguin processes. When originating from penguin processes $\mathcal{O}_{3-6}$, an equal amount of $q = u, d$ is generated and the process is dominated by the top quark penguin which results in a $\lambda_t \sim \lambda^2$ CKM prefactor. The $q = u$ case also has a tree contribution $\mathcal{O}^u_{1,2}$ which is then proportional to $\lambda_u \sim \lambda^4$. Thus *a priori* it seems difficult to judge whether the loop suppression or the CKM suppression is more effective.[13] Inspecting Fig. 6 and taking into account that WA is the leading effect we see that the answer depends on q^2 and the Dirac structure: C_6 dominates the isospin asymmetry for $B \to K^* ll$ but for $B \to Kll$ the $C_{2,4}$ contributions are of similar magnitude to C_6.

(ii) *QLSS:* QLSS is dominated by the charm loop as the latter originates from the tree operators $\mathcal{O}^c_{1,2}$. Whereas this contribution is not CKM suppressed $\lambda_c \sim \lambda^2$ it is of course loop suppressed.

(iii) $\mathcal{O}_8$: The chromomagnetic $\mathcal{O}_8$ contribution has been discussed in a separate paper [6]. For $B \to K^{(*)}$ the transition matrix element is found it to be rather small, as compared to the QCD penguin form factors $T_1(0)$. The total and isospin violating parts were found to be in the 6% and 2% range, as compared to $T_1(0)$, respectively. An interesting aspect is the large strong phase attributed to LD contributions. The phase is of importance for CP violation in new physics searches in $D \to V\gamma$ [45], but not for CP-averaged isospin as the latter is only sensitive to the real part of strong phases, at least in the linear approximation cf. (18). Furthermore we should point out that we neglect the $\mathcal{O}'_8$ contribution in the SM, as $C'_8/C_8 \simeq m_s/m_b$ by virtue of the MFV symmetry.

Some of the points discussed above and in the previous subsection are summarized in Table III.

VI. ISOSPIN ASYMMETRIES IN $B \to \rho\gamma/ll$

$B \to \rho$ decays[14] differ from $B \to K^*$ decays in two important respects: (1) WCs of the operators $\mathcal{O}_{1,2}$ are not

[12]We differ from these references in that we compute WA and $\mathcal{O}_8$ in LCSR which includes LD contributions as argued at the beginning of Sec. IV B. Moreover we include twist-3 contributions for WA for the reasons mentioned in Sec. V A 4. The QLSS contributions are effectively treated in the same way. Whereas their result is small it differs from ours quantitatively which is explained by the differences mentioned above.

[13]For $D \to V\gamma$ and decays such as $D_s^+ \to \rho^+\gamma$ there is no CKM suppression at all and since all other subprocesses are small, WA dominates these decays as we have argued in [45] and in Appendix A.

[14]In this work we refrain from including the isospin asymmetry $B \to \pi ll$. $B^+ \to \pi^+ ll$, but not the neutral mode, has only been observed recently by the LHCb Collaboration [46]. Another logical extension would be to consider a ρ-ω asymmetry as in [9]. We refrain from doing so mainly because the latter suffers from a large theoretical uncertainty in the actual difference, not to be confused with the separate values, of the ρ and ω form factors. This situation could be improved considerably through a dedicated study of the respective ratio of decay constants; both transversal and longitudinal.

CKM suppressed (cf. Table III), and (2) $B^0 \to \rho^0$, by virtue of $\rho^0 \sim (\bar{u}u - \bar{d}d)$, contains additional diagrams with different arrangements of the four quark operators, and as a consequence also couples to color octet operators [octet with respect to the basis (19)]. We shall see shortly that the first point is effectively irrelevant as the relevant CKM angle $\alpha_{\rm CKM} = 89(4)^\circ$ [20] chooses to be close to Pythagorian perfection.

More precisely the $\mathcal{O}_{1,2}$ contribution in the SM comes with a CKM prefactor

$$\frac{\lambda_u^{bd}}{\lambda_t^{bd}} = -\left|\frac{\lambda_u^{bd}}{\lambda_t^{bd}}\right| e^{-i\alpha_{\rm CKM}}, \tag{63}$$

where $\lambda_i^{bd} \equiv V_{id}^* V_{ib}$, in close analogy to $\lambda \equiv \lambda_i^{bs} \equiv V_{id}^* V_{ib}$ used previously. Since the CP-averaged isospin asymmetry is sensitive to the real part, giving $\cos\alpha_{\rm CKM} = 0.02(7)$, the relatively large magnitude of $\lambda_u^{bd}/\lambda_t^{bd}$ is overruled and thus the overall contribution from $\mathcal{O}_{1,2}$ is very small. Essentially there is then no interference of the $\mathcal{O}_{1,2}|_{\rm WA}$ with the leading contributions. This is why the non-CP-averaged isospin asymmetry leads to rather different results (already in the SM; cf. Sec. VI C).

A. Extending the effective Hamiltonian for $B^0 \to \rho^0\gamma/ll$

For the $B^0 \to \rho^0\gamma/ll$ decay ($\rho^0 \sim \bar{u}u - \bar{d}d$), the basis (19) has to be extended to include

$$O_i^{\rm WA} = \bar{q}\Gamma_1 b\bar{s}\Gamma_2 q \Rightarrow O_i^{\rm WA,8} = \frac{1}{4}\bar{q}\lambda^a\Gamma_1 b\bar{s}\lambda^a\Gamma_2 q, \tag{64}$$

so that for example $O_1^{\rm WA,8} = \frac{1}{4}\bar{q}\lambda^a b\bar{s}\lambda^a q$, and we modify the effective Hamiltonian (20) to

$$\mathcal{H}^{{\rm WA},q} = -\frac{G_F}{\sqrt{2}}\lambda_t \sum_{i=i}^{10}[a_i^q O_i^{\rm WA} + a_i^{8q} O_i^{\rm WA,8}]. \tag{65}$$

In spite of all these operators being present, the basic situation presented in Table I has not changed: our calculation only picks up six linearly independent combinations of WCs in the $B^0 \to \rho^0\gamma/ll$ case. We therefore choose to present the isospin asymmetry for the ρ meson in the following schematic way:

$$\rho^\pm \leftrightarrow a_i^u, \qquad \rho^0 \leftrightarrow \tilde{a}_i^d = c_i^d a_i^d + c_i^{8d} a_i^{8d} + c_i^{8u} a_i^{8u} \tag{66}$$

with c_i^x given in Appendix F 2.

B. Isospin asymmetries in $B \to \rho\gamma/ll$ in the SM

The SM values of the new color octet coefficients are

$$\begin{aligned} a_1^{8q} &= -a_2^{8q} = a_3^{8q} = -a_4^{8q} = -4C_5, \\ a_5^{8q} &= -a_6^{8q} = -a_7^{8q} = a_8^{8q} = 2C_3 - 2\delta_{qu}\frac{\lambda_u}{\lambda_t}C_1, \\ a_9^{8q} &= a_{10}^{8q} = 0. \end{aligned} \tag{67}$$

The ones for the color singlet operators are the same as for the K^* (21). The formulas for $\tilde{a}$, in relation to ρ^0 (66), are given in Appendix F 6 a for the SM.

Our results for $B \to \rho ll$, including breakdowns of operator dependence, are shown in Figs. 7 and 9, and tabulated data is given in Appendix F 1 in Table XI. The experimental measurement of the isospin asymmetry is defined differently to the K^* case, as [47]

$$\begin{aligned} \Delta(\rho\gamma) &= \frac{\tau_{B^0}}{2\tau_{B^+}}\frac{\mathcal{B}(B^+ \to \rho^+\gamma)}{\mathcal{B}(B^0 \to \rho^0\gamma)} - 1 \\ &= \frac{-2\bar{a}_I(\rho\gamma)}{1 + \bar{a}_I(\rho\gamma)} \overset{a_I(\rho\gamma)\ll 1}{\approx} -2\bar{a}_I(\rho\gamma) \end{aligned} \tag{68}$$

$[a_I(\rho\gamma) = -\Delta(\rho\gamma)/(2 + \Delta(\rho\gamma))]$ where a CP-averaged branching fraction is used. In this normalization, our result compares with the experimental result as [3]

$$\Delta(\rho\gamma)_{\rm HFAG} = -46(17)\%, \qquad \Delta(\rho\gamma)_{\rm LZ} = -10(6)\%. \tag{69}$$

We shall quote Δ in percentage even though, contrary to $-1 \le a_I \le 1$, Δ is not bounded when $a_I \to -1$. For completeness we further quote our result for the CP-averaged isospin asymmetry in $B \to \rho\gamma$ in the SM as

$$\bar{a}_I(\rho\gamma)_{\rm HFAG} = 30\binom{-13}{+16}\%, \qquad \bar{a}_I(\rho\gamma)_{\rm LZ} = 5.2(2.8)\%, \tag{70}$$

where we have used Eqs. (69) and (68) for computing what we call the HFAG value above. Our result is comparable to that obtained in [9][15] and somewhat larger than that in [48], principally due to a different choice of $\alpha_{\rm CKM}$. Our SM result is marginally consistent with the current experimental value, that is to say they are exactly two standard deviations apart. There is another way one can reflect on the experimental value (69); namely, one can extract $|V_{\rm td}/V_{\rm ts}|$ from the ratio of branching fractions $R_{\rho/K^*} = \mathcal{B}(B \to \rho\gamma)/\mathcal{B}(B \to K^*\gamma)$ which can be applied for charged and neutral case separately. In view of the fact, to be discussed in the next section, that the isospin splitting of the ratios of the ρ and K^* channel is accidentally small (i.e. SM: $R_{\rho^0/K^{*0}} \approx R_{\rho^+/K^{*+}}$ for current CKM angles), we may infer from Table 12 in Ref. [9] that

$$\left|\frac{V_{\rm td}}{V_{\rm ts}}\right|_{R_{\rho^0/K^{*0}}} = 0.229(25\%), \quad \left|\frac{V_{\rm td}}{V_{\rm ts}}\right|_{R_{\rho^+/K^{*+}}} = 0.165(25\%), \quad \left|\frac{V_{\rm td}}{V_{\rm ts}}\right|_{\rm PDG[19]} = 0.211(7), \tag{71}$$

and we have quoted the current value from the Particle Data Group (PDG) for comparison. We have given a rough

[15]Note that the authors of Ref. [9] use the opposite sign convention for $\Delta(\rho\gamma)$.

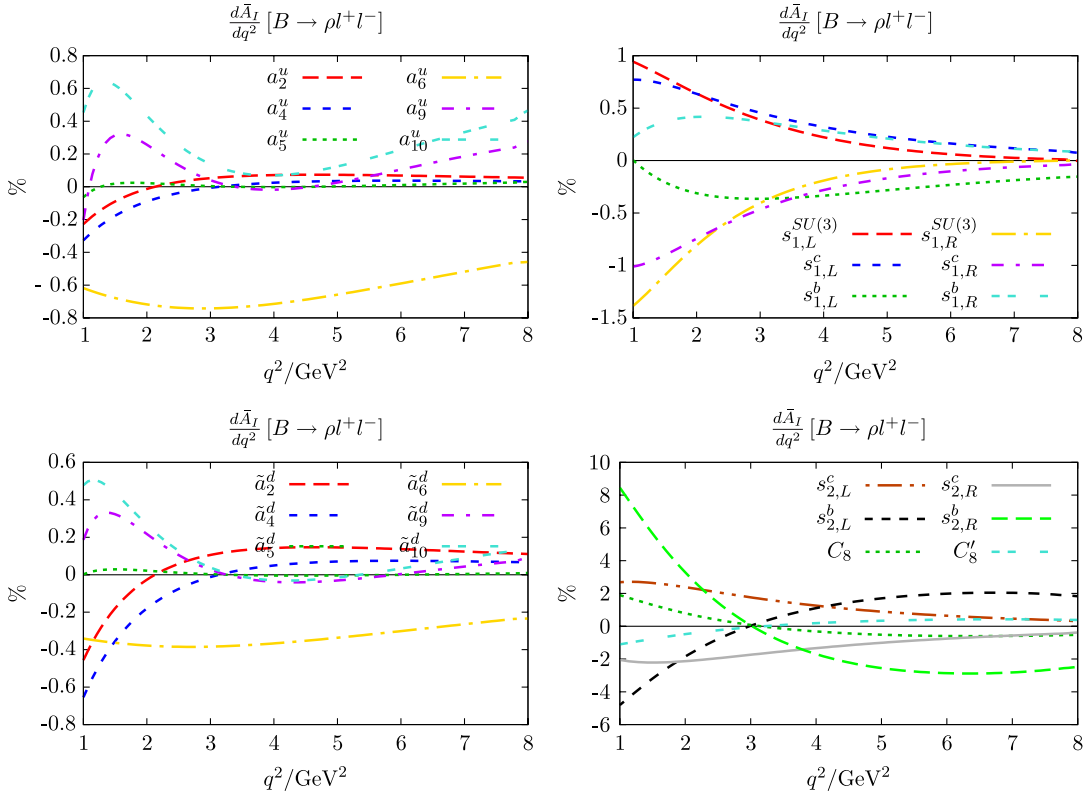

FIG. 9 (color online). Breakdown of contributions of WA (a_i), QLSS ($s^f_{x,\chi}$), and $\mathcal{O}_8^{(\prime)}$ to the isospin asymmetry $B \to \rho ll$ in the linear approximation (18). We have split the contributions as detailed in Table II into different graphs in order to make them more readable. Note that we use $a_i^u = 0.1$, $\tilde{a}_i^d = 0.1$, and $s^f_{x,\chi} = 1$ to produce these figures, as in the tables.

estimate of the error which is mainly due to the $B \to \rho\gamma$ branching fraction (cf. Appendix E 4). Thus we infer that the discrepancy in $\Delta(\rho\gamma)$ (69) is presumably due to the ρ^+- rather than the ρ^0 channel.

C. On subtleties of *CP* averaging the isospin asymmetries

In this paper we have computed CP-averaged quantities which resultsin the linear approximation to taking the real part of the strong and weak phase separately, whereas no CP average implies taking the real part of the product of the strong and weak phase. Schematically,

$$\begin{aligned} &CP \text{ average: } \mathrm{Re}[e^{i\delta_{\text{strong}}}]\mathrm{Re}[e^{i\phi_{\text{weak}}}], \\ &\text{no } CP \text{ average: } \mathrm{Re}[e^{i\delta_{\text{strong}}} e^{i\phi_{\text{weak}}}]. \end{aligned} \tag{72}$$

To be more precise the weak and the strong phase is the difference between the isospin-violating and the isospin-conserving amplitude. Thus in general there can be significant differences if both δ_{strong} and ϕ_{weak} are sizeable.

Are there sizeable strong phase differences? The isospin conserving amplitude has a very small strong phase in the region we are considering and thus the question is whether there is a sizeable strong phase in the isospin violating amplitude. The answer to this is no for $q^2 = 0$, as only $\mathcal{O}_8(')$ contributes with a strong phase at leading order in α_s (which is at least small in the SM). For $1\ \mathrm{GeV}^2 \le q^2 \le 4m_c^2$, however, the answer is yes: the photon emitted from a light quark converts via an intermediate ρ, ω meson and gives rise to a tail in the imaginary part. This is the case for all IR isospin violation and we refer the reader to Fig. 4 (left) in [6] for an illustration.

Are there large sizeable weak phase differences? In the SM this is the case for $B \to \rho(b \to d)$ as can be seen from (63) with $\alpha_{\text{CKM}} = 89(4)$ but not for $B \to K, K^*(b \to s)$. In BSM scenarios this question is open modulo constraints, in particular, CP observables.

We summarize the conclusions to be drawn from the discussion above in Table IV. The plots for the non-CP-averaged isospin asymmetries in $B \to \rho ll$ are

TABLE IV. $\overline{CP}$ effect stands for CP-averaging effect on the isospin asymmetries and ✗(✓) mean (in)significant. Overview of the conclusions to be drawn from the analysis of Sec. VI C. Note that an enhancement of $\mathcal{O}_8$ or sizeable radiative corrections to WA or QLSS would raise δ_{strong} and could shift the situation slightly.

$\overline{CP}$ effect	$B \to (K^*, \rho)\gamma$	$B \to K^{(*)}ll$	$B \to \rho ll$
SM	✗	✗	✓
BSM ($\phi_{\text{weak}}^{\text{BSM}}$)	✗	✓	✓

TABLE V. Constraints on WCs a_i^q from $B \to K^*\gamma$ at 2σ, assuming no accidental cancellations occur, along with SM values. We assume $0 < \bar{a}_I(K^*\gamma) < 10\%$, and derive constraints from Table X assuming that only a single coefficient a_i^q deviates from its SM value. SM values are calculated from (21) and Table VIII. All constraints are for the real part of these coefficients; the imaginary part is not constrained by the isospin asymmetry.

$B \to K^*\gamma$	Min.	SM	Max.		Min.	SM	Max.
a_2^u	−0.39	−0.068	0.25	a_2^d	−0.24	−0.068	0.11
a_4^u	−0.38	−0.068	0.25	a_4^d	−0.24	−0.068	0.10
a_5^u	−0.41	−0.021	0.37	a_5^d	−0.67	−0.028	0.61
a_6^u	−0.62	0.021	0.57	a_6^d	−1.0	0.028	1.0
a_9^u	−0.049	0	0.049	a_9^d	−0.080	0	0.080
a_{10}^u	−0.048	0	0.048	a_{10}^d	−0.080	0	0.080

shown in Fig. 9. We see that the asymmetries raise up to $\pm 5\%$ in the 1 GeV$^2 \leq q^2 \leq 4m_c^2$ region.

In general it might therefore be interesting to measure non-CP-averaged isospin asymmetries in future experimental determinations. This is certainly possible for the K^* and the ρ but not for the K, as it is observed through K_S^0 which is a superposition of the strangeness eigenstates K^0 and $\bar{K}^0$.

VII. ISOSPIN ASYMMETRIES BEYOND THE SM

The extension of the SM basis was discussed throughout the main text and summarized in Sec. V A. Possibly we should reemphasize, for the sake of clarity, that $\mathcal{O}'_{7,9,10}$ operators of $V + A$ chirality are of no interest to the isospin asymmetry as they do not violate isospin. Of course if they become extremely large then they would affect the rate. Yet it is already known that they cannot be too large; see e.g. [49–51]. The various contributions of the extended basis are detailed in Figs. 8 and 9 and tabulated in Tables IX, X, and XI (Appendix F 1) for the K, K^* and ρ channels, respectively. One aspect that is immediately apparent from these graphs is that there are overwhelmingly many contributions that can give rise to a sizeable isospin asymmetry at low q^2. In fact there are so many that by the rules of probability one would expect cancellations in the generic case. Fortunately this is where the q^2 spectrum should help us, should there be new physics; one cannot expect to be unlucky over the entire q^2 range.

In Sec. V A 3 we discussed that only for leading twist and SM chirality the K and the $K_\parallel^*$ are related. As noted there this link breaks down in the presence of right-handed currents, which are only partially constrained, and thus in a generic scenario the link between the K and the K^* isospin asymmetry is lost. The reader can convince himself or herself of this fact directly from the corresponding tables and figures referred to above.

A. Constraints on isospin sensitive four Fermi operators

We shall now briefly turn to the question to what extent these operators are already constrained. We identify nonleptonic decays[16] as well as $B \to \rho/K^*\gamma$ isospin asymmetries themselves as the main sources for constraints:

(i) $B \to \rho/K^*\gamma$ *isospin asymmetries*: the experimental values are quoted in (62) and (69), respectively. These isospin asymmertries are sensitive to $a^q_{2,4,5,6,9,10}$ of WA, in particular. Of course one number such as $\bar{a}_I(K^*\gamma)$ cannot seriously bound 12 numbers. We might though give indicative constraints by imposing that each of the coefficients shall not be more than two standard deviations away from the central value, which roughly amounts to $0 < \bar{a}_I(K^*\gamma) < 10\%$ and $6 < \bar{a}_I(\rho\gamma) < 67\%$ $[-80\% < \Delta(\rho\gamma) < -12\%]$. The results of this procedure are collected in Tables V and VI, respectively.

(ii) *Nonleptonic decays*: four Fermi operators do affect nonleptonic decays such as $B \to \rho/\pi K^{(*)}$, $B_s \to K^{(*)}\phi$, etc. The disadvantage is that they are difficult to predict from a theoretical viewpoint, especially in the absence of a first principle approach to final state rescattering. The uncertainty in strong phases obscures interference effects which affects all observables, let alone CP asymmetries. The advantage though is that there is a plethora of channels which allows theorists to constrain certain weak topologies, see e.g. [52–54], and permits them to cross-check their methods. Interesting constraints on four Fermi operators, such as the so-called electroweak penguins present in the SM, have been obtained in Refs. [55,56] for instance in the framework of QCD factorization. We would like to add two remarks. First, these operators do partially overlap with ours and would indeed bring in additional constraints. Yet only global fits lead to solid constraints which is beyond the scope of this work. Second, from the

[16] $\Delta F = 2$ constraints from neutral meson oscillations, usually rather severe, are presumably not very strong. More precisely if we are to compare SM/MFV type operator $\mathcal{O}^{\text{MFV}}_{\Delta B=2} \approx |\lambda_t|^2 G_F/16\pi^2 (\bar{b}\Gamma_1 s_L)(\bar{b}\Gamma_2 s_L)$ (with $\Gamma_{1,2}$ specific Dirac structures) then by integrating out either b quarks or saturating light quarks with intermediate hadronic states one would expect to get a $G_F \times (m_b^2, \Lambda^2_{\text{QCD}}) \approx (10^{-4}, 10^{-6})$ suppression in each case.

TABLE VI. Constraints on operators a_i^q from $B \to \rho\gamma$ at 2σ, assuming no accidental cancellations occur, along with SM values. We assume $6\% < \bar{a}_I(\rho\gamma) < 67\%$ and derive as described below Table V. Again note that we list the real part only as this is what enters the CP-averaged isospin asymmetry. Since our calculated SM value is the lower bound of this range (within uncertainties), we quote the SM value of the coefficient and the other bound; the true value is expected to lie in this range.

$B \to \rho\gamma$	SM	Bound		SM	Bound
a_2^u	−0.068	−4.1	$\tilde{a}_2^d$	−0.068	−2.1
a_4^u	−0.068	−4.0	$\tilde{a}_4^d$	−0.068	−2.0
a_5^u	−0.021	4.9	$\tilde{a}_5^d$	−0.028	8.1
a_6^u	0.021	−7.6	$\tilde{a}_6^d$	0.028	−13
a_9^u	0	0.56	$\tilde{a}_9^d$	0	0.94
a_{10}^u	0	0.56	$\tilde{a}_{10}^d$	0	0.93

plots in Refs. [55,56] one infers that it is rather unlikely that the NP contributions to the WC exceeds the SM values by a factor of 5 but could easily be out by a factor of 2. In view of the multitude of channels this might very well be true for SM operators. It seems more difficult to come to a quick judgement for non SM operators (by which we mean operators with small WCs). Partial studies do exist; e.g. an interesting direction, in view of right-handed currents, is the investigation of polarization in $B \to VV$ decays [54] which was carried out in [57] in the framework of QCD factorization.

B. $B \to K^*/\rho\gamma$ isospin asymmetry splitting—(quasi-)SM null test

The closeness of $\alpha_{\rm CKM}$ to 90° may be exploited to predict an observable with much smaller theoretical uncertainty, albeit at the expense of larger current experimental uncertainty.

Our prediction is essentially that $\bar{a}_I(\rho\gamma)$ and $\bar{a}_I(K^*\gamma)$ should be similar, up to form factor and hadronic parameter differences.[17] A major source of uncertainty in determining $\bar{a}_I(K^*\gamma)$ and $\bar{a}_I(\rho\gamma)$, however, is the renormalization scale used to compute the WCs, and because of this it is worthwhile to calculate a quantity in which the leading scale dependence and form factor differences cancel, namely,

$$\delta_{a_I} \equiv 1 - \frac{\bar{a}_I(\rho\gamma)}{\bar{a}_I(K^*\gamma)} R_{\rho K^*} = 1 + \frac{\Delta(\rho\gamma)}{(2+\Delta(\rho\gamma))\bar{a}_I(K^*\gamma)} R_{\rho K^*}, \tag{73}$$

where

$$R_{\rho K^*} \equiv \sqrt{\frac{\bar{\Gamma}(B \to \rho\gamma)}{\bar{\Gamma}(B \to K^*\gamma)}} \left| \frac{V_{\rm ts}}{V_{\rm td}} \right|, \tag{74}$$

and a barred partial width $\bar{\Gamma}$ implies a CP average, and omission of charges implies an isospin average.[18] The dominant contributions to the right-hand side of (73) are

$$a_I(V\gamma) \approx \frac{C_6 + C_5/3}{C_7^{\rm eff}} \frac{f_V^\perp F^{\rm WA}(0)}{T_1^V(0)} + \cdots, \qquad \bar{\Gamma}(B \to V\gamma) \approx \frac{3\alpha c_F}{8\pi} |\lambda_t C_7^{\rm eff}|^2 |T_1^V(0)|^2, \tag{75}$$

where the dots stand for $C_{3,4}$ contributions—which are small as the K^* and ρ cases are very similar—quark masses, and $B^0 \to \rho^0$ diagrams at $\mathcal{O}(\alpha_s^2)$ where the different structure of the ρ^0 matters even for small $\cos\alpha_{\rm CKM}$. The function $f_V^\perp F^{\rm WA}(0)$ stands for final state emission where we have explicitly factored out the $f^\perp$ decay constant as compared with (33). More precisely, $f_V^\perp F^{\rm WA}(q^2) = \sum_{i=2,4}(F_i^d(q^2) - F_i^u(q^2))$ ($i = 2, 4$ are the operators proportional to $C_6 + C_5/3$) in the notation of (33), and $F^{\rm WA}$ is the same for the K^* and the ρ in our approximation up to small corrections from different Gegenbauer moments. The correction factor $R_{\rho K^*}$ serves the purpose of eliminating the form factor ratio as $\bar{a}_I(\rho\gamma)/\bar{a}_I(K^*\gamma) \simeq T_1^{B\to K^*}(0)/T_1^{B\to\rho}(0)$ which follows from Eq. (75). Since the WA contribution $f^\perp F^{\rm WA}(0)$ is essentially proportional to $f^\perp$, it then follows that

$$\delta_{a_I} = 1 - f_\rho^\perp/f_{K^*}^\perp + \text{small corrections}, \tag{76}$$

where the principal source of uncertainty, the scale dependence of $C_6 + C_5/3$, drops out. Note that by "small corrections" we mean small as compared to 1. The quantity δ_{a_I} is particularly sensitive to corrections to the isospin asymmetry and we therefore include terms quadratic in WA amplitudes present in (17) but neglected in (18) and elsewhere. Comparing our prediction with a naive combination of PDG [20] results for these quantities gives

$$[\delta_{a_I}]_{\rm exp} = -4.0(3.5), \qquad [\delta_{a_I}]_{\rm LZ} = 0.10(11). \tag{77}$$

The theoretical uncertainty should be compared with 1 as it is a ratio, as above and thus is at 11%, is under rather good control, as compared to roughly 50% in the individual asymmetries. See Appendix E 4 for the experimental input used as well as brief comments on the uncertainty. Let us briefly add that the uncertainty due to the difference in B meson lifetimes and $|V_{\rm ts}/V_{\rm td}|$ is negligible. Experimental and theoretical values agree within uncertainties, though the central value is very different and an improved experimental

[17] An extension to $q^2 > 0$ is not straightforward as the isospin asymmetries of the K^* and ρ^* do differ qualitatively: $C_9^{\rm eff}(q^2)$ contributes a small weak phase to the leading amplitude which partially alleviates the $\cos\alpha_{\rm CKM}$ suppression.

[18] For the ρ meson this implies $\bar{\Gamma}(B\to\rho\gamma) = \frac{1}{2}\bar{\Gamma}(B^+\to\rho^+\gamma) + \bar{\Gamma}(B^0\to\rho^0\gamma)$ due to $\rho^0 \sim (\bar{u}u - \bar{d}d)/\sqrt{2}$ as discussed previously.

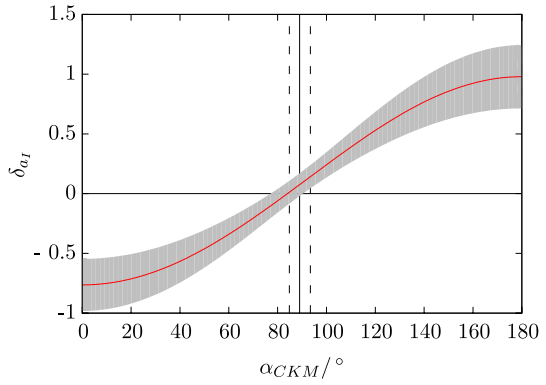

FIG. 10 (color online). Plot of the effective ρ to K^* isospin asymmetry difference δ_{a_I} (73). Vertical lines indicate the current experimental value of $\alpha_{\rm CKM}$ [20] and its uncertainty. At the present small value of $\cos\alpha_{\rm CKM}$, δ_{a_I} is well determined theoretically.

determination is desirable since the theoretical errors are under good control. The experimental uncertainty due to all four branching fractions involved in δ_{a_I} is rather similar, and thus *all* of them need to be reduced to significantly improve the overall uncertainty. It should also be added that if the asymmetries are measured in the same experiment (some) systematic uncertainties can be expected to cancel.

The behavior of δ_{a_I} and its uncertainty as a function of $\alpha_{\rm CKM}$ are shown in Fig. 10. We provide a fit for this plot,

$$[\delta_{a_I}]_{\rm LZ} = 0.10\text{–}0.87\cos\alpha_{\rm CKM}, \tag{78}$$

where the 1σ bounds are given by $[\delta_{a_I}]_{\rm LZ} \pm [\sigma]_{\rm LZ}$ where $[\sigma]_{\rm LZ} = 0.10 + 0.14\cos^2\alpha_{\rm CKM}$ is a good fit for the error band shown in Fig. 10.

It is clear that the structure of the SM is responsible for the smallness of δ_{a_I} (73). In general the quantity δ_{a_I} is thus highly sensitive to new physics. Two examples are as follows:

(i) *Non-MFV isospin violation*: For example, $(a_i^q|_{b\to s})/(a_i^q|_{b\to d}) \neq \lambda_t^{bs}/\lambda_t^{bd}$; cf. Eq. (19) and thereafter for the definition of a_i^q.

(ii) *UV isospin violation*: Four fermi operators of the type (19) in unequal proportion of $q = u, d$ quarks. Such a difference is sensitive to the structure of the $K^{*,0}$ and ρ^0 parton content.

We provide some example values for the case of UV isospin violation in Table VII.

TABLE VII. Effect of varying a_i^d from their SM values on the isospin splitting δ_{a_I}. We fix all a_i^q to their SM values and then alter a single one by the specified amount. More precisely $\delta_{a_I}[a_8^d + x] \leftrightarrow \delta_{a_I}[a_8^{d,\rm SM} + x]$ above. The resulting variation of δ_{a_I} can be large and is primarily the result of the ρ^0 coupling to a different combination of a_i as discussed in Sec. VI A, and is therefore an example of UV isospin violation (but not MFV violation). The uncertainties quoted in this table do not include uncertainty from varying the renormalization scale; this would require a computation of the scale dependence of the Hamiltonian (65) and is thus beyond the scope of this work. The renormalization scale is taken to be the usual central value, $\mu = 4.7$ GeV.

x	$\delta_{a_I}^{a_1^d+x}$	$\delta_{a_I}^{a_8^d+x}$
−0.3	1.16(15)	1.71(20)
−0.2	0.82(11)	1.21(13)
−0.1	0.47(9)	0.67(9)
0.1	−0.29(14)	−0.51(15)
0.2	−0.68(18)	−1.14(21)
0.3	−1.08(23)	−1.78(28)

VIII. CONCLUSION

Isospin violating effects considered in this paper are of the UV type, i.e. $H^{\rm eff}$ is asymmetric under $u \leftrightarrow d$, as well as IR-isospin violation which manifests itself in photon emission from the spectator quark. We have found that CP-averaged isospin asymmetries in the SM are small, below 1.5%, for $B \to (K, K^*\rho)ll$ at lepton pair momentum 1 GeV$^2 \le q^2 \le 4m_c^2$ as can be inferred from Figs. 6 and 8 as well as the actual breakdown of the various operator contributions. In fact in the SM the $(K, K^*)ll$ and ρll are somewhat accidentally small. In the former case the large Wilson coefficient C_2^u is suppressed by a small CKM prefactor $|\lambda_u/\lambda_t| \simeq \lambda^2 \approx 0.04$ and in the latter case it is the smallness of $\cos\alpha_{\rm CKM}$ which suppresses the tree-level WC C_2^u. The latter point is also the reason why the non-CP-averged isospin asymmetry for $B \to \rho ll$ deviates from the CP-averged one; cf. Sec. VI C. Not performing the CP average, which is possible for the ρ and K^*, is certainly an interesting option for the former *per se*; cf. Fig. 8 (bottom) and for the latter in the presence of new weak phases.

Isospin asymmetries of $B \to K^*/\rho\gamma$ are a bit higher, around 5% each, due to the photon pole enhancement and are measured with reasonable accuracy (62) and (69). Whereas the K^* experimental result is in perfect agreement with our prediction, the ρ asymmetry is off by 2 standard deviations and calls for further experimental data. In both cases we use these results to give indicative constraints on the WA WCs; cf. Tables V and VI, by demanding that no coefficient is more than 2 standard deviations away from the experimental results. The smallness of $\cos\alpha_{\rm CKM}$ implies that the $K^*/\rho\gamma$ SM isospin asymmetries are structurally very similar, resulting in the almost identical numerical result, which prompted us to define a (quasi)null test of the SM δ_{a_I} in Sec. VII B.

We have not systematically investigated the isospin asymmetry in the high q^2 region in this work. Nevertheless we have argued that it has to be small as it is (i) no longer artificially enhanced as at low q^2 by the photon pole, through which isospin effects propagate, and (ii) its contribution is further suppressed relative to the form factor contributions as the latter feel the closeness of the t channel pole at $q^2 = m_{B_s^*}^2$. On grounds of these arguments, modulo magic cancellation at low q^2, one expects the isospin asymmetry to decrease. We should add that the authors of Ref. [44] had come to the same conclusion using arguments of a high q^2 OPE.

We have introduced the most general basis of dimension six operators for WA (19) and QLSS (38) and have detailed various contributions in Tables IX, X, and XI in Appendix F 1 as well as Figs. 8 and 9 in Sec. VII, respectively. Generic selection rules for the $B \to Kll$, valid for any scalar $\to$ scalar ll transition, were discussed in Sec. V A 1. Selection rules for WA, which are more stringent, were worked out in Sec. V A 2 for vectors and pseudoscalars. After applying all selection rules 24 and 10 operators remain for a vector and pseudoscalar meson final state, which compares with 7 operators in the SM for the K^* and the K meson. In view of the large number of operators that can contribute, as detailed in Fig. 6 and Tables IX and X, respectively, one might even wonder whether by the laws of probability cancellation of new physics is the rule rather than the exception. One would hope that a refined experimental analysis in q^2 would reveal the deviation in one bin or another. In this paper we have not attempted to constrain the four Fermi operators through nonleptonic decays but have, for the time being,[19] contented ourselves with a few generic remarks in Sec. VII A. In the future data from isospin asymmetries in $B \to P, V\gamma/ll$ could be combined with data in nonleptonic decays $B \to PP, PV, VV$ to constrain four Fermi operators of $bs(d)qq$ type more effectively.

On the theoretical side the SM isospin prediction would benefit from an evaluation at $\mathcal{O}(\alpha_s)$ of the WA contribution. This computation would also be beneficial to understand $D^0 \to Vll/\gamma$ decays [45]. For the BSM analysis a computation of QLSS within LCSR would be desirable for the reasons mentioned at the beginning of the Sec. IV B.

We explained why the K and the $K_\parallel^*$ contribution are linked at leading twist and for left-handed currents only. Thus the relation between the Kll and K^*ll asymmetry is therefore already only approximate in the SM and lost entirely should there be sizeable $V + A$ structures. In view of the experimental results we therefore conclude: Whereas it is very plausible that the K isospin asymmetry is larger or very different from the K^* isospin asymmetry, it remains mysterious at this moment why it would be sizeable at high q^2 at all. In fact, in view of this and the smallness of the prediction in the low q^2 region, cf. Fig. 6 (top, right), the measured deviation of the integrated isospin asymmetry in $B \to Kll$ of the LHCb Collaboration [2] away from zero by 4 standard deviations is somewhat puzzling. More statistics, especially in the neutral channel, is therefore eagerly awaited.

[19]Tables IX, X, and XI can be obtained from the authors upon request.

ACKNOWLEDGMENTS

This work has benefited from discussion and or correspondence with Christoph Bobeth, Greig Cowan, Ulrik Egede, Thorsten Feldmann, Gudrun Hiller, Franz Muheim, Leonardo Vernazza, and especially Steve Playfer. Part of the computations in this paper were performed by the help of FeynCalc [68]. R. Z. gratefully acknowledges the support of STFC.

APPENDIX A: $\mathcal{B}(B^0 \to K^{*0}\gamma)/\mathcal{B}(B_s \to \phi\gamma)$

The LHCb Collaboration has recently measured [58] the ratio of branching fractions of $B^0 \to K^{*0}\gamma$ to $B_s \to \phi\gamma$ to be

$$R_{K^*\phi} \equiv \frac{\mathcal{B}(B^0 \to K^{*0}\gamma)}{\mathcal{B}(B_s^0 \to \phi\gamma)} = 1.23(6)_{\rm stat}(4)_{\rm syst}(10)_{f_s/f_d}, \tag{A1}$$

where the uncertainties are statistical, systematic, and due to s, d fragmentation.

In the SM the difference to unity of (A1) is mainly due to the ratio of form factors. Generically a difference can arise from WA and this is where it connects to the rest of this work. We shall give an update of the form factor ratio below and discuss an example of how an enhancement of one of the operators in (19) can lead to sizeable deviations from the SM value.

1. Form factor ratio update

We present a phenomenological update of the form factor ratio,

$$r_{K^*\phi} = \frac{T_1^{B\to K^*\gamma}(0)}{T_1^{B_s\to\phi\gamma}(0)} = 0.89(10)\%, \tag{A2}$$

using the results in [16] with the same hadronic input as in [6]. The uncertainty consists of an estimate of violation of semiglobal quark hadron duality as well as a parametric error. The first uncertainty is obtained by varying the continuum thresholds $s_0^{B\to K^*, B_s\to\phi}$ separately and adding them in quadrature. It leads to a $\Delta_{s_0} \approx 4\%$ uncertainty. We fix $s_0^{B\to K^*}$, $s_0^{B_s\to\phi} = 35(1), 36(1)\ \mathrm{GeV}^2$ which is consistent with $s_0^{B\to K^*} - s_0^{B_s\to\phi} \approx m_{B_s}^2 - m_{B_d}^2$. The second

uncertainty is obtained by varying all other parameters and adding them in quadrature which leads to a $\Delta_{\text{para}} \approx 6\%$ uncertainty. Possibly we should add that we vary the K^* and ϕ decay constants separately but vary $f^\perp$ and $f^\parallel$ in a correlated way as the ratio is known from lattice QCD to a high precision. This leads to either a $(\Delta^2_{\text{para}} + \Delta^2_{s_0})^{1/2} = 7\%$ or $\Delta_{\text{para}} + \Delta_{s_0} = 10\%$ error depending on whether the two uncertainties are added in quadrature or linearly. We chose to quote the more conservative error in Eq. (A2) above.

It would seem worthwhile to compare the central value with previous determinations. Taking the ratio of the individual form factor predictions in [16] we get $r_{K^*\phi} = 0.95 + 0.93(a_1(K^*) - 0.1)$. In this formula $a_1^\perp(K^*) = a_1^\parallel(K^*)$ was assumed which is still a reasonable rule in view of current determinations $a_1^\perp(K^*) = 0.04(3)$ and $a_1^\parallel(K^*) = 0.06(4)$ as used in [16]. Taking the average value of the two Gegenbauer moments one gets $r_{K^*\phi} = 0.91$, a value rather close to (A2).[20]

One might further wonder why $r_{K^*\phi}$ is about 18% lower than a naive estimate $f_{K^*}^\perp/f_\phi^\perp$. We identify four main effects: (1) -6% due to $m_\phi \neq m_{K^*}$, (2) -3% $s_0^{B\to K^*} \neq s_0^{B_s\to\phi}$, (3) -5% due to $a_1(K^*) \neq a_1(\phi) = 0$, and (4) -2% due to $a_2(K^*) \neq a_2(\phi)$ which adds up to 16% and consists of the bulk effect.

2. Prediction of $\mathcal{B}(B^0 \to K^{*0}\gamma)/\mathcal{B}(B_s \to \phi\gamma)$ and BSM effect of WA

The theoretical prediction in the SM is proportional to the form factor ratio

$$R_{K^*\phi} = |r_{K^*\phi}|^2 c_{K^*\phi}(1 + \delta_{\text{WA}}) \tag{A3}$$

times a phase space factor (whose uncertainty is almost entirely from to the uncertainty in τ_{B_s})

$$c_{K^*\gamma} = \frac{\tau_{B^0}}{\tau_{B_s}}\left(\frac{m_{B^0}}{m_{B_s}}\right)^3\left(\frac{1 - m^2_{K^{*0}}/m^2_{B^0}}{1 - m^2_\phi/m^2_{B_s}}\right)^3 = 1.01(2); \tag{A4}$$

and a small correction for WA: $\delta_{\text{WA}} = -0.02(2)$. Thus essentially $R_{K^*\phi}|_{\text{SM}} \approx |r_{K^*\phi}|^2$ Finally we shall requote experimental ratio (A1) besides our prediction assembling all three quantities in (A3):

$$\begin{aligned} R_{K^*\phi}|_{\text{LHCb}} &= 1.23(6)_{\text{stat}}(4)_{\text{syst}}(10)_{f_s/f_d}, \\ R_{K^*\phi}|_{\text{LZ}} &= 0.78(18). \end{aligned} \tag{A5}$$

The theory uncertainty is almost entirely due to the form factor ratio uncertainty (A2) which is after all not small. Thus new physics would need to manifest itself rather prominently[21] in order to surface above the form factor uncertainty, the possibility of which we shall illustrate just below.

The WA processes in $B_s \to \phi$ decay couples to a unique set of operators, and so we can modify the WCs in such a way as to shift this amplitude without affecting any other process considered in this work. By way of example, making the shift $a_7^{u,d,s} \to a_7^{u,d,s} - 0.5$ leads to $\delta_{\text{WA}} \to 0.5(3)$, and therefore $R_{K^*\phi} \to 1.2(3)$, without affecting any other flavor changing neutral currents process we are considering. This result cannot be derived by a simple rescaling of the results in Table X because the effect of Gegenbauer moments in the $B_s \to \phi$ WA amplitudes are significant.

An extension of this analysis to the differential branching fractions $(B^0)B_s \to K^{*0}(\phi)\mu^+\mu^-$, which have recently been measured by the LHCb Collaboration [59], would be interesting and is deferred to later work.

APPENDIX B: DISTRIBUTION AMPLITUDES

1. Light meson DA

We shall briefly summarize and define the DA used throughout this paper. For further references we refer the reader to the classic review [60], the LCSR review [31], and the thorough paper on higher twist DA [28]. The 2-particle DA for the pseudoscalar at twist-2 (ϕ_K) and -3 ($\phi_{p,\sigma}$) (e.g. [17]) is given by

$$\begin{aligned} &\langle K(p)|\bar{s}(x)_a[x,z]q(z)_b|0\rangle \\ &= \int_0^1 du e^{i(up\cdot x + \bar{u}p\cdot z)}\Big[i\frac{f_K}{4N_c}[\not{p}\gamma_5]_{ba}\phi_K(u) \\ &\quad - i\frac{\mu_K^2}{4N_c}[\gamma_5]_{ba}\phi_p(u) - i\frac{\mu_K^2}{24N_c}p_\mu(x-z)_\nu \\ &\quad \times [\sigma^{\mu\nu}\gamma_5]_{ba}\phi_\sigma(u)\Big] + \text{higher twist}, \end{aligned} \tag{B1}$$

where a, b are Dirac indices, $\bar{u} \equiv 1 - u$, $\mu_K^2 \equiv f_K m_K^2/(m_s + m_q)$, and the $[x,z]$, here and hereafter, represent a QCD Wilson line to make the matrix element gauge invariant. The asymptotic forms[22] of the DA functions are

$$\phi_K(u) = \phi_\sigma(u) = 6\bar{u}u \qquad \phi_p(u) = 1. \tag{B2}$$

From the appendix of [17] we see that upon neglecting quark masses and 3-particle DAs, equations of motion constrain $\phi_{p,\sigma}(u)$ to their asymptotic forms. $\phi_K(u)$ is expanded in Gegenbauer moments as usual.

The 2-particle DA for the vector meson at twist-2 ($\phi_{\parallel,\perp}$) and -3 ($g_\perp^{(v,a)}$) (e.g. [16]) is

[20]In [9] $r_{K^*\phi} = 0.99(13)$ was quoted based on some input from lattice QCD on the ratio of f_{B_s}/f_{B_d} for which there is no reason if the $f_{B_{d,s}}$ are taken from sum rules to the same order which is a consistent procedure.

[21]Similar remarks would apply to ratio of the kind $\mathcal{B}(B^0 \to \rho^{*0}\gamma)/\mathcal{B}(B^0 \to \omega\gamma)$, as discussed in a previous footnote.

[22]By asymptotic we mean, as usual, for $\mu_F \to \infty$. All DA depend on the factorization scale μ_F of the LC-OPE which we do not indicate explicitly.

$$\langle K^*(p,\eta)|\bar{s}(x)_a[x,z]q(z)_b|0\rangle = \int_0^1 du e^{i(up\cdot x+\bar{u}p\cdot z)}\Big\{\frac{f_{K^*}^{\perp}}{4N_c}\Big[(\not{\eta}\not{p})_{ba}\phi_\perp(u) - \frac{i}{2}(1)_{ba}(\eta\cdot(x-z))m_{K^*}^2 h_\parallel^{(s)}(u)$$
$$- i(\sigma_{\mu\nu})_{ba}p^\mu(x-z)^\nu\frac{\eta\cdot(x-z)}{(p\cdot(x-z))^2}m_{K^*}^2 h_\parallel^{(t)}(u)\Big]$$
$$+\frac{m_{K^*}f_{K^*}}{4N_c}\Big[(\not{p})_{ba}\frac{\eta\cdot(x-z)}{p\cdot(x-z)}\phi_\parallel(u) + \Big(\not{\eta} - \not{p}\frac{\eta\cdot(x-z)}{p\cdot(x-z)}\Big)_{ba}g_\perp^{(v)}(u)$$
$$+\frac{1}{4}\epsilon_{\mu\nu\rho\sigma}\eta^\nu p^\rho(x-z)^\sigma(\gamma^\mu\gamma_5)_{ba}g_\perp^{(a)}(u)\Big]\Big\} + \text{higher twist.} \tag{B3}$$

The asymptotic DAs are

$$\phi_\perp(u) = \phi_\parallel(u) = g_\perp^{(a)}(u) = h_\parallel^{(s)}(u) = 6\bar{u}u$$
$$g_\perp^{(v)}(u) = \frac{3}{4}(1+(u-\bar{u})^2) \qquad h_\parallel^{(t)}(u) = 3(u-\bar{u})^2. \tag{B4}$$

In fact, these functions overparametrize the K^* state and are related by QCD equations of motion [28]. In the limit of three massless quark flavors, the relevant constraint for QLSS reads [8][23]

$$\int_0^u dv[\phi_\parallel(v) - g_\perp^{(v)}(v)]$$
$$= \bar{u}\Big(g_\perp^{(v)}(u) - \frac{g_\perp^{(a)\prime}(u)}{4}\Big) - \frac{g_\perp^{(a)}(u)}{4}, \tag{B5}$$

which is used to eliminate the integral from (47). We also require the identity

$$uh_\parallel^{(t)}(u) + \frac{u}{2}h_\parallel^{(s)\prime}(u) = 2\int_0^u (h_\parallel^{(t)}(v) - \phi_\perp(v))dv \tag{B6}$$

in order to show gauge invariance in O_2^{WA} results in Appendix F 3. To this end we note that Eqs. (B5) and (B6) follow from equations (4.15) and (4.16) and (3.21) and (3.22) in [28].

2. Photon DA

The leading twist 2 photon DA [27] is

$$\langle\gamma(q,\epsilon)|\bar{q}_a(x)[x,z]q_b(z)|0\rangle$$
$$= ie\int_0^1 d^4y\epsilon_\mu^* e^{iq\cdot y}\langle 0|T\bar{q}_a(x)[x,z]q_b(z)j_{\mathrm{em}}^\mu(y)|0\rangle$$
$$= \frac{iQ_q\langle\bar{q}q\rangle}{4N_c}\int_0^1 du e^{i(uq\cdot x+\bar{u}q\cdot z)}(\phi_\gamma(u)\sigma^{\alpha\beta}\epsilon_\alpha q_\beta$$
$$+ (x-z)\cdot\epsilon)_{ba} + \text{higher twist.} \tag{B7}$$

The first and second term on the last line correspond to the left-hand side of equation (2.7) of [27] and second term on the right-hand side of the same equation. The reason Eq. (B7) is not gauge invariant is that $[x,z]$ does not contain the QED (quantum electrodynamical) Wilson line as we expand in the external field to first order. Furthermore we have assumed the Lorentz gauge $\partial\cdot A = 0$ through $A_\mu \to \epsilon_\mu e^{iq\cdot x}$.[24] Note that the perturbative photon contribution has to be included separately. The asymptotic photon DA is given by

$$\phi_\gamma(u) = 6\chi\bar{u}u, \tag{B8}$$

where χ is the magnetic susceptibility of the quark condensate, calculated to be $\chi = -3.15(10)\ \mathrm{GeV}^{-2}$ at $\mu = 1$ GeV in [27] (the sign is adjusted to our convention of the covariant derivative).

3. B-meson DA

The B-meson DA used in the QLSS diagrams is given in [37,38],

$$\langle 0|\bar{q}_a(x)[x,z]b_b(0)|B(p_B)\rangle$$
$$= \frac{-if_Bm_B}{4N_c}\int_0^\infty dl_+ e^{-il\cdot x}\Big[\frac{1+\not{v}}{2}\Big\{\phi_+(l_+)\not{n}_+$$
$$+\phi_-(l_+)\Big(\not{n}_- - l_+\gamma_\perp^\nu\frac{\partial}{\partial l_\perp^\nu}\Big)\Big\}\gamma_5\Big]_{ba}\Big|_{l=\frac{l_+n_+}{2}}, \tag{B9}$$

where $p_B = m_Bv$ and n_+ and n_- are lightlike vectors

$$n_+^2 = n_-^2 = 0, \qquad n_+\cdot n_- = 2, \tag{B10}$$

for which $n_\pm = (1,0,0,\pm1)$ is a possible parametrization. This allows an arbitrary vector x to be written as

$$x^\mu = \frac{x_+n_+^\mu + x_-n_-^\mu}{2} + x_\perp^\mu \tag{B11}$$

and the scalar product of two such vectors reads:

$$x\cdot y = \frac{1}{2}(x_+y_- + x_-y_+) + x_\perp\cdot y_\perp. \tag{B12}$$

[23]This may be obtained from the Eq. (8) in [8] assuming that $\phi_\parallel(u) = \phi_\parallel(\bar{u})$ and likewise for $g_\perp^{(v)}$ and $g_\perp^{(a)}$ which is valid up to small isospin violating terms. It may more properly be derived directly from the equation of motion in [28].

[24]By working with a plane wave the Lorentz gauge is a natural choice. Note still adhering to the plane wave picture the axial gauge $n\cdot A = 0$ with $A_\mu \to (\epsilon_\mu - (n\cdot\epsilon)/(n\cdot q)q_\mu)e^{iq\cdot x}$ is an alternative. It would amount to replacing the polarization vector accordingly in the formulas above.

The kinematics required for $B \to K^{(*)}(\gamma^* \to ll)$ are

$$p_+ = m_B - \frac{q^2}{m_B}, \quad p_- = 0, \quad q_+ = \frac{q^2}{m_B}, \quad q_- = m_B, \tag{B13}$$

with $p_\perp = q_\perp = 0$.

Furthermore we take ϕ_+ and ϕ_- to be the model functions defined in [61]

$$\phi_+(\omega) = \frac{\omega}{\omega_0^2} e^{-\omega/\omega_0}, \qquad \phi_-(\omega) = \frac{1}{\omega_0} e^{-\omega/\omega_0}, \tag{B14}$$

with $\omega_0 = 2\Lambda_{\mathrm{HQET}}/3 \simeq 0.4$ GeV. Our results contain the moment functions

$$\lambda_\pm^{-1}(q^2) = \int_0^\infty dl_+ \frac{\phi_\pm(\omega)}{l_+ - q^2/m_B - i\epsilon} \tag{B15}$$

which evaluate to

$$\begin{aligned} \lambda_+^{-1}(q^2) &= \frac{1}{\omega_0}[1 + ye^{-y}(i\pi - \mathrm{Ei}(y))], \\ \lambda_-^{-1}(q^2) &= \frac{e^{-y}}{\omega_0}(i\pi - \mathrm{Ei}(y)), \end{aligned} \tag{B16}$$

where $y = q^2/\omega_0 m_B$ and the function Ei is the exponential integral.

a. On corrections for QLSS within QCDF

We would like to discuss the origin of the $\mathcal{O}(q^2/m_B^2)$ corrections due to neglecting the l_- direction and the $l_\perp$ derivative alluded to in Sec. IV. Further comments can be found in that section.

(i) *Neglecting the l_- direction:* We wish to stress a particular feature of the B-meson DA: it takes the form of a function of a light-cone coordinate. In the B-meson rest frame all components of the spectator quark momentum are expected to be of comparable magnitude $\mathcal{O}(\Lambda_{\mathrm{QCD}})$ and thus the special role of l_+ originates from the dynamics. It turns out that to leading order in $1/m_B$ the short distance part of the matrix element is only sensitive to the l_+ component of the light quark momentum,[25] and hence a light-cone DA is what is required [38]. The next-leading order diagram in Fig. 5 with photon emission next to the B meson is sensitive to $(q-l)^2 = q^2 + l^2 - q_+ l_- - q_- l_+$ [$q_\perp = 0$ in the notation of (B12)] with $q_- = m_B$ and $q_+ = m_B(q^2/m_B^2)$. Thus at $q^2 = 0$ the process depends only on the l_+ direction but becomes increasingly sensitive to the l_- direction as q^2 rises. At $q^2 = 4m_c^2$ this amounts to about a 30% effect ($q_+/q_- \simeq 0.3$).

(ii) *Neglecting the $l_\perp$ derivative:* The derivative with respect to $l_\perp$ will be $1/m_B$ suppressed, as compared to the other term coupling to $\phi_-(l_+)$, except for the case where the photon is emitted from the light quark originating from the B meson (same diagram as discussed in the previous point). The effect on the corresponding light quark propagator S_F is

$$\begin{aligned} & l_+ \gamma_\perp^\rho \frac{\partial}{\partial l_\perp^\rho} \gamma_5 \gamma^\mu S_F(q-l) \\ &= i l_+ \gamma_5 \gamma_\perp^\rho \gamma^\mu \left(\frac{\gamma_\perp^\rho}{(q-l)^2} + 2\frac{\not{q} - \not{l}}{(q-l)^4} l_\perp^\rho \right) \\ &= \mathcal{O}(\Lambda_{\mathrm{QCD}}/m_B). \end{aligned} \tag{B17}$$

This comes about as follows. The second term vanishes by setting $l_\perp = 0$ after taking the derivative. To analyze the first term we contract $\gamma_\perp^\rho \not{\epsilon} \gamma_{\perp,\rho}$ with a polarization vector ϵ_μ, using the light-cone decomposition (B11),

$$\begin{aligned} l_+ \gamma_\perp^\rho \not{\epsilon} \gamma_{\perp,\rho} &= -l_+[\not{n}_+ \epsilon_+ + \not{n}_- \epsilon_-] \\ &\quad + l_+ \underbrace{\gamma_\perp^\rho \not{\epsilon}_\perp \gamma_{\perp,\rho}}_{=0}, \end{aligned} \tag{B18}$$

where the first part must be compared with the other structure coupling to $\phi_-(l_+)$:

$$i\not{n}_- \not{\epsilon}(\not{q} - \not{l}) = \frac{i}{4}\not{n}_-[\epsilon_+ q_- + \not{\epsilon}_\perp \not{n}_+(q_+ + l_+)]. \tag{B19}$$

We therefore see that the derivative term is subleading in the ϵ_+ coefficient by $l_+/q_- = \mathcal{O}(\Lambda_{\mathrm{QCD}}/m_B)$. The ϵ_- coefficient must be related by gauge invariance; see Appendix D 2 for further discussion. At last we would like to mention that it would be interesting to study whether there is any significant change for $0 < q^2 < 4m_c^2$.

APPENDIX C: HELICITY PROJECTORS

As hinted in the main text, the basis $\mathcal{T}_{1,2,3}$, or more precisely $\mathcal{T}_{2,3}$, is not ideal for addressing physical quantities. In the decay rate this emerges in two ways. First a particular direction, namely, zero helicity has to be $\mathcal{O}(m_V)$ (10) and furthermore the directions $\mathcal{T}_{2,3}$ are not orthogonal to each other. In the main text we have given the transformation to the helicity basis $h_{0,\pm}$ in Eq. (5). We shall give the Lorentz structures for the latter and discuss a few more details. As in (3) we define

$$\begin{aligned} & {}_{\mathrm{out}}\langle V(p,\eta) l^+(l_1) l^-(l_2) \,|\, B(p+q)\rangle_{\mathrm{in}} \\ &= \frac{G_F}{\sqrt{2}} \lambda_t \frac{\alpha}{q^2 \pi} (\mathcal{T}^{V\mu} \bar{u}(l_1) \gamma_\mu v(l_2) + \mathcal{T}^{A\mu} \bar{u}(l_1) \gamma_\mu \gamma_5 v(l_2)), \end{aligned}$$

where

$$\mathcal{T}^{(V,A)\mu} = \sum_{i=\pm,0} h^{(V,A)} P_i^\mu, \tag{C1}$$

and the helicity basis tensors are given by

[25] This is the component in the lightlike direction which is parallel to the final state light meson.

$$P_{\pm}^{\mu} = \frac{1}{\sqrt{2}}\Big[2\epsilon^{\mu\nu\rho\sigma}\eta_\nu p_\rho q_\sigma \mp \frac{i}{\sqrt{\lambda_V}}(\lambda_V m_B^2 \eta^\mu - 2(\eta\cdot q) \times ((1-\hat{m}_V^2-\hat{q}^2)p^\mu - 2\hat{m}_V^2 q^\mu))\Big],$$

$$P_0^{\mu} = \frac{4i\hat{m}_V}{\sqrt{2\hat{q}^2\lambda_V}}(\eta\cdot q)[2\hat{q}^2 p^\mu - (1-\hat{m}_V^2-\hat{q}^2)q^\mu].$$

Writing $\vec{P}_h = (P_0, P_+, P_-)$ and $\vec{P} = (P_1, P_2, P_3)$, suppressing a Lorentz index for the time being, the transformation follows from the transformation (5) through $\vec{P}_h = (B^T)^{-1}\vec{P}$. The Lorentz structures have the following properties: $q\cdot P_{\pm,0} = 0$ and $p\cdot P_{\pm} = 0$. It seems worthwhile to mention that the m_V factor in P_0^μ cancels against the $1/m_V^2$ originating from the polarization sum: $\sum_{\rm pol} = \eta_\mu\eta_\nu = (p_\mu p_\nu/m_V^2 - g_{\mu\nu})$. This assures finiteness of the rate as m_V approaches zero, provided that $h_0 = \mathcal{O}(m_V^0)$.

APPENDIX D: GAUGE INVARIANCE

1. WA contact terms and gauge invariance

Before discussing the problem in more detail let us state a few general facts, some of which have already been stated in the main text.

(i) GI (23) is satisfied in Q_b and Q_q terms separately.

(ii) When there is ISR as well as FSR then one needs to approximate ISR and FSR consistently in order for (i) to be true.

(iii) In the neutral case (i.e. $Q_b = Q_q$), (ii) can be circumvented, at the cost of (i), as ISR and FSR are separately gauge invariant.

(iv) Statement (ii) can be circumvented in the case when the four quark operator is of the current-current type [$\mathcal{O}_{5-8}^{\rm WA}$ (19)]. In this case FSR corresponds to a contact term, up to corrections $\mathcal{O}(m_{q,s})$, which is easily computed using the weak WI.

In previous computations [4,5], as discussed in [29] in more clarity, (iv) applied as in the SM only $\mathcal{O}_{5-8}^{\rm WA}$ type (21) are significant in the absence of CKM suppression; then (ii) does not apply as there is either only ISR or FSR; cf. Table I. Inspecting Table I we see that $\mathcal{O}_4^{\rm WA}$ for the K is the only problematic case which we shall discuss in some more detail in Sec. D 1 a below. Furthermore statement (iv) is explained in Sec. D 1 b. The modification of the issue of contact terms for $q^2 = 0$, which implies substituting the quark condensate terms $\langle qq\rangle/q^2$ for the photon DA, is outlined in Appendix D 3 c.

a. Eliminating parasitic cuts—spurious momentum k

It is at this point we must point out that factorizing the WA matrix elements conceals a problem in constructing sum rules: the problem of parasitic cuts. As shown in Fig. 11 (left) a naïvely constructed sum rule will receive contributions from cuts which do not have the same quantum numbers as the B meson. A solution to this problem was introduced in [62] where spurious momentum k is introduced at the weak vertex, which gives the second cut in Fig. 11 (left) momentum $(p_B - k)^2$ which is distinct from p_B^2 of the first cut. How the effect of the momentum k is eliminated from the final result is to be discussed shortly below. We use the momentum assignments shown in Fig. 11 (right) and reuse the modified basis tensors from [6], which are given by

$$p_T^\rho = i\Big[Q^\rho - \frac{q^2}{Q\cdot(p_B+p)}(p_B+p)^\rho\Big],$$
$$\bar{p}_{\bar{T}}^\rho = i\Big[k^\rho - \frac{k\cdot Q}{Q\cdot(p_B+p)}(p_B+p)^\rho\Big], \tag{D1}$$

where $Q \equiv q - k$. Amongst the possible six invariants, four are fixed as

$$p^2 = m_{V,P}^2 = 0 \qquad k^2 = 0 \qquad Q^2 = q^2, \tag{D2}$$

and the remaining two invariants p_B^2 and $P^2 = (p_B - k)^2$ correspond to the two cuts shown in Fig. 11 (left). p_B^2 is the dispersion variable and the second cut variable $P^2 = (p_B - k)^2$ is the only trace of the spurious momentum. This is eliminated by setting $P^2 = m_B^2$ as $p_B^2 \simeq m_B^2$ by virtue of Eq. (29). After projection onto this extended

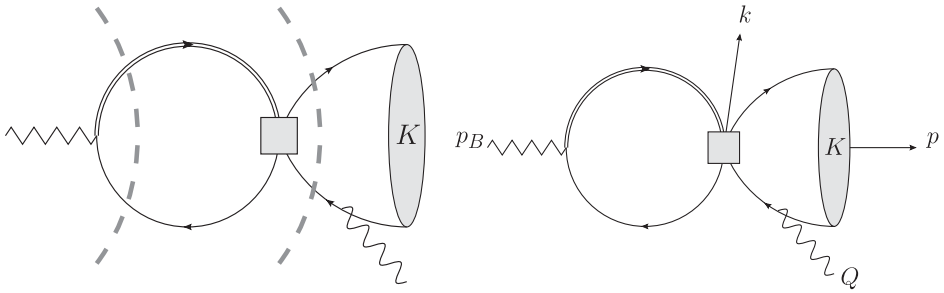

FIG. 11. Left: momentum assignments for $B \to K\gamma^*$ including an additional momentum at the weak vertex. Right: dashed lines denote possible cuts with momentum $(p+q)^2$ flowing through them, which contribute to a naïve sum rule. The right-hand cut is a parasite because the lines it cuts do not have the quantum numbers of the B meson so should not contribute to a dispersion relation for the B-meson current J_B.

basis, the coefficient of p_T^ρ corresponds to the coefficient of P_T^ρ which appears in the decay rate.

b. Vector and axial 4-quark operators and the weak WI

In this subsection we dwell in more detail on how point (iv) at the beginning of this appendix unfolds. According to statement (ii) ISR and FSR then ought to be treated consistently, as for instance outlined in the previous subsection, in order to maintain GI. The problem in distinguishing the two cuts shown in Fig. 11 (right) applies only to the FSR diagram.[26] We shall see just below that in the case where the current with kaon quantum numbers is of the vector and axial type the diagram is a pure contact term by virtue of the weak WI and only produces a gauge variant part. This means that it does not carry any nontrivial dynamics and that its sole purpose is to render the matrix element gauge invariant. Furthermore we note that adding a spurious momentum does not have any impact on the diagram. In two subsequent paragraphs we are going to show this through the weak WI and infer the same result by sketching an explicit computation.

Weak WI: Consider the FSR for the operator $\mathcal{O}_6^{\mathrm{WA}}$ at leading order $\mathcal{O}(\alpha_s^0)$,

$$\begin{aligned}\langle K^*\gamma|\bar{s}\gamma^\mu q|0\rangle\langle 0|\bar{q}\gamma_\mu\gamma_5 b|B\rangle &= -ef_B(p_B)_\mu\epsilon_\nu\int_x e^{-ip_B\cdot x}\langle K^*|T\bar{s}\gamma^\mu q(x)J^\nu_{\mathrm{em}}(0)|0\rangle\\ &= -ef_B\epsilon_\nu\int_x e^{-ip_B\cdot x}\langle K^*|i\partial_\mu\{T\bar{s}\gamma^\mu q(x)J^\nu_{\mathrm{em}}(0)\}|0\rangle\\ &= ie(Q_q-Q_s)f_B\epsilon_\nu\langle K^*(p,\eta)|\bar{s}\gamma^\nu q(0)|0\rangle\\ &= ie(Q_q-Q_s)f_Bf_{K^*}m_{K^*}(\eta\cdot\epsilon),\end{aligned} \tag{D3}$$

where we have used $\langle 0|\bar{q}\gamma_\mu\gamma_5 b(0)|B(p+q)\rangle = if_B(p+q)_\mu$ in the first equality,

$$\text{weak WI: } \partial_\mu\bar{s}\gamma^\mu q(x) = \mathcal{O}(m_s-m_q)\to 0 \tag{D4}$$

in the second equality, and $[Q,\mathcal{O}] = Q_{\mathcal{O}}\mathcal{O}$ ($Q=\int d^3x J^0_{\mathrm{em}}$) in the third equality. The last step is due to the definition of the K^* decay constant: $\langle K^*(p,\eta)|\bar{s}\gamma^\nu q(0)|0\rangle = m_{K^*}f_{K^*}\eta^\nu$. As stated previously this contribution is a pure gauge variant term. Adding a spurious momentum $p_B\to p_B-k$ would not change anything in the derivation. Similarly we find for the K,

$$\langle K\gamma|\bar{s}\gamma^\mu\gamma_5 q|0\rangle\langle 0|\bar{q}\gamma_\mu\gamma_5 b|B\rangle = e(Q_q-Q_s)f_Bf_K(p\cdot\epsilon). \tag{D5}$$

We would like to remark that the results in (D3) and (D5) are correct to all orders in QCD (with $m_q=0$).

In summary the weak WI (D4) replaces the computation. In the next paragraph we shall outline the main points of the explicit LC-OPE computation which comes to the same conclusion.

Explicit computation: we would like to mention one additional point: the reader may wonder whether we could have simply used the K^* DAs in (B3), worked out the result, and not had to concern ourselves with arguments based on WIs. It turns out that (B3) is in fact insufficient for this purpose and the Wandzura–Wilczek type relation (B5) has to be used. We have checked that this leads to the same result up to $O(m_{K^*}^2)$ terms. The latter are of twist-4 and expected to be there as we have consistently neglected them throughout this work.

c. Remarks on gauge invariance and contact terms at $q^2 = 0$

At $q^2=0$ the $\langle\bar{q}q\rangle$ term from the light quark propagator, originating from the interpolating current J_B, have to replaced by the photon DA. This gives rise to a puzzle as the former are gauge variant whereas DA are usually GI. The resolution is, as we shall see, that the photon DA is QED gauge variant.

Generally for $q^2\neq 0$ and for $\mathcal{O}_{5-8}^{\mathrm{WA}}$ the term with FSR produces solely a gauge variant contact term proportional to Q_q-Q_b; cf. (D3) as discussed in Sec. D 1 b. GI is restored by a gauge variant term coming from ISR. As discussed in the main text Sec. III E for $q^2=0$ the $Q_q\langle\bar{q}q\rangle$ is replaced by a photon DA term as depicted in Fig. 4. This means that the ISR and FSR cancellation of gauge noninvariant terms at the $(Q_q-Q_b)\langle\bar{q}q\rangle$ level implies that the matrix element used for the photon DA, which is usually gauge invariant, is gauge variant. This is indeed the case as the QED Wilson line is absent in the matrix element (B7) as we expand in the external electromagnetic field. This can be seen explicitly from the corresponding matrix element which is the sum of an explicit gauge invariant plus a gauge variant term. We have checked that, by working in the Lorentz gauge $\partial\cdot A=0$,[27] which is consistent with $A_\mu\to\epsilon_\mu e^{iq\cdot x}$, the gauge variant term [corresponding to the second term on the right-hand side of (B7)] conspires with the gauge variant terms from the other diagram in

[26]For ISR radiation the second cut corresponds to the kaon, as the momentum flowing into a 4-quark operator is the kaon final state momentum.

[27]Note, the Lorentz gauge does still allow for residual gauge transformations of the form $\epsilon_\mu\to\epsilon_\mu+q_\mu$ for example.

Fig. 2(b) (right) to produce a term proportional to $Q_q - Q_b$ which combines with the contact term Eq. (D3) and leads to a gauge invariant result.

2. QLSS and gauge invariance

The issue of GI for spectator scattering, in Sec. IV, at $q^2 \neq 0$ is not straightforward. In principle we would expect the two diagrams, by which we mean photon emission form the spectator quark, in Fig. 5 to be GI. The computation used in [11],[28] which we reproduced in this paper for non-SM operators, can only be expected to respect GI at leading order. Yet, since GI mixes different orders, a rigourous test cannot be expected. The recipe of the pragmatist is then subtract the amount of next leading term that renders the leading term GI. We shall discuss it in more detail below and see that a pole in $1/q^2$ supports our argumentation from another point of view.

In full generality, the $B \to K^* l^+ l^-$ decay may be parametrized:

$$\begin{aligned}\langle K^*(\eta, p)\gamma^*(q, \mu)|\mathcal{H}_{\text{eff}}|B(p+q)\rangle \\ \equiv U^\mu(q^2) = (\eta\cdot q)p^\mu U_p(q^2) + (\eta\cdot q)q^\mu U_q(q^2) \\ + \eta^\mu(p\cdot q)U_\eta(q^2) + i\epsilon^{\mu\nu\rho\sigma}\eta_\nu p_\rho q_\sigma U_\epsilon(q^2). \quad \text{(D6)}\end{aligned}$$

QED GI requires the following WI to hold:

$$\begin{aligned}0 = q_\mu U^\mu(q^2) \\ = (\eta\cdot q)[(p\cdot q)U_p(q^2) + q^2 U_q(q^2) + (p\cdot q)U_\eta(q^2)].\end{aligned} \quad \text{(D7)}$$

In the best of all worlds, where GI is obeyed exactly, we may choose to eliminate any function by virtue of the equation above. For example we could solve for either

$$\times \quad U_q(q^2) \to -\frac{p\cdot q}{q^2}[U_p(q^2) + U_\eta(q^2)], \quad \text{(D8)}$$

$$\checkmark \quad U_p(q^2) \to -U_\eta(q^2) - \frac{q^2}{p\cdot q}U_q(q^2). \quad \text{(D9)}$$

For (D8) to be well defined the following relation must hold:

$$U_p(0) + U_\eta(0) = 0, \quad \text{(D10)}$$

or $U_q(q^2)$ behaves as $1/q^2$, which is not acceptable.[29] Since $U_p p_\mu$ is power suppressed with respect to $U_q q_\mu$, cf. (B13), we cannot expect (D10) to hold; however, applying (D9) does work since in contrast to (D8) it does not contain any m_B^2/q^2 enhancement. Note for the K meson the same discussion applies with $U_\eta|_K = 0$ from the start. The term U_ϵ is of no relevance for the discussion here.

We will illustrate this procedure in the case of $B \to K l^+ l^-$. The result in this case is

$$\begin{aligned}U^\mu &\propto \frac{(l_+ m_B - 2q^2)p^\mu + 2(p\cdot q)q^\mu}{l_+ m_B - q^2} \\ &= 2\frac{(p\cdot q)q^\mu - q^2 p^\mu}{l_+ m_B - q^2} + \frac{l_+ m_B p^\mu}{l_+ m_B - q^2}.\end{aligned} \quad \text{(D11)}$$

Our procedure (D9) ($U_\eta|_K = 0$) demands that $U_p = -(q^2/(p\cdot q))2(p\cdot q)(l_+ m_B - q^2)$, which amounts to dropping the second term on the right-hand side. This ensures GI. We reemphasize that if the $1/m_b$ expansion was implemented to all orders GI would have been automatic.

APPENDIX E: DETAILS OF CALCULATION

1. Input values

Here we summarize the numerical input to our calculation for the convenience of the reader. We compute α_s using 2-loop running with 4 or 5 active flavors, with $M_Z = 91.1876(21)$ GeV, $\alpha_s(M_Z) = 0.1184(7)$, and $m_b(m_b) = 4.18(3)$ GeV in the $\overline{\text{MS}}$ scheme [20]. We use b and c quark masses adapted for the pole mass scheme $m_c = 1.4(1)$ and $m_b = 4.7(1)$ GeV in all other cases. We use a lattice average $f_B = 191(5)$ [35,36] when not calculating sum rules, i.e. in the computation of $F_{(2,4),i}$ (33). Inputs used to compute WCs are given below Table VIII. We compute the CKM matrix elements using a Wolfenstein

TABLE VIII. WCs at $\mu = m_b$ and $\mu = \sqrt{m_b \Lambda_H}$ at NNLL order for $m_b = 4.7$ GeV, $M_W = 80.4$ GeV, $\sin^2\theta_W = 0.23$, $m_t = 177$ GeV, $\Lambda_H = 0.5$ GeV, and $\Lambda^{(5)}_{\text{QCD}} = 214$ MeV in two different bases. Three loop running for α_s is used. The BBL basis we use is that defined in [14]; it is equivalent to the traditional basis defined in [13] at leading order. We use the CMM basis [15] for loop calculations. The BBL coefficients presented here are defined in terms of a linear transform of the CMM coefficients as explained in the text.

	$\mu = m_b$		$\mu = \sqrt{m_b\Lambda_H}$	
	CMM	BBL	CMM	BBL
C_1	−0.2622	−0.1311	−0.5636	−0.2818
C_2	1.0087	1.0524	1.0299	1.1238
C_3	−0.0051	0.0110	−0.0175	0.0194
C_4	−0.0778	−0.0316	−0.1718	−0.0524
C_5	0.0003	0.0087	0.0012	0.0132
C_6	0.0009	−0.0371	0.0042	−0.0775
C_7^{eff}	−0.2975		−0.3351	
C_8^{eff}	−0.1569		−0.1828	
C_9	4.0354		4.4207	
C_{10}	−4.2496		−4.2496	

[28] These authors do not discuss the QED GI.

[29] More precisely integrability of the rate, which we expect, is incompatible with $1/q^2$ behavior. Note this pole cannot be compensated by virtual correction as in $\gamma \to ll$ which leads to $1/q^2$ in $|h_\pm|^2$ (7).

parametrization expanding up to $\mathcal{O}(\lambda^2)$ [63,64] with the parameters $\lambda = 0.2254(7)$, $A = 0.81(2)$, $\bar{\rho} = 0.131(26)$, and $\bar{\eta} = 0.345(14)$ [20]. For the α_{CKM} dependence of δ_{a_l} (73), we fix the magnitude $|\lambda_u/\lambda_t|$ from the Wolfenstein parametrization. All hadronic inputs for the light mesons are as given in our previous paper [6]. The new input $\mu_K^2 = f_K m_K^2/m_s$ is computed using $m_s(2\ \mathrm{GeV}) = 95(5)$ MeV [20]. The condensates $\langle\bar{q}q\rangle$ and $\langle\bar{q}Gq\rangle$ are taken to be $\langle\bar{q}q\rangle(1\ \mathrm{GeV}) = (-0.24(1)\ \mathrm{GeV})^3$ and $\langle\bar{q}Gq\rangle(1\ \mathrm{GeV}) = (0.8(1)\ \mathrm{GeV})^2\langle\bar{q}q\rangle$ [6].

2. Error estimation

We compute error estimates in the following way: the central value of a result is computed using the central values of all inputs. To compute the error, we then generate a list of pseudorandom sample points from the probability distributions of the input parameters, and compute the result for each sample point.

For a function $f(x)$, where x represents all N input parameters and is thus N dimensional, the variance is estimated as

$$\sigma^2 = \frac{1}{n-1}\sum_{i=1}^{n}(f(x_i) - f(x_c))^2, \tag{E1}$$

where x_c is the central values of the input parameters, and not included in x_i, and n is the number of sample points used to compute an error estimate, excluding the central value x_c. The points x_i are generated from the N-dimensional probability distribution of input parameters; note that x_i is varied for all parameters simultaneously, so *none* of its elements are equal to the central value of any input parameter. In effect, this is a primitive Monte Carlo integration over the input parameter distribution space. All input parameters are assumed to be Gaussian distributed with standard deviation equal to their quoted error, except for the renormalization scale, to be discussed below. We assign the functions $h_{0,\pm}$ and h_T an error of 20%, which arises from the uncertainty in the form factors T_i, $A_{1,3}$, V, and $f_{+,T}$ and nonform factor corrections. We impose this at the level of the h functions so that constraints such as (10) and $h_+ \sim \mathcal{O}(1/m_B)$ are maintained.

To compute the scale uncertainty only 3 points are sampled: μ, $\mu/2$, and 2μ. The renormalization scale is set to μ to compute the central value of a result. The error is computed as

$$\sigma_\mu^2 = \frac{1}{2n-1}\sum_{i=1}^{n}\left[\left(f\left(\frac{\mu}{2}\right) - f(\mu)\right)^2 + (f(2\mu) - f(\mu))^2\right], \tag{E2}$$

although in practice this is implemented by generating a $2n$ pseudorandom number y_i in [0,1] and selecting $\mu/2$ or 2μ depending on whether $y > 0.5$. This may then be incorporated into the same procedure as sampling all other input parameters. We take the central renormalization scale $\mu = m_b = 4.7$ GeV for all processes except QLSS and $\mathcal{O}_8$, which we take to be $\mu' = \sqrt{\Lambda_H \mu}$, where $\Lambda_H = 0.5(2)$ GeV as in [6].

3. Wilson coefficients

Although we specify our results in the BBL basis [13] our calculation is carried out in the CMM basis [15]

$$\mathcal{H}_{\mathrm{eff}} = \frac{G_F}{\sqrt{2}}\left(\sum_{i=1}^{2}(\lambda_u C_i^{\mathrm{CMM}}\mathcal{Q}_i^u + \lambda_c C_i^{\mathrm{CMM}}\mathcal{Q}_i^c) - \lambda_t\sum_{i=3}^{10} C_i^{\mathrm{CMM}}\mathcal{Q}_i\right), \tag{E3}$$

where $\mathcal{Q}_{7-10} = \mathcal{O}_{7-10}$ and the four quark operators are given by

$$\begin{aligned}
\mathcal{Q}_1^q &= 4(\bar{s}_L\gamma_\mu T^a q_L)(\bar{q}\gamma^\mu T^a b_L),\\
\mathcal{Q}_2^q &= 4(\bar{s}_L\gamma_\mu q_L)(\bar{q}\gamma^\mu b_L),\\
\mathcal{Q}_3 &= 4(\bar{s}_L\gamma_\mu b_L)\sum_q(\bar{q}\gamma^\mu q),\\
\mathcal{Q}_4 &= 4(\bar{s}_L\gamma_\mu T^a b_L)\sum_q(\bar{q}\gamma^\mu T^a q),\\
\mathcal{Q}_5 &= 4(\bar{s}_L\gamma_\mu\gamma_\nu\gamma_\rho b_L)\sum_q(\bar{q}\gamma^\mu\gamma^\nu\gamma^\rho q),\\
\mathcal{Q}_6 &= 4(\bar{s}_L\gamma_\mu\gamma_\nu\gamma_\rho T^a b_L)\sum_q(\bar{q}\gamma^\mu\gamma^\nu\gamma^\rho T^a q),
\end{aligned} \tag{E4}$$

with $2q_L = (1-\gamma_5)q$. We transform into the BBL basis following the recipe in Appendix A of [14]; our C_i are equivalent to the $\bar{C}_i$ in [14] and are *defined* by a linear transform from C_i^{CMM}. This linear transform reproduces BBL WCs at $O(\alpha_s^0)$.

We calculate the WCs to NNLL order. The calculation is carried out as described in the appendix of [14] using the full anomalous dimension matrix computed in [65], at fixed $N_f = 5$, and initial conditions are computed at $\mu = M_W$ as described therein using the NNLO expressions in [66] for C_{1-6} and $C_{9,10}$ and those in [67] for $C_{7,8}^{\mathrm{eff}}$. An example of the result of this calculation is given in Table VIII.

4. Numerical evaluation of δ_{a_l} from PDG values

In terms of experimentally measured quantities, δ_{a_l} is

$$\delta_{a_l} = 1 - \left|\frac{V_{\mathrm{ts}}}{V_{\mathrm{td}}}\right|\frac{2\frac{\tau_{B^+}}{\tau_{B^0}}\mathcal{B}(B^0\to\rho^0\gamma) - \mathcal{B}(B^+\to\rho^+\gamma)}{\frac{\tau_{B^+}}{\tau_{B^0}}\mathcal{B}(B^0\to K^{*0}\gamma) - \mathcal{B}(B^+\to K^{*+}\gamma)} \times\sqrt{\frac{\frac{\tau_{B^+}}{\tau_{B^0}}\mathcal{B}(B^0\to K^{*0}\gamma) + \mathcal{B}(B^+\to K^{*+}\gamma)}{2\frac{\tau_{B^+}}{\tau_{B^0}}\mathcal{B}(B^0\to\rho^0\gamma) + \mathcal{B}(B^+\to\rho^+\gamma)}}. \tag{E5}$$

We use the values [20]

$$\frac{\tau_{B^+}}{\tau_{B^0}} = 1.079(7), \qquad \left|\frac{V_{td}}{V_{ts}}\right| = 0.211(7),$$
$$\mathcal{B}(B^+ \to \rho^+\gamma) = 9.8(2.5) \times 10^{-7},$$
$$\mathcal{B}(B^0 \to \rho^0\gamma) = 8.6(1.5) \times 10^{-7},$$
$$\mathcal{B}(B^+ \to K^{*+}\gamma) = 4.21(18) \times 10^{-5},$$
$$\mathcal{B}(B^0 \to K^{*0}\gamma) = 4.33(15) \times 10^{-5}, \tag{E6}$$

and combine all errors in quadrature to get the result (77). The main error comes from the ratio of differences, that is to say the isospin asymmetries themselves, with approximately equal parts from the numerator and the denominator.

APPENDIX F: RESULTS

1. Tabulated results for four Fermi operators

We provide numerical data corresponding to Figs. 6 and 8 in Tables X and IX, at 1 GeV^2 intervals in q^2. Data for Figs. 7 and 9 are given in Table XI. We also provide data for $B \to (K^*, \rho)\gamma$, denoted by $q^2 = 0$ in Tables X and XI, respectively.

2. Effective coefficients in $B^0 \to \rho^0$ decay

Here we collect the formulas for $\tilde{a}_i^d$ omitted from Sec. VI.

$$\tilde{a}_2^d = a_2^d + \frac{1}{6}(-a_2^u - a_3^u + 4a_6^u - 4a_7^u + 3a_{10}^u) + \frac{2}{9}(-a_2^{8u} - a_3^{8u} + 4a_6^{8u} - 4a_7^{8u} + 3a_{10}^{8u}) + \frac{1}{12}(-a_2^d - a_3^d + 4a_6^d - 4a_7^d + 3a_{10}^d) + \frac{1}{9}(-a_2^{8d} - a_3^{8d} + 4a_6^{8d} - 4a_7^{8d} + 3a_{10}^{8d}), \tag{F1}$$

$$\tilde{a}_4^d = a_4^d + \frac{1}{6}(-a_1^u - a_4^u + 4a_5^u - 4a_8^u + 3a_9^u) + \frac{2}{9}(-a_1^{8u} - a_4^{8u} + 4a_5^{8u} - 4a_8^{8u} + 3a_9^{8u}) + \frac{1}{12}(-a_1^d - a_4^d + 4a_5^d - 4a_8^d + 3a_9^d) + \frac{1}{9}(-a_1^{8d} - a_4^{8d} + 4a_5^{8d} - 4a_8^{8d} + 3a_9^{8d}), \tag{F2}$$

$$\tilde{a}_5^d = a_5^d + \frac{1}{12}(2(a_5^d - a_5^u) + 2(a_8^d - a_8^u) + (a_4^d - a_4^u) - (a_1^d - a_1^u)) + \frac{1}{9}(2(a_5^{8d} - a_5^{8u}) + 2(a_8^{8d} - a_8^{8u}) + (a_4^{8d} - a_4^{8u}) - (a_1^{8d} - a_1^{8u})), \tag{F3}$$

TABLE IX. Breakdown of contributions to $B \to Kll$ isospin asymmetry in SM operator coefficients C_i, and in a generalized basis of four quark WA operators with coefficients a_i and QLSS contributions with coefficients $s^q_{x\chi}$. We use $a_i^q = 0.1$ and $s^q_{x,\chi} = 1$ to produce these values.

	q^2/GeV^2							
$B \to Kll$	1	2	3	4	5	6	7	8
$a_4^u = 0.1$	0.35%	0.14%	−0.03%	−0.15%	−0.23%	−0.27%	−0.28%	−0.25%
a_8^u	0.68%	0.60%	0.63%	0.64%	0.62%	0.58%	0.53%	0.47%
a_4^d	−0.10%	−0.13%	−0.18%	−0.21%	−0.22%	−0.23%	−0.22%	−0.20%
a_8^d	0.35%	0.31%	0.33%	0.33%	0.32%	0.30%	0.27%	0.24%
$s^{SU(3)}_{1(R,L)} = 1$	1.28%	0.68%	0.35%	0.18%	0.08%	0.04%	0.01%	−0.01%
$s^c_{1(R,L)}$	0.88%	0.60%	0.39%	0.25%	0.16%	0.11%	0.07%	0.04%
$s^b_{1(R,L)}$	−0.20%	−0.34%	−0.31%	−0.25%	−0.20%	−0.15%	−0.12%	−0.09%
$s^c_{2(R,L)}$	−4.68%	−3.94%	−3.13%	−2.46%	−1.96%	−1.57%	−1.25%	−0.91%
$s^b_{2(R,L)}$	5.03%	1.75%	0.03%	−1.04%	−1.76%	−2.25%	−2.51%	−2.44%
C_1 Table VIII	−0.00%	−0.00%	−0.00%	−0.00%	−0.00%	−0.00%	−0.00%	−0.00%
C_2	−0.84%	−0.45%	−0.22%	−0.10%	−0.03%	0.01%	0.03%	0.04%
C_3	0.02%	0.04%	0.04%	0.04%	0.04%	0.04%	0.03%	0.03%
C_4	−0.11%	−0.21%	−0.28%	−0.31%	−0.31%	−0.29%	−0.27%	−0.24%
C_5	0.01%	−0.00%	−0.01%	−0.02%	−0.03%	−0.03%	−0.03%	−0.03%
C_6	0.20%	0.23%	0.30%	0.35%	0.39%	0.41%	0.39%	0.34%
C_8^{eff}	−0.22%	−0.09%	−0.02%	0.02%	0.05%	0.08%	0.09%	0.09%
SM total	−0.93%	−0.48%	−0.20%	−0.01%	0.12%	0.20%	0.24%	0.24%

TABLE X. Breakdown of contributions to $B \to K^* ll$ isospin asymmetry in SM operator coefficients C_i, and in a generalized basis of four quark WA operators with coefficients a_i and QLSS contributions with coefficients $s^q_{x\chi}$. We use $a^q_i = 0.1$ and $s^q_{x,\chi} = 1$ to produce these values. The $q^2 = 0$ value corresponds to the process $B \to K^* \gamma$ and is computed slightly differently to $B \to K^* ll$ as described in Sec. III E. The value for s^f_{1R} and s^f_{2L} are zero at $q^2 = 0$ as a consequence of $h_+(0) = 0$ in our approximation.

	q^2/GeV^2								
$B \to K^* ll$	0	1	2	3	4	5	6	7	8
$a^u_2 = 0.1$	−1.55%	−0.22%	−0.00%	0.06%	0.08%	0.08%	0.07%	0.06%	0.06%
a^u_4	−1.58%	−0.33%	−0.09%	−0.00%	0.02%	0.03%	0.04%	0.03%	0.03%
a^u_5	1.29%	−0.07%	0.02%	0.00%	−0.00%	0.00%	0.01%	0.02%	0.03%
a^u_6	−0.84%	−0.53%	−0.64%	−0.67%	−0.65%	−0.60%	−0.54%	−0.47%	−0.42%
a^u_9	10.3%	−0.20%	0.23%	0.03%	−0.02%	0.02%	0.10%	0.17%	0.26%
a^u_{10}	10.5%	0.43%	0.40%	0.13%	0.08%	0.14%	0.24%	0.34%	0.47%
$a^d_2 = 0.1$	−2.85%	−0.40%	−0.00%	0.12%	0.15%	0.15%	0.14%	0.12%	0.11%
a^d_4	−2.91%	−0.61%	−0.17%	−0.01%	0.05%	0.07%	0.07%	0.07%	0.06%
a^d_5	0.78%	0.00%	0.02%	0.00%	−0.00%	−0.00%	−0.00%	0.00%	0.01%
a^d_6	−0.50%	−0.30%	−0.34%	−0.35%	−0.33%	−0.31%	−0.27%	−0.24%	−0.21%
a^d_9	6.23%	0.18%	0.20%	0.02%	−0.04%	−0.03%	0.00%	0.04%	0.08%
a^d_{10}	6.29%	0.45%	0.24%	0.03%	−0.03%	−0.01%	0.04%	0.09%	0.16%
$s^{SU(3)}_{1R} = 1$	0.00%	−1.26%	−0.75%	−0.38%	−0.18%	−0.08%	−0.03%	−0.01%	0.00%
s^c_{1R}	0.00%	−0.90%	−0.67%	−0.43%	−0.26%	−0.16%	−0.10%	−0.06%	−0.03%
s^b_{1R}	0.01%	0.20%	0.38%	0.34%	0.26%	0.19%	0.14%	0.10%	0.08%
$s^{SU(3)}_{1L}$	−0.28%	0.81%	0.58%	0.36%	0.21%	0.12%	0.06%	0.03%	−0.00%
s^c_{1L}	−0.40%	0.67%	0.57%	0.42%	0.30%	0.22%	0.16%	0.11%	0.07%
s^b_{1L}	0.95%	−0.00%	−0.28%	−0.33%	−0.31%	−0.26%	−0.22%	−0.18%	−0.14%
s^c_{2R}	1.59%	−1.82%	−1.96%	−1.64%	−1.27%	−0.97%	−0.73%	−0.54%	−0.36%
s^b_{2R}	5.03%	8.33%	3.25%	0.12%	−1.56%	−2.38%	−2.67%	−2.62%	−2.28%
s^c_{2L}	0.02%	2.43%	2.21%	1.66%	1.19%	0.85%	0.61%	0.44%	0.29%
s^b_{2L}	0.05%	−4.60%	−1.84%	−0.05%	0.98%	1.56%	1.83%	1.88%	1.69%
C_1 Table VIII	−0.01%	−0.00%	−0.00%	−0.00%	−0.00%	−0.00%	−0.00%	−0.00%	−0.00%
C_2	0.11%	−0.71%	−0.44%	−0.24%	−0.12%	−0.06%	−0.02%	0.01%	0.03%
C_3	0.09%	0.01%	0.04%	0.04%	0.05%	0.04%	0.04%	0.03%	0.03%
C_4	−0.98%	−0.08%	−0.25%	−0.30%	−0.31%	−0.30%	−0.28%	−0.26%	−0.24%
C_5	−0.51%	−0.09%	−0.02%	0.01%	0.02%	0.02%	0.02%	0.02%	0.01%
C_6	6.41%	1.40%	0.40%	0.03%	−0.11%	−0.17%	−0.18%	−0.18%	−0.17%
C^{eff}_8	−0.19%	−0.34%	−0.14%	−0.02%	0.05%	0.09%	0.10%	0.10%	0.09%
SM total	4.92%	0.18%	−0.42%	−0.48%	−0.44%	−0.38%	−0.33%	−0.28%	−0.24%

$$\tilde{a}^d_6 = a^d_6 + \frac{1}{12}(2(a^d_6 - a^u_6) + 2(a^d_7 - a^u_7) + (a^d_2 - a^u_2) - (a^d_3 - a^u_3)) + \frac{1}{9}(2(a^{8d}_6 - a^{8u}_6) + 2(a^{8d}_7 - a^{8u}_7) + (a^{8d}_2 - a^{8u}_2) - (a^{8d}_3 - a^{8u}_3)), \tag{F4}$$

$$\tilde{a}^d_9 = a^d_9 + \frac{1}{6}(a^d_9 - a^u_9) + \frac{1}{12}((a^d_1 - a^u_1) + (a^d_4 - a^u_4)) + \frac{1}{9}((a^{8d}_1 - a^{8u}_1) + (a^{8d}_4 - a^{8u}_4)), \tag{F5}$$

$$\tilde{a}^d_{10} = a^d_{10} + \frac{1}{6}(a^d_{10} - a^u_{10}) + \frac{1}{12}((a^d_2 - a^u_2) + (a^d_3 - a^u_3)) + \frac{1}{9}((a^{8d}_2 - a^{8u}_2) + (a^{8d}_3 - a^{8u}_3)). \tag{F6}$$

a. Effective coefficients in $B^0 \to \rho^0$ decay in the SM

The effective coefficients in $B^0 \to \rho^0$ decay in the SM for $B^0 \to \rho^0$ are

TABLE XI. Breakdown of contributions to $B \to \rho ll$ isospin asymmetry in SM operator coefficients C_i, and in a generalized basis of four quark WA operators with coefficients a_i and QLSS contributions with coefficients $s^q_{x\chi}$. We use $a^u_i = 0.1$, $\tilde{a}^d_i = 0.1$ and $s^q_{x,\chi} = 1$ to produce these values. The modified four quark coefficients $\tilde{a}_i$ are explained in Sec. VI. The $q^2 = 0$ value corresponds to the process $B \to \rho\gamma$ and is computed slightly differently to $B \to \rho ll$ as described in Sec. III E. The value for s^f_{1R} and s^f_{2L} are zero at $q^2 = 0$ as a consequence of $h_+(0) = 0$ in our approximation.

	q^2/GeV^2								
$B \to \rho ll$	0	1	2	3	4	5	6	7	8
$a^u_2 = 0.1$	−1.55%	−0.23%	−0.01%	0.05%	0.07%	0.07%	0.07%	0.06%	0.06%
a^u_4	−1.59%	−0.33%	−0.09%	−0.01%	0.02%	0.04%	0.04%	0.04%	0.03%
a^u_5	1.25%	−0.06%	0.02%	0.00%	−0.00%	0.00%	0.01%	0.02%	0.03%
a^u_6	−0.81%	−0.62%	−0.72%	−0.74%	−0.71%	−0.66%	−0.59%	−0.52%	−0.46%
a^u_9	11.0%	−0.20%	0.26%	0.04%	−0.02%	0.03%	0.11%	0.19%	0.28%
a^u_{10}	11.1%	0.45%	0.43%	0.14%	0.07%	0.12%	0.23%	0.33%	0.47%
$\tilde{a}^d_2 = 0.1$	−3.10%	−0.46%	−0.03%	0.11%	0.14%	0.15%	0.14%	0.12%	0.11%
$\tilde{a}^d_4$	−3.17%	−0.65%	−0.18%	−0.01%	0.05%	0.07%	0.07%	0.07%	0.07%
$\tilde{a}^d_5$	0.76%	0.00%	0.02%	0.00%	−0.00%	−0.00%	−0.00%	0.00%	0.01%
$\tilde{a}^d_6$	−0.48%	−0.34%	−0.38%	−0.38%	−0.37%	−0.34%	−0.30%	−0.26%	−0.23%
$\tilde{a}^d_9$	6.62%	0.19%	0.22%	0.03%	−0.04%	−0.03%	0.00%	0.04%	0.09%
$\tilde{a}^d_{10}$	6.68%	0.48%	0.27%	0.04%	−0.03%	−0.01%	0.03%	0.09%	0.16%
$s^{SU(3)}_{1R} = 1$	0.00%	−1.39%	−0.81%	−0.41%	−0.19%	−0.08%	−0.03%	−0.01%	0.00%
s^c_{1R}	0.00%	−1.01%	−0.74%	−0.47%	−0.28%	−0.17%	−0.10%	−0.06%	−0.03%
s^b_{1R}	0.01%	0.22%	0.42%	0.37%	0.29%	0.21%	0.15%	0.11%	0.08%
$s^{SU(3)}_{1L}$	−0.40%	0.94%	0.64%	0.39%	0.22%	0.12%	0.06%	0.03%	−0.00%
s^c_{1L}	−0.44%	0.77%	0.64%	0.45%	0.32%	0.23%	0.16%	0.12%	0.07%
s^b_{1L}	1.12%	0.00%	−0.31%	−0.36%	−0.33%	−0.28%	−0.23%	−0.19%	−0.15%
s^c_{2R}	1.76%	−2.05%	−2.13%	−1.74%	−1.34%	−1.01%	−0.76%	−0.57%	−0.38%
s^b_{2R}	4.02%	8.46%	3.29%	0.06%	−1.70%	−2.55%	−2.86%	−2.82%	−2.47%
s^c_{2L}	0.02%	2.69%	2.38%	1.76%	1.26%	0.89%	0.64%	0.46%	0.30%
s^b_{2L}	0.05%	−4.81%	−1.85%	0.03%	1.11%	1.70%	1.99%	2.04%	1.83%
C_1 Table VIII	0.01%	0.02%	0.01%	0.01%	0.00%	0.00%	−0.00%	−0.00%	−0.00%
C_2	0.01%	−1.46%	−1.00%	−0.65%	−0.40%	−0.23%	−0.11%	−0.02%	0.09%
C_3	0.08%	0.01%	0.04%	0.05%	0.05%	0.05%	0.04%	0.04%	0.03%
C_4	−0.93%	−0.09%	−0.28%	−0.34%	−0.35%	−0.33%	−0.31%	−0.28%	−0.26%
C_5	−0.54%	−0.10%	−0.02%	0.01%	0.02%	0.02%	0.02%	0.02%	0.01%
C_6	6.74%	1.51%	0.46%	0.06%	−0.10%	−0.16%	−0.18%	−0.18%	−0.18%
C^{eff}_8	−0.14%	−0.35%	−0.14%	−0.01%	0.06%	0.09%	0.11%	0.11%	0.09%
SM total	5.22%	−0.45%	−0.93%	−0.87%	−0.72%	−0.57%	−0.43%	−0.32%	−0.21%

$$\begin{aligned}
\tilde{a}^d_2 &= \tilde{a}^d_4 = 2\left(\frac{C_5}{N_c} + C_6\right),\\
\tilde{a}^d_5 &= -\tilde{a}^d_6 = \left(\frac{C_3}{N_c} + C_4\right) + \frac{\lambda_u}{\lambda_t}\left(C_1 + \frac{C_2}{N_c}\right),\\
\tilde{a}^d_9 &= \tilde{a}^d_{10} = 0,
\end{aligned} \tag{F7}$$

where we have used the formulas of the previous section and Eqs. (21) and (67) Note, we recognize the well-known color suppressed tree-level combination $C_1 + C_2/N_c$ in the formula above.

3. Weak annihilation formulas

We list the functions defined on the right-hand side of (33). Any function not listed is zero and there are many as can be inferred from Table I. The functions ρ_{C_b} an ρ_{C_d} are derived from the dispersion representation of the Passarino-Veltman functions

$$\begin{aligned}
C_b &= C_0(p_B^2, p_B^2 - m_B^2, q^2, 0, m_b^2, 0),\\
C_d &= C_0(p_B^2, p_B^2 - m_B^2, q^2, m_b^2, 0, m_b^2),
\end{aligned} \tag{F8}$$

which are given in Appendix H of [6] (note that $C_b = C_a|_{u=1}$ and $C_d = C_c|_{u=1}$).

The functions in (33) which apply at $|q^2| > 1$ GeV^2 are given in Sec. F 6 a, and the functions in (36) which apply at $q^2 = 0$ are given in Sec. F 6 b.

a. WA formulas $|q^2| > 1$ GeV^2

Defining, as before, $d \equiv -\frac{\sqrt{2}m_B m_V}{\sqrt{q^2}E}$, we get,

$$f^q_{2,A}(q^2,u) = 2\pi^2\phi_\perp(u)\left(\frac{Q_q}{(u-1)m_B^2 - uq^2} - \frac{Q_b}{um_B^2 - uq^2 + q^2}\right), \tag{F9}$$

$$d\cdot f^q_{2,0}(q^2,u) = \frac{32\pi^2 m_{K^*}^2 m_B^2}{(m_B^2-q^2)^2} h_\parallel^{(s)\prime}(u)\left[\frac{\bar{u}Q_b}{um_B^2 + \bar{u}q^2} - \frac{uQ_q}{\bar{u}m_B^2 + uq^2}\right], \tag{F10}$$

$$f^q_{4,V}(q^2,u) = -2\pi^2\phi_\perp(u)\left(\frac{Q_b}{um_B^2 - uq^2 + q^2} + \frac{Q_q}{-um_B^2 + m_B^2 + uq^2}\right), \tag{F11}$$

$$\begin{aligned}\rho^q_{5,V}(q^2,s) = \frac{3}{2}m_b f_{K^*} m_{K^*}(s(s-q^2)^3)^{-1}\Big((m_b^2-s)(Q_b-Q_q)(s^2-(q^2)^2) - sQ_b(2m_b^2q^2 - sq^2 + s^2)\\ \times\log\left(\frac{sm_b^2}{m_b^2q^2 - sq^2 + s^2}\right) + sQ_q q^2(2m_b^2 + q^2 - s)\log\left(\frac{s(m_b^2+q^2-s)}{m_b^2q^2}\right)\Big),\end{aligned} \tag{F12}$$

$$V^q_{5,V}(q^2) = \frac{2\pi^2 f_{K^*} m_{K^*}(m_b^2Q_q - Q_b q^2)}{m_b^2 q^2}, \tag{F13}$$

$$\begin{aligned}\rho^q_{6,A}(q^2,s) = \frac{3}{2}m_b f_{K^*} m_{K^*}(s^2(s-q^2)^3(q^2-m_B^2))^{-1}\Big((m_b^2-s)(s-q^2)(m_b^2(Q_b-Q_q)(-sq^2+(q^2)^2+2s^2)\\ - s(s-q^2)(s(Q_b-Q_q) - 2Q_b q^2)) + s^2Q_q q^2(-2m_b^2(s-q^2) + 2m_b^4 + (s-q^2)^2)\log\left(\frac{s(m_b^2+q^2-s)}{m_b^2q^2}\right)\\ + s^2Q_b(-2sm_b^2(s-q^2) - 2m_b^4q^2 + s(s-q^2)^2)\log\left(\frac{sm_b^2}{m_b^2q^2 - sq^2 + s^2}\right)\Big),\end{aligned} \tag{F14}$$

$$V^q_{6,A}(q^2) = -\frac{2\pi^2 f_{K^*} m_{K^*}(-m_b^2q^2(Q_b - 3Q_q) + m_b^4Q_q + Q_b(q^2)^2)}{m_b^2q^2(m_B^2 - q^2)}, \tag{F15}$$

$$\begin{aligned}d\cdot\rho^q_{6,0}(q^2,s) = 3m_b m_B^2 f_{K^*} m_{K^*}(s^2(s-q^2)^3(m_B^2-q^2))^{-1}\Big(2s^2m_b^4Q_b\log\left(\frac{sm_b^2}{m_b^2q^2 - sq^2 + s^2}\right)\\ - 2s^2m_b^2Q_q(m_b^2 + q^2 - s)\log\left(\frac{s(m_b^2+q^2-s)}{m_b^2q^2}\right)\\ + (m_b^2-s)(Q_b-Q_q)(s-q^2)(m_b^2(q^2-3s) + s(s-q^2))\Big),\end{aligned} \tag{F16}$$

$$d\cdot V^q_{6,0}(q^2) = \frac{8\pi^2 m_B^2 f_{K^*} m_{K^*} Q_q}{q^2(m_B^2 - q^2)}, \tag{F17}$$

$$\rho^q_{9,V}(q^2,s) = \frac{3}{2}(s(s-q^2)^3)^{-1} f^{\perp}_{K^*}\Big(-2sm_b^4 Q_b q^2 \log\Big(\frac{sm_b^2}{m_b^2 q^2 - sq^2 + s^2}\Big) + (m_b^2 - s)(s-q^2)(m_b^2(Q_b - Q_q)(q^2+s) - s(Q_b+Q_q)(s-q^2)) + 2sm_b^4 Q_q q^2 \log\Big(\frac{s(m_b^2+q^2-s)}{m_b^2 q^2}\Big)\Big), \tag{F18}$$

$$V^q_{9,V}(q^2) = \frac{4\pi^2 f^{\perp}_{K^*}(m_b^2 Q_q - Q_b q^2)}{m_b q^2}, \tag{F19}$$

$$\rho^q_{10,A}(q^2,s) = -\frac{3}{2} f^{\perp}_{K^*}(s(s-q^2)^2(q^2-m_B^2))^{-1}\Big(-2sm_b^4 Q_b q^2 \log\Big(\frac{sm_b^2}{m_b^2 q^2 - sq^2 + s^2}\Big) + (m_b^2 - s)(s-q^2)(m_b^2(Q_b - Q_q)(q^2+s) - s(Q_b+Q_q)(s-q^2)) + 2sm_b^4 Q_q q^2 \log\Big(\frac{s(m_b^2+q^2-s)}{m_b^2 q^2}\Big)\Big), \tag{F20}$$

$$V^q_{10,A}(q^2) = \frac{4\pi^2(m_b^2 - q^2) f^{\perp}_{K^*}(m_b^2 Q_q - Q_b q^2)}{m_b q^2 (m_B^2 - q^2)}, \tag{F21}$$

$$d\cdot\rho^q_{10,0}(q^2,s) = -12m_B^2 m^2_{K^*} f^{\perp}_{K^*}((q^2-s)^2(m_B^2-q^2)^3)^{-1}\Big(m_b^2 Q_b(m_b^2(q^2+s) + 2s(s-q^2))\log\Big(\frac{sm_b^2}{m_b^2 q^2 - sq^2 + s^2}\Big) - (m_b^2 - s)(s-q^2)(2m_b^2(Q_b - Q_q) + (Q_b+Q_q)(s-q^2)) + m_b^2 Q_q(q^2+s)(m_b^2+q^2-s)\Big(-\log\Big(\frac{s(m_b^2+q^2-s)}{m_b^2 q^2}\Big)\Big)\Big), \tag{F22}$$

$$d\cdot V^q_{10,0}(q^2) = \frac{16\pi^2 m_B^2 m^2_{K^*}(m_b^2 - q^2) f^{\perp}_{K^*}(m_b^2 Q_q - Q_b q^2)}{m_b q^2 (q^2 - m_B^2)^3}, \tag{F23}$$

$$\rho^q_{4,T}(q^2,s) = -\frac{3}{2}\mu_K^2(m_B + m_K)(sm_B^2(2m_B^2 q^2 + m_B^4 - 4sq^2 + (q^2)^2))^{-1}(2sQ_b m_B^2(m_b^4 + s(m_B^2 - s))\rho_{C_d}(s) + 2sm_B^2 Q_q \rho_{C_b}(s)(m_b^2(m_B^2 + q^2 - 2s) + m_b^4 + s(s - m_B^2)) + (m_b^2 - s)(Q_b - Q_q)(m_b^2(m_B^2 + q^2 - 4s) + s(-3m_B^2 - q^2 + 4s))), \tag{F24}$$

$$V^q_{4,T}(q^2) = -\frac{4\pi^2 m_b \mu_K^2 Q_q (m_B + m_K)}{m_B^2 q^2}, \tag{F25}$$

$$f^q_{4,T}(q^2,u) = \frac{2\pi^2}{m_B^2}(m_B + m_K)\Big[\phi_P(u)\Big(\frac{\bar{u}Q_b}{um_B^2 + \bar{u}q^2} - \frac{uQ_q}{\bar{u}m_B^2 + uq^2}\Big) + \frac{\phi_\sigma(u)}{6}\Big(Q_b\frac{u(1+2\bar{u})m_B^2 + 2\bar{u}^2 q^2}{u(um_B^2 + \bar{u}q^2)^2} - Q_q\frac{\bar{u}(1+2u)m_B^2 + 2u^2 q^2}{\bar{u}(\bar{u}m_B^2 + uq^2)^2}\Big)\Big], \tag{F26}$$

$$\rho^q_{8,T}(q^2,s) = \frac{3}{2}m_b f_K(m_B + m_K)(s^2(s-q^2)^3)^{-1}\Big(2s^2 m_b^4 Q_b \log\Big(\frac{sm_b^2}{m_b^2 q^2 - sq^2 + s^2}\Big) - 2s^2 m_b^2 Q_q(m_b^2 + q^2 - s) \times \log\Big(\frac{s(m_b^2+q^2-s)}{m_b^2 q^2}\Big) + (m_b^2 - s)(Q_b - Q_q)(s-q^2)(m_b^2(q^2-3s) + s(s-q^2))\Big), \tag{F27}$$

$$V^q_{8,T}(q^2) = \frac{4\pi^2 f_K Q_q (m_B + m_K)}{q^2}. \tag{F28}$$

b. WA formulas $q^2 = 0$

$$\tilde{\rho}^{\,q,\gamma}_{5,V}(s) = \frac{2\pi^2 f_{K^*} m_{K^*} Q_q \phi_\gamma(\frac{m_b^2}{s})}{s}, \qquad V^{q,\gamma}_{5,V} = -\frac{2\pi^2 Q_b f_{K^*} m_{K^*}}{m_b^2}, \tag{F29}$$

$$\tilde{\rho}^{\,q,\gamma}_{6,A}(s) = -\frac{2\pi^2 f_{K^*} m_{K^*} Q_q (s\phi_\gamma(\frac{m_b^2}{s}) - 2)}{s m_B^2}, \qquad V^{q,\gamma}_{6,A} = \frac{2\pi^2 f_{K^*} m_{K^*} (Q_b - 2Q_q)}{m_B^2}, \tag{F30}$$

$$\tilde{\rho}^{\,q,\gamma}_{9,V}(s) = \frac{4\pi^2 m_b Q_q f^\perp_{K^*} \phi_\gamma(\frac{m_b^2}{s})}{s}, \qquad V^{q,\gamma}_{9,V} = -\frac{4\pi^2 Q_b f^\perp_{K^*}}{m_b}, \tag{F31}$$

$$\tilde{\rho}^{\,q,\gamma}_{10,A}(s) = \frac{4\pi^2 m_b Q_q f^\perp_{K^*} \phi_\gamma(\frac{m_b^2}{s})}{m_B^2}, \qquad V^{q,\gamma}_{10,A} = -\frac{4\pi^2 m_b Q_b f^\perp_{K^*}}{m_B^2}. \tag{F32}$$

[1] B. Aubert *et al.* (*BABAR* Collaboration), Phys. Rev. Lett. **102**, 091803 (2009); J.-T. Wei *et al.* (BELLE Collaboration), Phys. Rev. Lett. **103**, 171801 (2009).
[2] R. Aaij *et al.*, J. High Energy Phys. 07 (2012) 133.
[3] Y. Amhis *et al.* (Heavy Flavor Averaging Group), arXiv:1207.1158.
[4] A. Ali and V. M. Braun, Phys. Lett. B **359**, 223 (1995).
[5] A. Khodjamirian, G. Stoll, and D. Wyler, Phys. Lett. B **358**, 129 (1995).
[6] M. Dimou, J. Lyon, and R. Zwicky Phys. Rev. D **87**, 074008 (2013).
[7] H. Ishida and Y. Koide, arXiv:1305.7342.
[8] A. L. Kagan and M. Neubert, Phys. Lett. B **539**, 227 (2002).
[9] P. Ball, G. W. Jones, and R. Zwicky, Phys. Rev. D **75**, 054004 (2007).
[10] F. Mahmoudi, Comput. Phys. Commun. **178**, 745 (2008).
[11] T. Feldmann and J. Matias, J. High Energy Phys. 01 (2003) 074.
[12] A. Khodjamirian, Th. Mannel, and Y.-M. Wang, J. High Energy Phys. 02 (2013) 010.
[13] G. Buchalla, A. J. Buras, and M. E. Lautenbacher, Rev. Mod. Phys. **68**, 1125 (1996).
[14] M. Beneke, T. Feldmann, and D. Seidel, Nucl. Phys. **B612**, 25 (2001).
[15] K. G. Chetyrkin, M. Misiak, and M. Munz, Phys. Lett. B **400**, 206 (1997).
[16] P. Ball and R. Zwicky, Phys. Rev. D **71**, 014029 (2005).
[17] P. Ball and R. Zwicky, Phys. Rev. D **71**, 014015 (2005).
[18] B. Grinstein, M. J. Savage, and M. B. Wise, Nucl. Phys. **B319**, 271 (1989).
[19] J. Bijnens and N. Danielsson, Phys. Rev. D **75**, 014505 (2007).
[20] J. Beringer *et al.*, Phys. Rev. D **86**, 010001 (2012).
[21] S. W. Bosch and G. Buchalla, Nucl. Phys. **B621**, 459 (2002).
[22] R. S. Chivukula and H. Georgi, Phys. Lett. B **188**, 99 (1987).
[23] A. J. Buras, P. Gambino, M. Gorbahn, S. Jager, and L. Silvestrini, Phys. Lett. B **500**, 161 (2001).
[24] G. D'Ambrosio, G. F. Giudice, G. Isidori, and A. Strumia, Nucl. Phys. **B645**, 155 (2002).
[25] R. Zwicky and T. Fischbacher, Phys. Rev. D **80**, 076009 (2009).
[26] M. E. Albrecht, Th. Feldmann, and Th. Mannel, J. High Energy Phys. 10 (2010) 089.
[27] P. Ball, V. M. Braun, and N. Kivel, Nucl. Phys. **B649**, 263 (2003).
[28] P. Ball, V. M. Braun, Y. Koike, and K. Tanaka, Nucl. Phys. **B529**, 323 (1998).
[29] A. Khodjamirian and D. Wyler, arXiv:hep-ph/0111249.
[30] I. I. Balitsky, V. M. Braun, and A. V. Kolesnichenko, Nucl. Phys. **B312**, 509 (1989).
[31] P. Colangelo and A. Khodjamirian arXiv:hep-ph/0010175.
[32] M. A. Shifman, A. I. Vainshtein, and V. I. Zakharov, Nucl. Phys. **B147**, 385 (1979).
[33] M. A. Shifman, Prog. Theor. Phys. Suppl. **131**, 1 (1998).
[34] T. M. Aliev and V. L. Eletsky, Sov. J. Nucl. Phys. **38**, 936 (1983).
[35] A. Bazavov *et al.*, Phys. Rev. D **85**, 114506 (2012).
[36] H. Na C. J. Monahan, C. T. H. Davies, R. Horgan, G. Peter Lepage, and J. Shigemitsu, Phys. Rev. D **86**, 034506 (2012).
[37] M. Beneke and T. Feldmann, Nucl. Phys. **B592**, 3 (2000).
[38] M. Beneke, G. Buchalla, M. Neubert, and C. T. Sachrajda, Nucl. Phys. **B591**, 313 (2000).
[39] C. Kim, A. K. Leibovich, and T. Mehen, Phys. Rev. D **78**, 054024 (2008).
[40] M. Misiak, Phys. Lett. B **269**, 161 (1991).
[41] M. Ciuchini, E. Franco, G. Martinelli, L. Reina, and L. Silvestrini, Phys. Lett. B **316**, 127 (1993).

[42] B. Grinstein and D. Pirjol, Phys. Rev. D **70**, 114005 (2004).
[43] C. Bobeth, G. Hiller, and D. van Dyk, J. High Energy Phys. 07 (2010) 098.
[44] M. Beylich, G. Buchalla, and T. Feldmann, Eur. Phys. J. C **71**, 1635 (2011).
[45] J. Lyon and R. Zwicky arXiv:1210.6546.
[46] R. Aaij *et al.*, J. High Energy Phys. 12 (2012) 125.
[47] N. Taniguchi *et al.*, Phys. Rev. Lett. **101**, 111801 (2008).
[48] M. Beneke, Th. Feldmann, and D. Seidel, Eur. Phys. J. C **41**, 173 (2005).
[49] W. Altmannshofer, P. Paradisi, and D. M. Straub, J. High Energy Phys. 04 (2012) 008.
[50] W. Altmannshofer and D. M. Straub, J. High Energy Phys. 08 (2012) 121.
[51] S. Descotes-Genon, J. Matias, M. Ramon, and J. Virto, J. High Energy Phys. 01 (2013) 048.
[52] R. Fleischer and R. Knegjens, Eur. Phys. J. C **71**, 1532 (2011).
[53] M. Ciuchini, E. Franco, S. Mishima, and L. Silvestrini, J. High Energy Phys. 10 (2012) 029.
[54] B. Bhattacharya, A. Datta, and D. London Int. J. Mod. Phys. A **28**, 1350063 (2013).
[55] L. Hofer, D. Scherer, and L. Vernazza, J. High Energy Phys. 02 (2011) 080.
[56] L. Hofer and L. Vernazza, arXiv:1212.4785.
[57] M. Beneke, J. Rohrer, and D. Yang, Nucl. Phys. **B774**, 64 (2007).
[58] R. Aaij *et al.*, Nucl. Phys. **B867**, 1 (2013).
[59] R. Aaij *et al.*, J. High Energy Phys. 07 (2013) 084.
[60] V. L. Chernyak and A. R. Zhitnitsky, Phys. Rep. **112**, 173 (1984).
[61] A. G. Grozin and M. Neubert, Phys. Rev. D **55**, 272 (1997).
[62] A. Khodjamirian, Nucl. Phys. **B605**, 558 (2001).
[63] L. Wolfenstein, Phys. Rev. Lett. **51**, 1945 (1983).
[64] A. J. Buras, M. E. Lautenbacher, and G. Ostermaier, Phys. Rev. D **50**, 3433 (1994).
[65] M. Czakon, U. Haisch, and M. Misiak, J. High Energy Phys. 03 (2007) 008.
[66] C. Bobeth, M. Misiak, and J. Urban, Nucl. Phys. **B574**, 291 (2000).
[67] M. Misiak and M. Steinhauser, Nucl. Phys. **B683**, 277 (2004).
[68] R. Mertig, M. Bohm, and A. Denner, Comput. Phys. Commun. **64**, 345 (1991).